Technical Report CERC-94-2
February 1994

US Army Corps of Engineers
Waterways Experiment Station

Storm Evolution of Directional Seas in Shallow Water

by Charles E. Long
Coastal Engineering Research Center

Prepared for Headquarters, U.S. Army Corps of Engineers

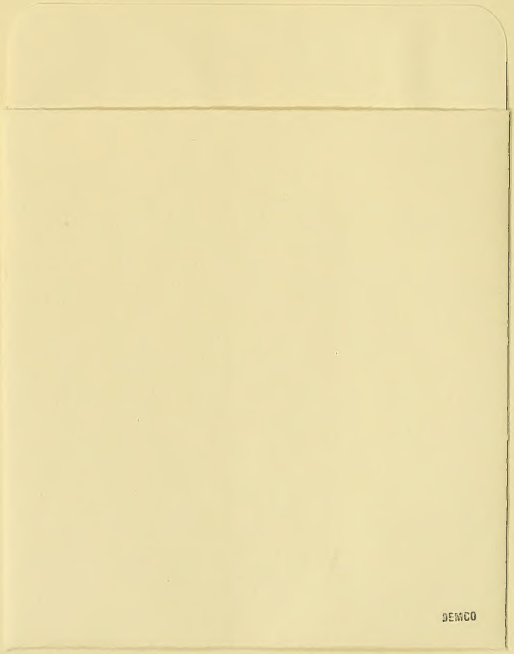

Technical Report CERC-94-2
February 1994

Storm Evolution of Directional Seas in Shallow Water

by Charles E. Long
Coastal Engineering Research Center

U.S. Army Corps of Engineers
Waterways Experiment Station
3909 Halls Ferry Road
Vicksburg, MS 39180-6199

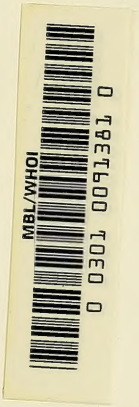

Final report

Approved for public release; distribution is unlimited

Prepared for U.S. Army Corps of Engineers
Washington, DC 20314-1000

Under Work Unit 32484

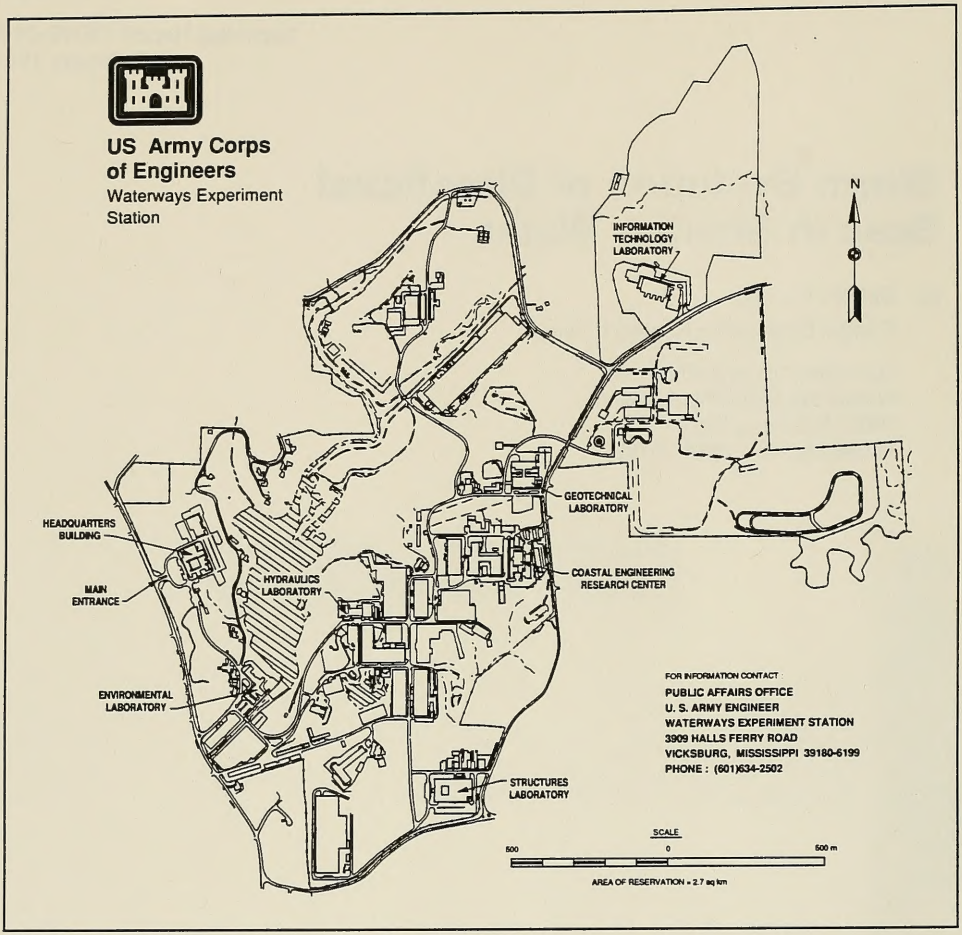

Waterways Experiment Station Cataloging-in-Publication Data

Long, Charles E.
Storm evolution of directional seas in shallow water / by Charles E. Long ; prepared for U.S. Army Corps of Engineers.
131 p. : ill. ; 28 cm. — (Technical report ; CERC-94-2
Includes bibliographic references.
1. Storm surges — Mathematics. 2. Spectral energy distribution. 3. Wind waves — Mathematics. 4. Time-series analysis. I. United States. Army. Corps of Engineers. II. U.S. Army Engineer Waterways Experiment Station. III. Title. IV. Series: Technical report (U.S. Army Engineer Waterways Experiment Station) ; CERC-94-2.
TA7 W34 no.CERC-94-2

Contents

Preface

This report illustrates the evolution of directionally distributed, shallow-water waves at times of high energy as measured with a high-resolution directional wave gauge. The work was motivated by the need for a complete description of storm wave fields incident on the nearshore to augment understanding and modeling of nearshore processes which affect coastal engineering projects. This effort was authorized by Headquarters, U.S. Army Corps of Engineers (HQUSACE), under Civil Works Research Work Unit 32484, Directionality of Waves in Shallow Water, Coastal Flooding Program. Funds were provided through the Coastal Engineering Research Center (CERC), U.S. Army Engineer Waterways Experiment Station (WES), under the program management of Ms. Carolyn M. Holmes, CERC. Messrs. John H. Lockhart, Jr., John G. Housley, Barry W. Holliday, and David A. Roellig were HQUSACE Technical Monitors.

This report was prepared by Dr. Charles E. Long at CERC's Field Research Facility (FRF) in Duck, NC, under the direct supervision of Mr. William A. Birkemeier, Chief, FRF, and Mr. Thomas W. Richardson, Chief, Engineering Development Division, CERC; and under the general supervision of Dr. James R. Houston and Mr. Charles C. Calhoun, Jr., Director and Assistant Director, CERC, respectively.

Data processing software was written by Dr. Joan M. Oltman-Shay of Quest Integrated, Inc., Seattle, WA. Physical maintenance of the directional gauge was done by the FRF dive team consisting of Messrs. Birkemeier, Michael W. Leffler, H. Carl Miller, Eugene W. Bichner, and Brian L. Scarborough. Gauge calibration was maintained by Mr. Kent K. Hathaway, FRF. Data acquisition and storage were done by Mr. Clifford F. Baron, FRF. Considerable assistance in data processing was provided by students contracted through the Cooperative Education Program: Ms. Wendy L. Smith of Old Dominion University, Mmes. Juliana Admadji and Janna Pemberton of Florida Institute of Technology, and Ms. Judy Roughton of College of the Albemarle, Elizabeth City, NC. Dr. R. T. Guza, Scripps Institution of Oceanography, and Mr. Lockhart provided several useful suggestions after reviewing a preliminary draft of this manuscript. The efforts of all of these individuals are appreciated.

At the time of publication of this report, Director of WES was Dr. Robert W. Whalin. Commander was COL Bruce K. Howard, EN.

1 Introduction

Ocean wind waves are among the dominant forcing mechanisms for nearshore dynamic processes. Of the broad suite of possible wave regimes, those associated with high energy are most important for engineering design. High-energy waves produce the most rapid changes in natural or renourished beach morphologies and are most likely, by definition, to exceed the strength or elevation of a coastal protective structure, resulting in costly damage or excessive overtopping. Complete knowledge of the types of extremely energetic natural wind wave fields that are incident on the nearshore is thus rather critical for efficient design of coastal engineering projects.

A complete wave field definition describes the way in which wave energy is distributed in both frequency and direction. Because of the difficulty in making high-resolution measurements of wave energy distributions, early engineering guidance treated a given sea state as consisting of a train of waves at a single frequency traveling in a single direction. While most wave fields are more complicated than this, there persists much guidance based on unidirectional, monochromatic waves, as evidenced in the *Shore Protection Manual* (SPM 1984). Advances in time series measurement and efficient analysis in the last three decades have provided considerable knowledge of the frequency distributions of wave energy, enabling the development of good theoretical models and improved physical models of wave processes with a consequent improvement in engineering guidance.

Detailed measurements of wave direction are more difficult. Only within the last decade have practical methods of directional wave measurement been available, and these are still expensive and logistically demanding. Until very recently, there were no long-term observations from which to extract the directional character of nearshore seas with any statistical confidence. To alleviate this lack of knowledge, the Field Research Facility (FRF) of the U.S. Army Engineer Waterways Experiment Station, Coastal Engineering Research Center, deployed a high-resolution directional wave gauge at its site near Duck, NC, in September 1986. Measurements covering a 5-year period, lasting through August 1991, enable considerable clarification of the directional nature of incident wind waves at this site.

The purpose of this report is to elucidate, by illustration, the nature of the frequency and directional distributions of wind wave energy during storm events occurring during the 5-year observation period. These results are

intended to assist numerical modelers in developing and testing theories of wave transformation across a continental shelf. Results also can be used by numerical and physical modelers to establish realistic seaward wind wave boundary conditions for models of nearshore processes. Illustrations are contained primarily in Appendix A. Chapters 2 and 3 of this report describe the experiment site, gauges, sampling pattern, storm definition, characterizing parameters, and format of displayed results. Common features of storm wave frequency-direction spectra are described, and some conjecture about unusual spectral properties, along with the appropriate path of future research, is presented in Chapter 4.

2 Measurement Scheme

Measurement Site

The FRF is located on the Outer Banks of North Carolina, just north of the village of Duck (Figure 1). The site is representative of many coastal sites characterized by a broad continental shelf, relatively mild bottom slope, and reasonably uniform longshore topography. The mild sloping bottom substantially dissipates wind waves in the nearshore so that attention can be focused on waves arriving from seaward. The uniform longshore topography allows the use of a spatial array of sensors to detect wave direction without contamination by a longshore inhomogeneity in the incident wave field. The facility, described by Birkemeier et al. (1985), has a permanent staff and computing facilities that are used to monitor, maintain, and error check the instrumentation on a day-to-day basis, and so minimize data losses from the myriad problems that can plague field data collection.

Regional and local topography

At the large environmental scale, the coastline in the vicinity of the FRF is nearly straight for several tens of kilometers north and south. It is oriented such that the shore-normal direction (facing seaward) is very nearly 70 deg from true north (70 deg T). Waves and onshore winds can approach this site along an easterly 180-deg arc from 340 to 160 deg T. The adjacent continental shelf is approximately 100 km wide, being narrower to the south where Cape Hatteras juts eastward. The direction of nearest approach of the 100-m isobath (the shelf break) is 10 deg to 15 deg south of east and is about 80 km distant from the FRF. A characteristic bottom slope for the shelf is 1 m/km, but, at a finer scale, the bathymetry is marked by numerous features of 1- to 10-km horizontal scales and 10-m vertical scales scattered irregularly across the shelf. Waves with periods near 10 sec begin to shoal at depths of 100 m, so that considerable refraction of wind waves propagating over the shelf is expected (U.S. Army Engineer District, Wilmington 1980).

Within a few kilometers of the FRF, the bathymetry is more regular. A complex bar system exists within about 300 m of the shore (Birkemeier 1984), and waves and currents have created some irregular bathymetry of the 600-m-long research pier (Miller, Birkemeier, and DeWall 1983). Away from these regions, isobaths are nearly shore-parallel. The bottom slope is nearly uniform at about 0.5 m/km and is reasonably dynamically stable, as indicated by

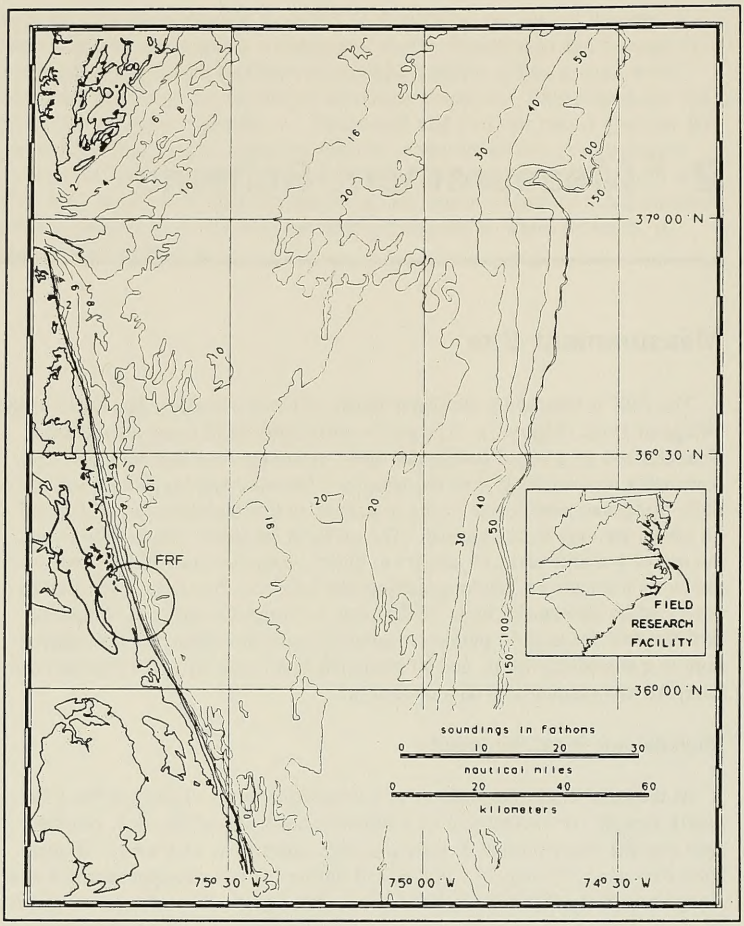

Figure 1. FRF location and offshore bathymetry

repeated surveys (Howd and Birkemeier 1987). Figure 2 illustrates the bathymetry over a region 600 m north to 600 m south of the pier and extending about 900 m offshore.

Regional climate

The site is subject to a variety of climates that give rise to a broad diversity in frequency and directionally distributed wave energy. Typical wind and wave climate for the period covered by this report can be roughly classified as four basic types (Miller et al. 1988; Leffler et al. 1989, 1990, 1991, 1992, 1993). First are low-wind situations, where the wave field is characteristically low-frequency swell propagating in from the open Atlantic Ocean. These

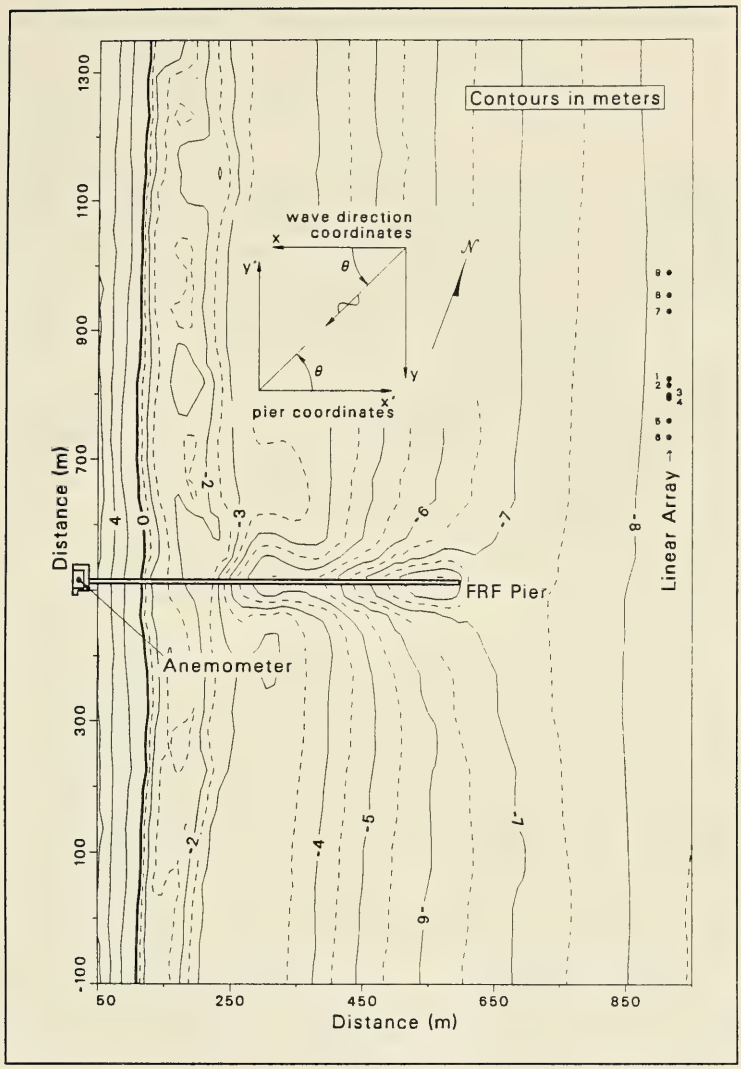

Figure 2. FRF nearshore bathymetry and instrument location

waves typically arrive from the east-to-southeast, and are normally present between storm events.

The second and most common type of wave-generating winds are from northeasters associated with atmospheric frontal passages. Fronts typically arrive from the west and have a northeast-southwest orientation. Active local

wave generation occurs after a frontal passage when strong winds arise in the northeast quadrant. A third type of storm is an extratropical depression that typically forms south of the FRF along the south Atlantic coast. These storms tend to migrate northward along the coast, creating high winds and waves from the east to northeast. Less frequent but more intense wave generators are hurricanes, the fourth type of disturbance. These originate in the equatorial Atlantic, migrate west to northwest, and can make landfall on the gulf and Atlantic coasts with very destructive winds and waves. No hurricanes made landfall at the FRF during the course of this study, but several passed by in the deeper Atlantic, creating a distinctive local field of high, long-period waves narrowly distributed in frequency and direction.

It is noted that the regional topography and climate limit the generalization of results obtained at the FRF to sites having similar characteristics. For example, one would not expect nearshore dynamics of sites on the Great Lakes, gulf, or west coasts of the United States to behave in the same way because their climates and bathymetries are different. Nonetheless, fundamental physical processes such as nonlinear wave behavior, wave breaking, and air-sea interaction, for which insights are gained by studies at the FRF, will be more universally applicable; the limitations are not too restrictive, and generalizations are justified.

Instrumentation

Data from two gauges are presented in this report. One gauge consists of a set of near-bottom-mounted pressure gauges, which together constitute a high-resolution directional wave gauge. This gauge provides estimates of the frequency-direction spectra of wind waves which are the basis of this report. The other gauge is an anemometer that gives a measure of local wind speed and direction. It provides a characterization of the larger wind field that generates some of the wave fields measured with the directional wave gauge. These gauges are described here briefly for completeness and because their properties affect the way data are interpreted.

High-resolution directional wave gauge

The directional wave gauge consists of two fundamental parts: (a) an array of gauges that sense sea surface displacement, and (b) an analysis algorithm that converts the data to an estimate of $S(f,\theta)$, the frequency-direction spectrum, where f is cyclic wave frequency and θ is wave direction.[1] The sensors are a set of nine near-bottom-mounted pressure gauges, laid out in a straight line along the 8-m isobath as shown in Figure 2. Spacing between the gauges follows the guidance given by Davis and Regier (1977) for the design of wave direction detectors. Pressure time series data from each gauge are converted to units of equivalent seawater depth, Fourier transformed, and converted to sea surface displacement Fourier transforms using linear wave

[1] For convenience, symbols and abbreviations are listed in the Notation (Appendix B).

theory. For each pair of gauges, raw cross-spectral estimates are then computed, ensemble averaged, and band averaged to create a smoothed cross-spectrum for each gauge pair. For each smoothed frequency, a matrix is formed of the cross-spectra for all possible pairs of gauges. This matrix is then fed to the directional estimation algorithm.

Wave energy directional distributions are computed using the Iterative Maximum Likelihood Estimator (IMLE), which was derived by Pawka (1982, 1983), and found to be a substantial improvement on the Maximum Likelihood Estimator (MLE) derived by Davis and Regier (1977). Specifically, the algorithm is Equations 1 - 4 in the paper by Pawka (1983) with convergence exponent $\beta = 1$, convergence coefficient $\gamma = 5$, and a maximum of 30 iterations.

In practice, all gauges of the FRF array are not used for all wave frequencies. Gauges with large separations are used for long, low-frequency waves. Closely spaced gauges are used for shorter waves to avoid loss of coherence for these waves at large spatial separations. Details of array sub-configurations and their associated frequencies are given by Long and Oltman-Shay (1991). Tests of the FRF array with artificial data indicate a directional resolution of 5 deg. This means it can resolve the peak of a single mode directional distribution to within 5 deg, or distinguish the peaks of a bimodal distribution when separated by 15 deg or more.

Anemometer

The reference anemometer used in this study was mounted atop the FRF laboratory building (Figure 2) at an elevation of 19.5 m above mean sea level. It has a nominal speed accuracy of ± 0.5 m/sec and direction accuracy of ± 3 deg. Speed and direction data are collected on separate channels, and results from each channel are simply averaged (not vector averaged). The proximity of the anemometer to the FRF building is known to cause low speed readings on some occasions in very high winds (Long and Hubertz 1988), but it is considered sufficiently reliable for the generally moderate winds encountered in this study. Though other anemometers have been deployed for shorter periods at the FRF, this one was consistently in use for the duration of this study. It follows that this gauge provides the most consistent local representation of the larger scale wind field.

Data Sampling Schemes

With few exceptions, data used in this report were obtained following the standard FRF sampling scheme. The pattern is to collect four contiguous records of 34-min duration (4,096 data points at a 2-Hz sampling rate) starting at 0100, 0700, 1300, and 1900 Eastern Standard Time (EST). When the characteristic wave height H_{mo} exceeds 2 m at a reference wave gauge (usually gauge #1 of the directional array), additional collections are made starting at 0400, 1000, 1600, and 2200 EST. This form of sampling gives good data

coverage of high energy conditions, but has a tendency to miss some of the details of initial transient conditions at the onset of a storm.

The anemometer data presented in this report are based on a subset of the overall FRF database. Wind speeds and directions are deduced from single 34-min records with start times of 0100, 0700, 1300, and 1900 EST. These particular records are the most reliable, having been checked by hand for use in the FRF annual reports (Leffler et al. 1992, 1993). The result is a very regular sampling of local winds, with gaps only for system maintenance or repair.

All possible data were processed from the directional wave gauge, so that normally there are samples from all the routine start times listed above. Four records of 34 min each (2 hr 16 min or 16,384 data points at 2 Hz) for each gauge were used in cross-spectral computation to ensure high confidence in the resulting cross-spectral matrix that is transformed in the IMLE algorithm. Fifteen half-overlapping segments of 2,048 points were processed for ensemble averages, and 10 subsequent frequency bands were averaged for a final resolution bandwidth $\Delta f = 0.00977$ Hz and a minimum of 160 degrees of freedom (excluding any gain in degrees of freedom from the lapped segments) in the final cross-spectral estimates. While this method gives very good results in estimates of $S(f,\theta)$, it has the effect of averaging all wave processes for the 2 hr 16 min records so that highly transient processes are smoothed somewhat. Results are not invalid, just rather strongly filtered. Shorter records can be used in future work if brief transients are important.

The bulk of $S(f,\theta)$ results were obtained by the method just described, but there were, on occasion, minor variations in sampling times and rates. During the SUPERDUCK experiment in September and October 1986 (Crowson et al. 1988), data collection start times were adjusted to conform to high and low tides, and so did not conform to the FRF normal collection pattern. Furthermore, a total of seven 34-min records were obtained in each collection. To maximize the number of $S(f,\theta)$ observations during SUPERDUCK, records 1 - 4 from a collection were processed, and then records 4 - 7 were processed, so that record 4 was used twice, but observations were still almost independent. Time series of parameters from these spectra thus appear rather oddly spaced, with pairs of samples appearing with 1 hr 42 min separations. During the DELILAH experiment of October 1990 (Birkemeier et al. 1991), data were collected for an additional 34 min and the sampling rate for all data was 4 Hz instead of 2 Hz. Thus, a collection had 10 records of 4,096 data points (about 17 min) each. For the data used here, wind speeds and directions during DELILAH were averaged for only 17 min instead of the usual 34 min. Directional array data were still processed in 2 hr 16 min total record lengths, but, in smoothing, 20 bands were averaged instead of 10, resulting in the same final resolution bandwidth (but more degrees of freedom).

General Working Data Set

The final working data set from which to extract storm data consists of 6,762 observations of $S(f,\theta)$ spanning the period from September 1986 to August 1991, or about 5 years. Two major gaps in data collection occurred during this time, affecting the seasonal coverage of storms and reducing their total number. After SUPERDUCK, full time collection of directional gauge data did not resume until late January 1987, so there is a gap in the time line of collections from November 1986 to January 1987. In December 1987, a fishing boat trawled a net along the line of the linear array of gauges, destroying about half of them. Parts replacement and repairs could not be effected until August 1988, so there is another gap from December 1987 to August 1988. Aside from these two major gaps, the record is substantially complete, excepting short periods for routine maintenance and calibration.

3 Storm Data

Event Definition

To extract storm data from the larger working data set, a definition of what is meant by a storm is necessary. For the purposes of this report, a storm is defined using the characteristic wave height H_{mo} and the length of time it exceeds a certain level. To isolate the largest events, it was required that H_{mo} exceed 2 m for times at least 24 hr apart, and not drop below 1 m in the interim. Wave conditions are normally relatively quiescent just before a storm, generally being low-amplitude, long-period swell from the southeast quadrant. To ensure at least one prestorm condition, data for a given event were extracted from the main database from the beginning of the day containing a prestorm condition to the end of the day during which H_{mo} first drops below 1 m.

Figure 3 shows a time series of H_{mo} from the directional gauge for all collections in the main database. Storm events that satisfy the above definition are identified by letter or number. Their nominal durations are marked by horizontal black bars. In all, 29 storm events were found and are referenced by the letters A to Z and the numbers 1 to 3. Note that Event 3 follows Event E.

Table 1 lists the storm events shown in Figure 3, along with the start and end dates defined by the criteria described above. Also shown are the maximum H_{mo} observed during the storm and a nominal duration, defined as the time elapsed from the first time H_{mo} exceeds 2 m to the last time it drops below 2 m. Linear interpolation between measured H_{mo} was used to obtain the exceedence times. Based on the definition of a storm described above, all durations should exceed 24 hr. Several do not, which illustrates the pitfalls of searching a 6,762-point database by eye. The shorter storms are retained here because they do not differ from the longer storms except by their durations.

Climatological Parameters

Several characterizing parameters are used in this report to describe a storm evolution. These parameters are given names and symbols common to

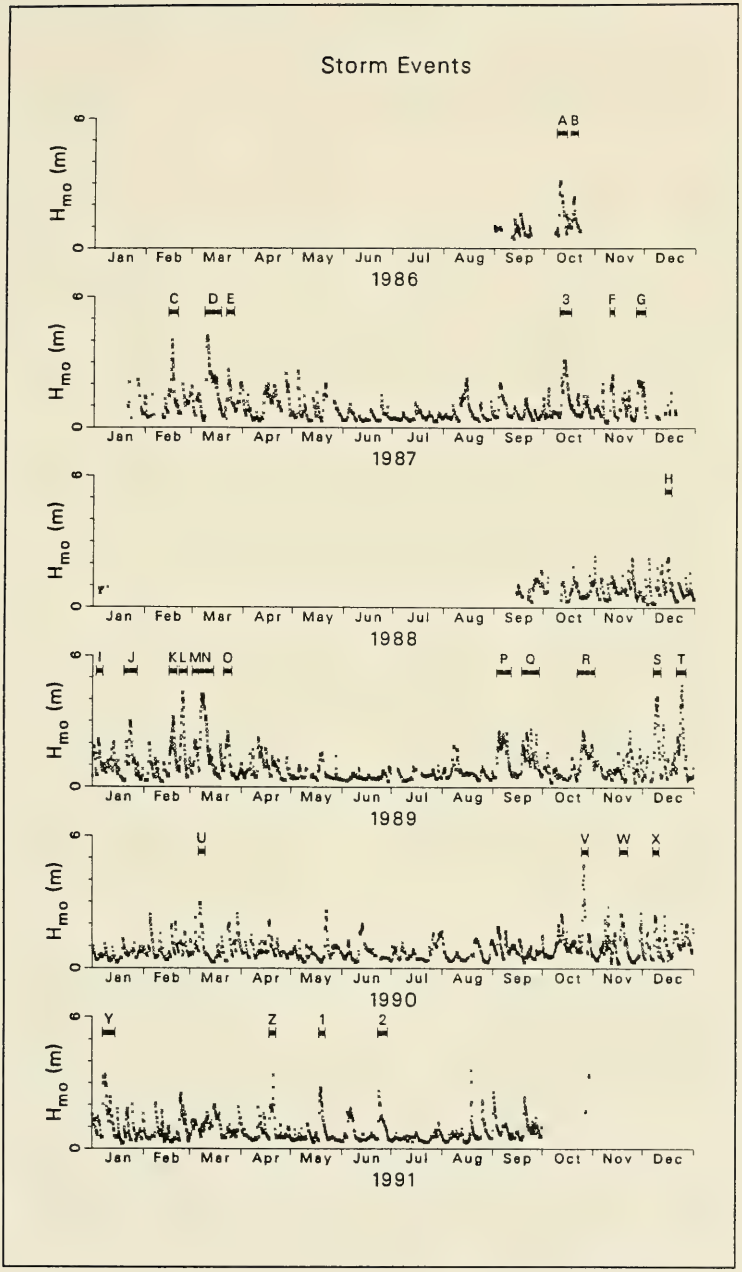

Figure 3. Time series of H_{mo} with storm events identified

Table 1
Storm Event Identification

Event	Start	End	H_{mo} m	duration hr
A	9 Oct 86	14 Oct 86	3.09	57.01
B	17 Oct 86	21 Oct 86	2.38	23.67
C	15 Feb 87	20 Feb 87	4.03	40.07
D	9 Mar 87	18 Mar 87	4.22	161.84
E	22 Mar 87	26 Mar 87	2.68	28.15
3	11 Oct 87	17 Oct 87	3.11	85.29
F	10 Nov 87	12 Nov 87	2.45	27.04
G	26 Nov 87	1 Dec 87	2.21	86.13
H	14 Dec 88	17 Dec 88	2.31	27.34
I	3 Jan 89	6 Jan 89	2.19	8.68
J	20 Jan 89	27 Jan 89	3.00	78.70
K	16 Feb 89	20 Feb 89	3.19	54.43
L	22 Feb 89	26 Feb 89	4.32	52.32
M	2 Mar 89	5 Mar 89	2.11	24.45
N	6 Mar 89	14 Mar 89	4.23	108.62
O	21 Mar 89	25 Mar 89	2.53	30.08
P	3 Sep 89	11 Sep 89	2.59	138.10
Q	18 Sep 89	28 Sep 89	2.68	199.53
R	22 Oct 89	1 Nov 89	2.63	38.02
S	7 Dec 89	11 Dec 89	4.17	61.76
T	21 Dec 89	26 Dec 89	4.68	91.00
U	6 Mar 90	9 Mar 90	2.96	22.25
V	25 Oct 90	28 Oct 90	4.70	44.31
W	17 Nov 90	21 Nov 90	2.51	42.70
X	7 Dec 90	10 Dec 90	2.41	24.07
Y	7 Jan 91	14 Jan 91	3.40	111.84
Z	18 Apr 91	21 Apr 91	3.38	51.00
1	18 May 91	21 May 91	2.82	33.22
2	23 Jun 91	28 Jun 91	2.66	21.05

wave analysis, but because there are several ways to compute each with the data at hand, they are defined specifically here. The parameter set consists of characteristic wave height H_{mo}, characteristic wave period T_p, characteristic wave direction θ_p, representative directional spread of wave energy $\delta\theta_p$, and water depth d.

Characteristic wave height H_{mo} is defined, as usual, as four times the standard deviation of sea surface displacement, based on variances contained in the frequency spectrum $S(f)$ between the low- and high-frequency cutoffs. In this analysis, $S(f)$ is computed as the average of the surface-corrected frequency spectra from each of the nine gauges in the linear array. This does not increase degrees of freedom (because all gauges are measuring the same

wave field), but it does reduce instrument noise. All analysis is done in discrete frequency space, and results are defined in terms of $N = 28$ frequency bands from $f_1 = 0.054$ Hz (the low-frequency bound) to $f_N = 0.319$ Hz (the high-frequency bound) in steps of $\Delta f = 0.00977$ Hz. The discrete frequency spectrum is given the symbol $S(f_n)$ so that characteristic wave height is

$$H_{mo} = 4 \left[\sum_{n=1}^{N} S(f_n)\, \Delta f \right]^{\frac{1}{2}} \tag{1}$$

Characteristic wave period, or peak period T_p is defined as the inverse of the peak frequency f_p deduced from the frequency spectrum; i.e., the discrete frequency at which $S(f_n)$ is maximum. This is the conventional definition of peak period, and is used here to be consistent with other wave studies. Thus, $T_p = 1/f_p$.

There are a number of ways to define peak direction θ_p. The one used here is the peak of the discrete frequency-direction spectrum $S(f_n,\theta_m)$ at the peak frequency; i.e., the discrete direction θ_p at which $S(f_p,\theta_m)$ is a maximum. Discrete directions θ_m range from $\theta_1 = -90$ deg to $\theta_M = \theta_{91} = 90$ deg in $\Delta\theta = 2$-deg increments. These angles represent the directions from which wave energy arrives relative to shore-normal, with -90 deg being waves travelling parallel to the beach from the south, 0 deg being waves arriving along the shore-normal axis, and +90 deg being waves travelling parallel to the beach from the north. A constraint on linear array analysis is that it cannot detect waves travelling seaward, so all waves are assumed to arrive from the seaward semicircle of azimuths.

A characteristic directional spread of wave energy $\delta\theta_p$ also is a very useful parameter for these data. It is also defined from $S(f_n,\theta_m)$ as being the angle that subtends the central half of the energy in the directional distribution at the peak frequency. Symbolically, an integral function $I(f,\theta)$ can be defined as

$$I(f,\theta) = \int_{-90}^{\theta} \frac{S(f,\phi)}{S(f)}\, d\phi \tag{2}$$

where $I(f,-90°) = 0$ and $I(f,90°) = 1$ identically because the integral of $S(f,\theta)$ with respect to direction defines $S(f)$. The arc that contains the central half of the energy at a given frequency begins at the angle θ_{25} for which $I(f,\theta_{25}) = 0.25$ and ends at the angle θ_{75} for which $I(f,\theta_{75}) = 0.75$. If θ_{25} and θ_{75} are determined at $f = f_p$, the peak directional spread is simply

$$\delta\theta_p = \theta_{75} - \theta_{25} \tag{3}$$

This parameter is robust in that it can be computed for any finite directional distribution and is meaningful in that it gives a small number for narrowly

distributed energy, and a large number for broadly distributed energy. Note that its use here differs from that of Long and Oltman-Shay (1991). Long and Oltman-Shay (1991) looked at the overall spread of $S(f,\theta)$. Examined here is the energy spread only at $f = f_p$, the most energetic frequency spectral line.

Water depths d reported here, and used for tide stage determination and surface correction of near-bottom pressure signals, are the medians of the mean depths determined from the nine pressure gauges for the duration of one collection. This was necessary because, while the pressure gauges are accurate at wind wave frequencies, they are susceptible to long-term drifts in their mean signals due to environmental changes and biological activity within the gauge sensing volumes. Use of median depths as representative depths for all the gauges eliminates the largest deviate mean depths. Comparison of resulting mean depths with the FRF tide gauge indicates an accuracy of about 0.1 m, which is sufficient for use here.

Data Presentation

The primary result of this study is the set of figures contained in Appendix A. For each of the events listed in Table 1, there are two types of display. One page contains time series of climatological parameters associated with the event. Following the climatology page for each event, subsequent pages contain sequences of frequency-direction spectral plots for select times within the event. Page A3 contains an index of events, showing the page in Appendix A where climatological parameters are displayed.

Climatological parameters displayed for the duration of each event are those described above, namely H_{mo}, T_p, d, $\delta\theta_p$, θ_p, wind direction, and wind speed. The reader is referred to the parametric plot for Event A on page A4 for an example. Wind direction and peak wave direction θ_p have been transformed to the same coordinate system (directions from which winds or waves arrive in degrees counterclockwise from shore-normal, as discussed earlier), and are drawn on the same set of axes. Plot symbols will then be collocated if wind and peak wave directions are aligned.

Because some events contain a large number of observations of $S(f,\theta)$, it is somewhat impractical logistically to display all observations for all events. Consequently, only certain select cases are illustrated in pages following the parametric plots. A prestorm condition, all observations up to and near the peak H_{mo} levels in a storm, and several observations during storm decay are displayed for all events. Shaded symbols in the graph of H_{mo} for a given event indicate which observations of $S(f,\theta)$ are plotted. For some storms of short duration, all observations are plotted.

Sequences of observed frequency-direction spectra, selected as noted, are illustrated on pages following the parametric plots. For example, selected cases from Event A, indicated by the shaded symbols on page A4, are shown as sequences of plots on pages A5 and A6. For each observation there are

four entities displayed: (a) a three-dimensional plot of the surface representing $S(f,\theta)$, (b) a linear graph of the frequency spectrum $S(f)$, (c) a linear graph of the direction spectrum $S(\theta)$ (defined below), and (d) a contour plot of $S(f,\theta)$. The same vertical scale is used for all three-dimensional plots of $S(f,\theta)$ within an event, so the relative importance of each observation can be assessed. Prestorm and storm decay conditions thus show low relief, and peak conditions tend to have the largest relief.

The linear plot of $S(f)$ is shown in the right panel of the three-dimensional box, with its abscissa parallel to the frequency axis of the $S(f,\theta)$ plot. The direction spectrum $S(\theta)$ is the directional analog of the frequency spectrum and shows the directional distribution of total energy. Computationally, it is found from

$$S(\theta) = \int_{f_1}^{f_N} S(f,\theta)\, df \tag{4}$$

and has units of square meters per degree. The analog with $S(f)$ can be seen from the definition of the frequency spectrum as

$$S(f) = \int_{-90}^{90} S(f,\theta)\, d\theta \tag{5}$$

with units of square meters per Hertz. The left panel of the three-dimensional box contains a linear graph of $S(\theta)$. Both $S(f)$ and $S(\theta)$ are drawn to constant scales derived from the maxima of these entities within an event.

The contour plot of $S(f,\theta)$ is shown below the three-dimensional box for each observation. Contour intervals are tenths of the maximum value of $S(f,\theta)$ of all observations in an event. Consequently, spectra having relatively low energy levels have both low relief in the three-dimensional plots and few, if any, lines in corresponding contour plots. Observations with higher energy levels have correspondingly more contour lines.

Because all four plotted entities within a given event are drawn to constant scales within an event, axis annotation is rather redundant. It is also space consuming. Consequently, axis annotation is drawn only for the upper left-hand set of plots on each page illustrating sequences of $S(f,\theta)$. Axis annotation for all other plot axes within an event is identical.

4 Discussion

The primary purpose of this report is to elucidate the directional distributions of nearshore wind wave energy in the context of evolving storms. With the illustrations in Appendix A for guidance, some fundamental properties of storm wave fields can be identified.

A primary question is whether a storm wave field can, in any sense, be reasonably approximated as unidirectional and monochromatic, or, perhaps, as corresponding to simple models of deep-ocean wave fields. A quick perusal of Appendix A shows, in a few observations, that a unidirectional, monochromatic model may be appropriate for some applications (examine, e.g., Event R and conditions near the peaks of Events V and W), but such conditions are relatively rare. Furthermore, narrow spreads of naturally occurring spectral energy in frequency and direction do not mean the waves are unidirectional and monochromatic. Real ocean waves are invariably groupy and subject to nonlinear interactions. These dynamically important properties can not be represented by unidirectional, monochromatic wave models, and the utility of such models is thereby somewhat restricted.

The wave fields of Appendix A do not appear to conform to models and observations of deep-ocean wave fields, either. For example, papers by Mitsuyasu et al. (1975) and Mitsuyasu and Uji (1989) indicate that $S(f,\theta)$ in the deep ocean is characterized by narrower directional spreads near the spectral peak frequency than in the spectral tails. Spectra shown in Appendix A appear generally to have maximum spreads near spectral peak frequencies. These observations mean that neither a single-wave-train model nor deep-ocean wave behavior is appropriate to characterize nearshore storm waves.

While the spectra of storm wave fields at the FRF are complicated, they are not without a remarkable similarity in structure that can be described, at least qualitatively. In this part of the report, these structural similarities are discussed, and some of the consequent research questions are posited.

Of the 29 storm events identified in this report, 25 have $S(f,\theta)$ with common structural features (described qualitatively below) through the progress of a storm. Four events, E, P, Q, and R, do not follow this pattern. Of these four, waves in Events P and Q are associated with Hurricanes Gabrielle and Hugo, respectively, both of which passed several hundred kilometers away

from the FRF. Well-dispersed, low-frequency wave trains with very narrow directional spreads are associated with these events and are characteristic of waves from distant sources. Events E and R may be natural deviates from the common pattern of the remaining 25 events.

Storm waves driven by wind systems identified in the FRF annual reports (Miller et al. 1988, Leffler et al. 1989, 1990, 1991, 1992, 1993) as Canadian high-pressure systems, frontal passages, or low-pressure cells forming west to south of the FRF have frequency-direction spectra with many common features. Most of these features are illustrated in Event N (pages A47 to A50), which exemplifies the set of events. The progression of these features as the storm evolves is as follows:

a. There is usually a prestorm wave field consisting of low energy, long period swell with moderate spread arriving from shore-normal to slightly south of shore-normal. For Event N, this is the first case illustrated on the top row of page A48.

b. During the primary growth stage, at the initial onset of winds, high-frequency, locally generated waves appear. Peak period usually drops from the pre-storm condition. Peak direction shifts nearly to align with wind, but not exactly (bottom-mounted pressure gauges can detect only intermediate to shallow water waves, so some refraction towards shore-normal will take place even in short fetches). Peak directional spreads are of order 10 deg to 20 deg, the smallest of any time in the storm. For Event N, this is the second case illustrated on the top row of page A48.

c. In the secondary growth stage (remainder of the top row and first two cases of the second row of plots on page A48 for Event N), peak period increases, and the frequency spectrum tends to conform to one of the conventional nearshore models, such as TMA (Bouws et al. 1985) or FRF (Miller and Vincent 1990). It is the directional distribution within $S(f,\theta)$ that is most curious. As energy at the peak period increases, so does the characteristic spread, perhaps indicating continued local growth plus additional energy radiating in from growth further offshore. Moreover, an additional lobe of energy appears at the peak frequency, aligned more nearly with shore-normal or, for Event N, well south of shore-normal. Furthermore, a secondary peak of high-frequency energy (identified as a ridge in three-dimensional plots of $S(f,\theta)$ or a second tail off the main lobe of energy in contour plots) appears, making a strongly bimodal high-frequency tail to the spectrum. The second energy ridge is aligned nearer to shore-normal, and ranges from 20 deg to 40 deg offset from the initial growth stage spectrum.

d. In the advanced growth stage (last two cases on the second row and first two cases on the bottom row of plots on page A48 for Event N), the spectral peak continues to move to lower frequencies and becomes centered at very nearly shore-normal. The spread is rather large, being of order 40 deg to 50 deg, and the secondary lobe of low-frequency

energy appears to be absorbed by the primary peak. The structure of the bimodal, high-frequency tail remains, and its energy increases.

e. As storm waves reach their peak wave energy, the directionally broad, energetic, low-frequency spectral peak and directionally bimodal, high-frequency tail of the spectra remain. If driving winds persist, this structure can continue relatively unchanged for some time. In Event N, for example, wind speed remains nearly constant at 16 to 18 m/sec, and wind direction persists at 60 deg to 80 deg from shore-normal for more than 2 days (see page A47). The sequence of observations on pages A48 to A50, showing $S(f,\theta)$ from 1300 on 7 Mar 89 to 1900 on 9 Mar 89, illustrate a structure that changes very little, suggesting that some equilibrium condition has been attained.

f. In the waning stages of a storm (the final plots on page A50 for spectra of Event N), winds usually decrease in speed and change direction. Active local wave generation abates, and the high-frequency part of the spectrum decays. Low-frequency waves that were generated offshore continue to arrive, still with a broad directional spread.

g. In the end stage, conditions generally return to the prestorm spectrum of low-frequency, low-energy swell, having broad directional spread and being centered near the shore-normal direction.

The above description was derived specifically from Event N, but the other 24 storm events have the same features to a greater or lesser degree. Even the two dissimilar storms, Events E and R mentioned above, have some of the same features. The ubiquitousness of these spectral patterns indicates a high degree of consistency in storm wave evolution at the FRF. The unexpected features of these spectra, low-frequency side lobe of energy in the secondary growth stage, as well as a directionally broad, low-frequency peak coupled with a bimodal high-frequency tail in the most energetic stages, require some explanation so that guidance appropriate to engineering projects can be derived.

There are a number of lines of approach for explaining these observations. Several of them require work that is beyond the scope of this report, but the nature of the necessary investigation can be mentioned here. A primitive question is whether the observed $S(f,\theta)$ are real or some artifact of the interaction of the true wave field and the IMLE algorithm as used with the FRF linear array of gauges. If the wave energy is all propagating onshore, there is no known reason to suspect the spectral estimation process. Tests using synthetic data indicate the system is well capable of resolving the broad directional spreads and 20-deg-separated bimodal distributions observed here. If there is wave energy reflected from nearshore, the directional estimation system used in this report cannot resolve it, and the reflected energy will appear to be coming from offshore. This question can be addressed with a more recently installed 360-deg array, but that analysis has not been completed at this writing. Nonetheless, it is unlikely that reflections will account for the present observations because the spectral pattern recurs at many tidal stages and over

many seasons, wherein nearshore reflectivity would be expected to vary considerably.

Another possibility is that linear wave theory is not adequate during high-energy conditions when the wave field may become saturated with highly nonlinear, actively breaking waves. While this may be true for the extreme storm of Event T, it is unlikely to be true for the very marginally energetic storm of Event I, which was inadvertently included in this analysis, and had an H_{mo} that exceeded 2 m for less than 9 hr. The common spectral pattern described above also occurs in Event I (see pages A33 and A34), so it is improbable that a saturated wave field accounts for these observations.

Two other possible causes for these results are a common structure in the overall driving wind fields or the net effect of the broad, shallow bathymetry of the continental shelf adjacent to the FRF. The anemometer used in this report is only a crude indicator of the larger wind systems that generate waves observed at the FRF. A possible line of future research to examine the larger systems would be to apply a wind field model like that used in the CERC Wave Information Studies (Resio, Vincent, and Corson 1982) to the storm events examined in this report.

In conjunction with this possible study would be the inclusion of a reasonably accurate bathymetry for the United States mid-Atlantic continental shelf. The shelf break, at depths of 60 to 100 m, is 80 to 100 km distant from the FRF (Figure 1). Waves with periods of 8 to 11 sec (common periods for waves observed at the FRF) begin to be influenced by the bottom at these depths. Consequently, considerable wave refraction is expected for intermediate and long waves generated over the shelf and in the deeper Atlantic by nonuniform wind fields associated with atmospheric fronts and low pressure systems. This condition may account for the directionally broad, low-frequency peaks and side lobes in observed storm spectra. However, a quantitative assessment of these effects should be made, either with a numerical model or with more extensive observations.

It is possible that the directionally bimodal, high-frequency spectra may be due to a hummock or linear bar just offshore of the FRF array that causes strong refraction for high-frequency waves. This hypothesis can be tested with a detailed bathymetric survey that extends beyond the area routinely measured by the FRF staff (generally, the area shown in Figure 2). Such a survey has not yet been done, but the results presented herein should provide strong motivation for such work. There is weak evidence against a local bathymetric effect in the present data set. In the later stages of Events A, Y, and 2, winds shifted to the southeast with just enough force to generate waves from that quadrant. Though rather faintly shown in the figures (see pages A6, A87, and A96), bimodal spectral structures appear in the southeast quadrant in forms roughly symmetric to those observed in the northeast quadrant. It is somewhat unlikely that a local bathymetric feature would induce this kind of symmetry in $S(f,\theta)$.

Another possible explanation for the present observations is nonlinear interactions among wave trains during their generation and propagation to the FRF directional gauge. Various interaction mechanisms have been proposed by the WAMDI Group (1988), Freilich, Guza, and Elgar (1990), Resio and Perrie (1991), and others. Testing these hypotheses requires more detailed spatial measurements of $S(f,\theta)$ than are currently available. However, an experiment can and should be designed for this purpose if the current results are to be fully explained.

By way of guidance for model testing and engineering design, a representative example of $S(f,\theta)$ for late stage growth and peak storm conditions is shown in Figure 4. It is simply an average of the 19 observations from the relatively stationary peak storm conditions of Event N. It contains the primary features noted above and represents a nearly stationary dynamic process that continued for 56 hr. It should be noted that although the high-frequency tail has a spectral density less than the spectral peak, the total energy in the part of the tail that is bimodal (found from the area under the frequency spectrum over the high-frequency range of frequencies) is roughly 25 percent to 50 percent of the total energy. Because the bimodal tail occurs at peak energy conditions, there is considerable energy in the tail region.

The key point is that a wave generation and transformation model at continental shelf and larger scales clearly must have a result that looks qualitatively like Figure 4 to represent conditions at the FRF with reasonable verity. Additionally, nearshore process models of the FRF will be improved if a spectrum like that in Figure 4 is used to describe the wave boundary condition outside the surf zone in high-energy cases.

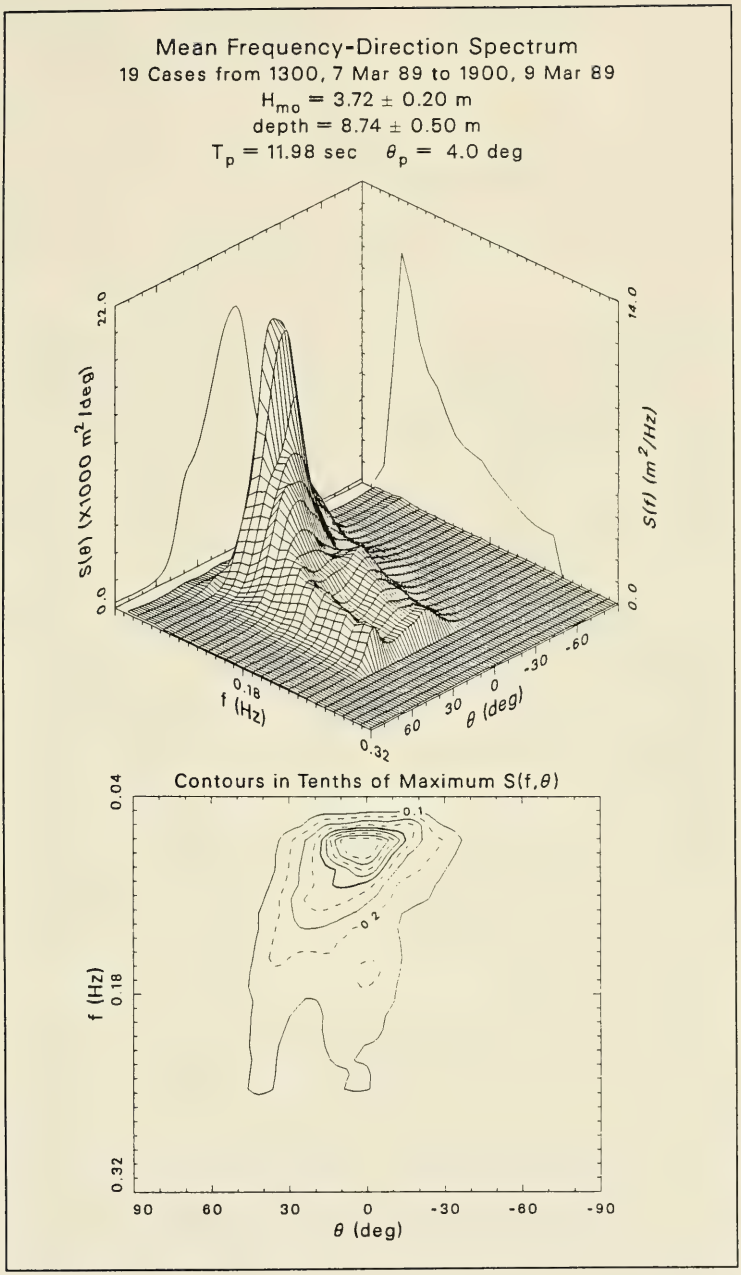

Figure 4. A characteristic storm spectrum from the FRF

5 Conclusion

This report elucidates the nature of frequency-direction spectra evolving during storm events occurring at the FRF. The primary result is a series of graphic presentations of spectra measured with a high-resolution directional wave gauge in an 8-m depth approximately 900 m offshore. Data from a 5-year observation period have been searched for storm events defined by a characteristic wave height in excess of 2 m at two points at least 24 hr apart in the same storm system. A total of 29 events have been isolated for closer scrutiny. Time series plots of climatic parameters and sequences of plots of $S(f,\theta)$ are used to reveal the evolutionary nature of storm wave fields.

The data indicate that there are two basic types of events: (a) high waves from strong but distant sources, and (b) localized wave generation from Canadian high-pressure systems, frontal passages, and atmospheric low-pressure cells passing the FRF from the west or south. Of the 29 events identified, 27 are of this latter type. Of the 27 localized events, 25 demonstrated very common patterns of spectral evolution. The patterns include initial localized waves aligned nearly with the local wind, directional broadening of spectral peaks as the wave fields grow, and a bifurcation of high-frequency spectral tails into two modes: (a) one nearly aligned with the wind, and (b) another, 20 deg to 40 deg away, aligned nearer to the shore-normal direction. One-quarter to one-half of the total energy is contained in the bimodal tails, a consideration of consequence because such spectra occur at the peaks of storms, and because the beating of such spectral waves against the shoreface can affect such nearshore processes as the patterns of beach erosion and infragravity wave generation.

The main conclusions here are that storm waves occur at the FRF with curious spectral shapes, and that accounting for the processes that give rise to those shapes is important. It is suggested that a more detailed coverage of wind, wave, and bathymetric observations over 100-km scales from the FRF is warranted. It is certain that nearshore processes driven by waves having such elaborately structured spectra will be different from estimates generated by over-simplified wave models (typically unidirectional and monochromatic) as even now still haunts engineering guidance. There is good reason to believe the spectra reported here are real and not some artifact of the analysis method used. Use of these results for testing wave generation and transformation models at scales of the continental shelf width, and as seaward wave boundary conditions for nearshore process models, will certainly yield more

realistic, meaningful, and accurate representations of nature, and thereby an improved coastal engineering science.

References

Birkemeier, W. A. (1984). "Time scales of nearshore profile changes," *Proceedings of the 19th Coastal Engineering Conference*, American Society of Civil Engineers, Houston, TX, 1507-1521.

Birkemeier, W. A., Miller, H. C., Wilhelm, S. D., DeWall, A. E., and Gorbics, C. S. (1985). "A user's guide to the Coastal Engineering Research Center's (CERC's) Field Research Facility," Technical Report CERC-85-1, U.S. Army Engineer Waterways Experiment Station, Vicksburg, MS.

Birkemeier, W. A., Hathaway, K. K., Smith, J. M., Baron, C. F., Leffler, M. W., and many others. "DELILAH experiment: Investigator's summary report," in preparation, U.S. Army Engineer Waterways Experiment Station, Vicksburg, MS.

Bouws, E., Gunther, H., Rosenthal, W., and Vincent, C. L. (1985). "Similarity of the wind wave spectrum in finite depth water: 1. Spectral form," *Journal of Geophysical Research* 90, 975-986.

Crowson, R. A., Birkemeier, W. A., Klein, H. M., and Miller, H. C. (1988). "SUPERDUCK nearshore processes experiment: Summary of studies, CERC Field Research Facility," Technical Report CERC-88-12, U.S. Army Engineer Waterways Experiment Station, Vicksburg, MS.

Davis, R. E., and Regier, L. A. (1977). "Methods for estimating directional wave spectra from multi-element arrays," *Journal of Marine Research* 35, 453-477.

Freilich, M. H., Guza, R. T., and Elgar, S. L. (1990). "Observations of nonlinear effects in directional spectra of shoaling gravity waves," *Journal of Geophysical Research* 95, 9645-9656.

Howd, P. A., and Birkemeier, W. A. (1987). "Storm-induced morphology changes during DUCK85," *Proceedings of Coastal Sediments '87*, American Society of Civil Engineers, New Orleans, LA, 834-847.

Leffler, M. W., Baron, C. F., Scarborough, B. L., Hathaway, K. K., and Hayes, R. T. (1991). "Annual data summary for 1989, CERC Field Research Facility," Technical Report CERC-91-9, U.S. Army Engineer Waterways Experiment Station, Vicksburg, MS.

_____. (1992). "Annual data summary for 1990, CERC Field Research Facility," Technical Report CERC-92-3, U.S. Army Engineer Waterways Experiment Station, Vicksburg, MS.

Leffler, M. W., Baron, C. F., Scarborough, B. L., and Hathaway, K. K. (1993). "Annual data summary for 1991, CERC Field Research Facility," Technical Report CERC-93-9, U.S. Army Engineer Waterways Experiment Station, Vicksburg, MS.

Leffler, M. W., Hathaway, K. K., Scarborough, B. L., Baron, C. F., and Miller, H. C. (1989). "Annual data summary for 1987, CERC Field Research Facility," Technical Report CERC-89-10, U.S. Army Engineer Waterways Experiment Station, Vicksburg, MS.

_____. (1990). "Annual data summary for 1988, CERC Field Research Facility," Technical Report CERC-90-13, U.S. Army Engineer Waterways Experiment Station, Vicksburg, MS.

Long, C. E. and Hubertz, J. M. (1988). "Nearshore wind-stress measurements: background, preliminary field work and experiment design," Miscellaneous Paper CERC-88-14, U.S. Army Engineer Waterways Experiment Station, Vicksburg, MS.

Long, C. E., and Oltman-Shay, J. M. (1991). "Directional characteristics of waves in shallow water," Technical Report CERC-91-1, U.S. Army Engineer Waterways Experiment Station, Vicksburg, MS.

Miller, H. C., Birkemeier, W. A., and DeWall, A. E. (1983). "Effects of CERC research pier on nearshore processes," *Proceedings of Coastal Structures '83*, American Society of Civil Engineers, Arlington, VA, 769-784.

Miller, H. C., Militello, A., Leffler, M. W., Grogg, W. E., Jr., and Scarborough, B. L. (1988). "Annual data summary for 1986, CERC Field Research Facility," Technical Report CERC-88-8, U.S. Army Engineer Waterways Experiment Station, Vicksburg, MS.

Miller, H. C., and Vincent, C. L. (1990). "FRF spectrum: TMA with Kitaigorodskii's f^{-4} scaling," *Journal of Waterway, Port, Coastal, and Ocean Engineering* 116, 57-77.

Mitsuyasu, H., Tasai, F, Suhara, T., Mizuno, S., Ohkusu, M., Honda, T., and Rikiishi, K. (1975). "Observations of the directional spectrum of ocean waves using a cloverleaf buoy," *Journal of Physical Oceanography* 5, 750-760.

Mitsuyasu, H., and Uji, T. (1989). "A comparison of observed and calculated directional wave spectra in the East China Sea," *Journal of the Oceanographical Society of Japan* 45, 338-349.

Pawka, S. S. (1982). "Wave directional characteristics on a partially sheltered coast," Ph.D. diss., Scripps Institution of Oceanography, University of California, San Diego, CA.

_____. (1983). "Island shadows in wave directional spectra," *Journal of Geophysical Research* 88, 2579-2591.

Resio, D., and Perrie, W. (1991). "A numerical study of nonlinear energy fluxes due to wave-wave interactions, Part 1, Methodology and basic results," *Journal of Fluid Mechanics* 223, 603-629.

Resio, D. T., Vincent, C. L., and Corson, W. D. (1982). "Objective specification of atlantic ocean wind fields from historical data," WIS Report 4, U.S. Army Engineer Waterways Experiment Station, Vicksburg, MS.

Shore protection manual. (1984). 4th ed., 2 Vol, U.S. Army Engineer Waterways Experiment Station, U.S. Government Printing Office, Washington, DC.

U.S. Army Engineer District, Wilmington. (1980). *Manteo (Shallowbag) Bay, North Carolina, general design memorandum, phase II*, Wilmington, NC.

WAMDI Group, The. 1988. "The WAM model - a third generation ocean wave prediction model," *Journal of Physical Oceanography* 18, 1775-1810.

Appendix A
Event Time Series and Spectral Sequences

Index

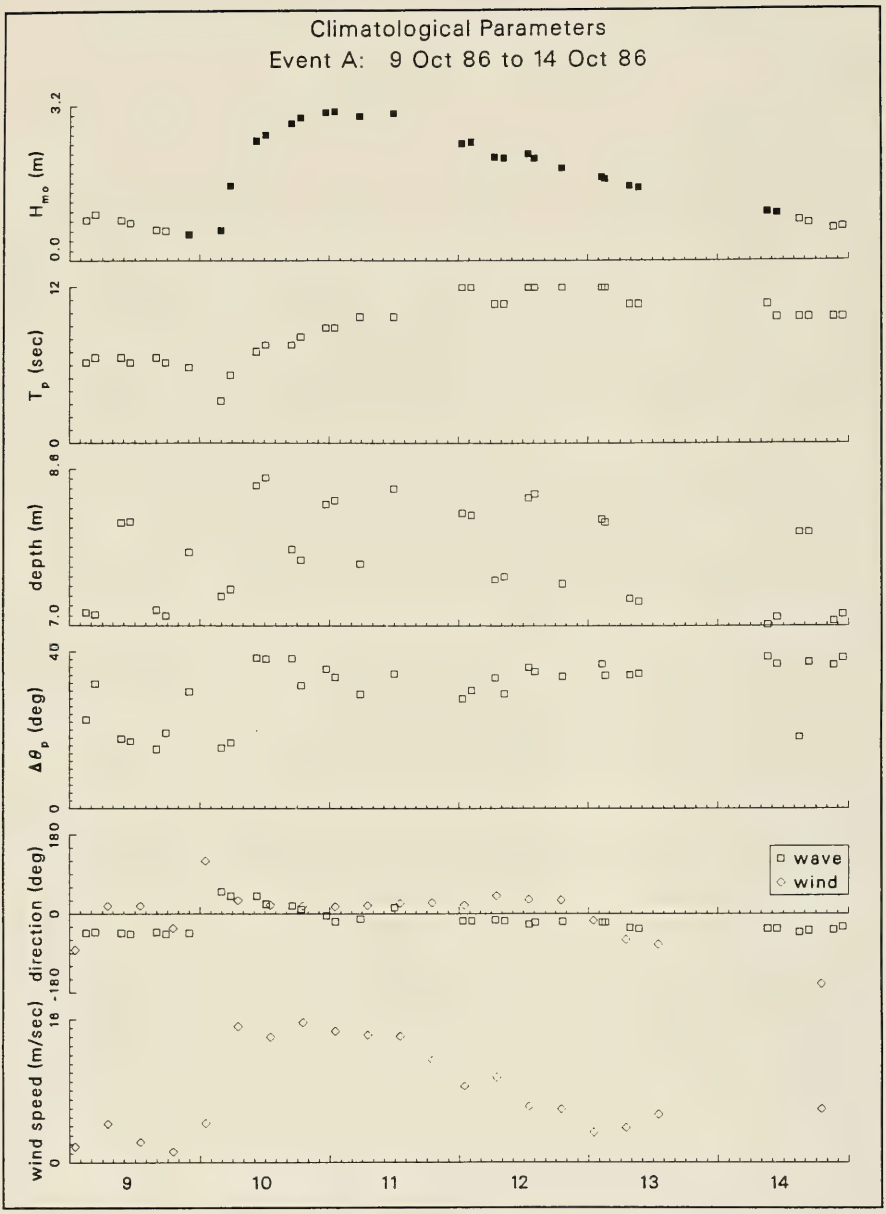
Climatological Parameters
Event A: 9 Oct 86 to 14 Oct 86
H_{mo} (m)
3.2
0.0
T_p (sec)
12
0
depth (m)
8.0
7.0
$\Delta\theta_p$ (deg)
40
0
direction (deg)
180
0
-180
wave
wind
wind speed (m/sec)
16
0
9
10
11
12
13
14

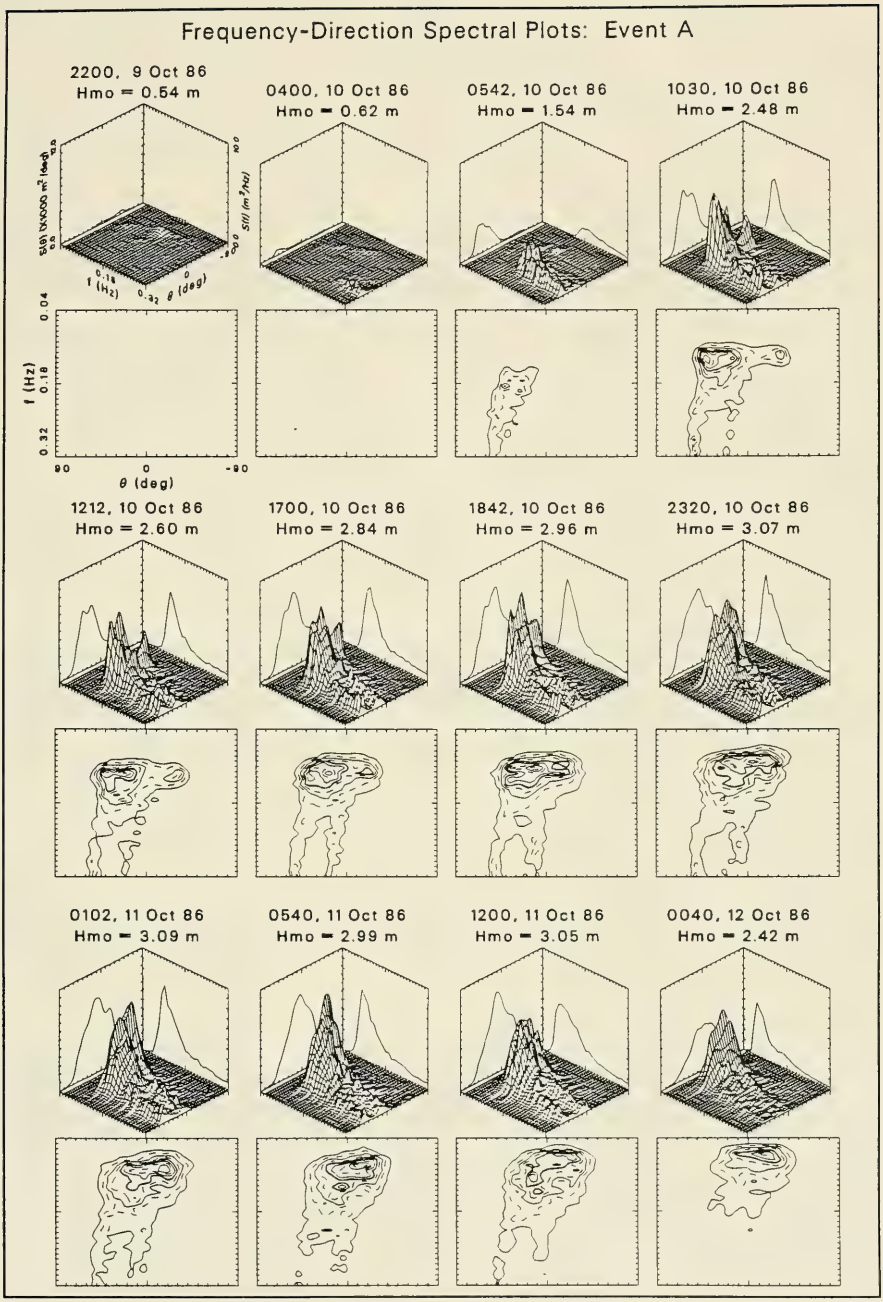
Frequency-Direction Spectral Plots: Event A
2200, 9 Oct 86
Hmo = 0.54 m
0400, 10 Oct 86
Hmo = 0.62 m
0542, 10 Oct 86
Hmo = 1.54 m
1030, 10 Oct 86
Hmo = 2.48 m
1212, 10 Oct 86
Hmo = 2.60 m
1700, 10 Oct 86
Hmo = 2.84 m
1842, 10 Oct 86
Hmo = 2.96 m
2320, 10 Oct 86
Hmo = 3.07 m
0102, 11 Oct 86
Hmo = 3.09 m
0540, 11 Oct 86
Hmo = 2.99 m
1200, 11 Oct 86
Hmo = 3.05 m
0040, 12 Oct 86
Hmo = 2.42 m
f (Hz)
0.04
0.18
0.32
90
0
-90
θ (deg)

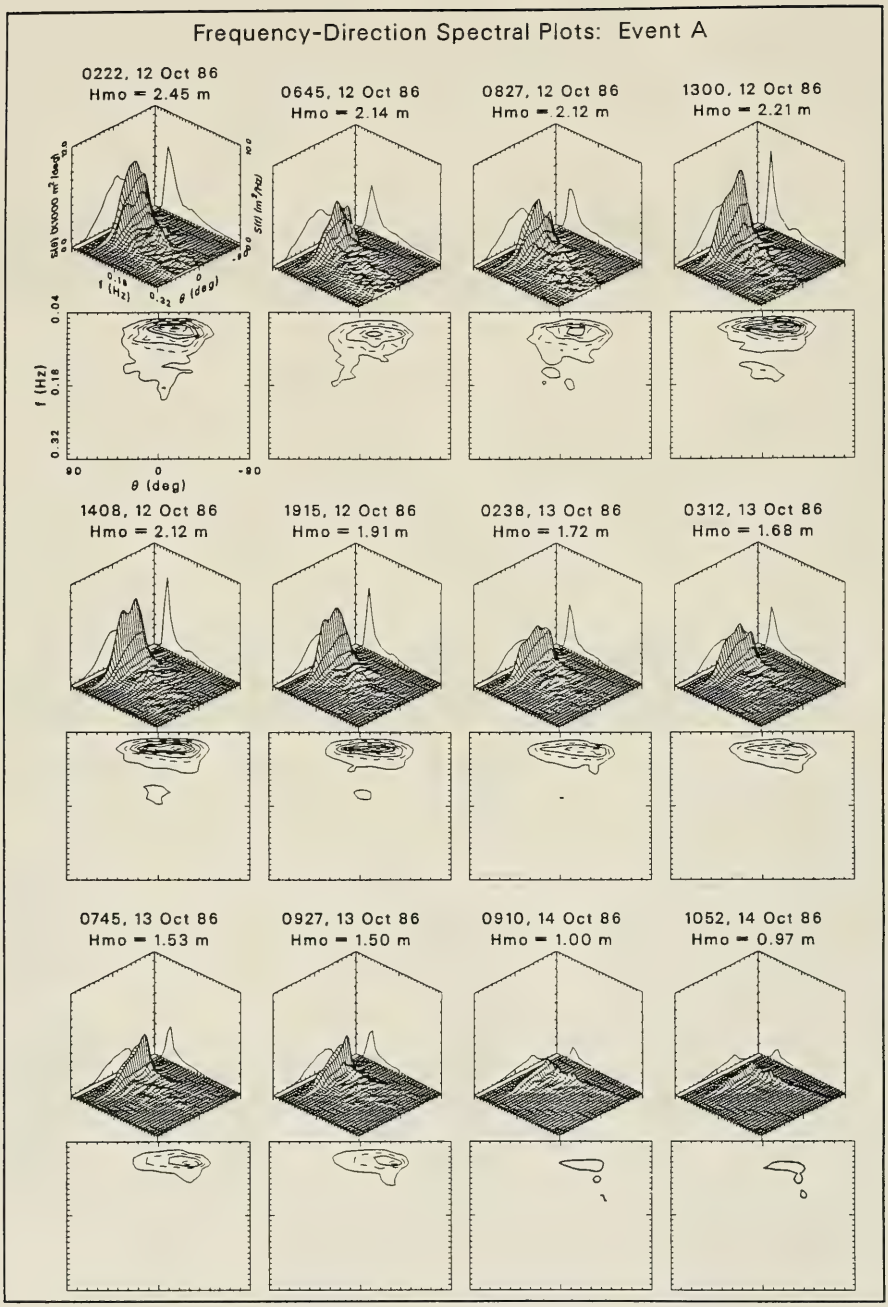
Frequency-Direction Spectral Plots: Event A
0222, 12 Oct 86
Hmo = 2.45 m
0645, 12 Oct 86
Hmo = 2.14 m
0827, 12 Oct 86
Hmo = 2.12 m
1300, 12 Oct 86
Hmo = 2.21 m
1408, 12 Oct 86
Hmo = 2.12 m
1915, 12 Oct 86
Hmo = 1.91 m
0238, 13 Oct 86
Hmo = 1.72 m
0312, 13 Oct 86
Hmo = 1.68 m
0745, 13 Oct 86
Hmo = 1.53 m
0927, 13 Oct 86
Hmo = 1.50 m
0910, 14 Oct 86
Hmo = 1.00 m
1052, 14 Oct 86
Hmo = 0.97 m
f (Hz)
θ (deg)

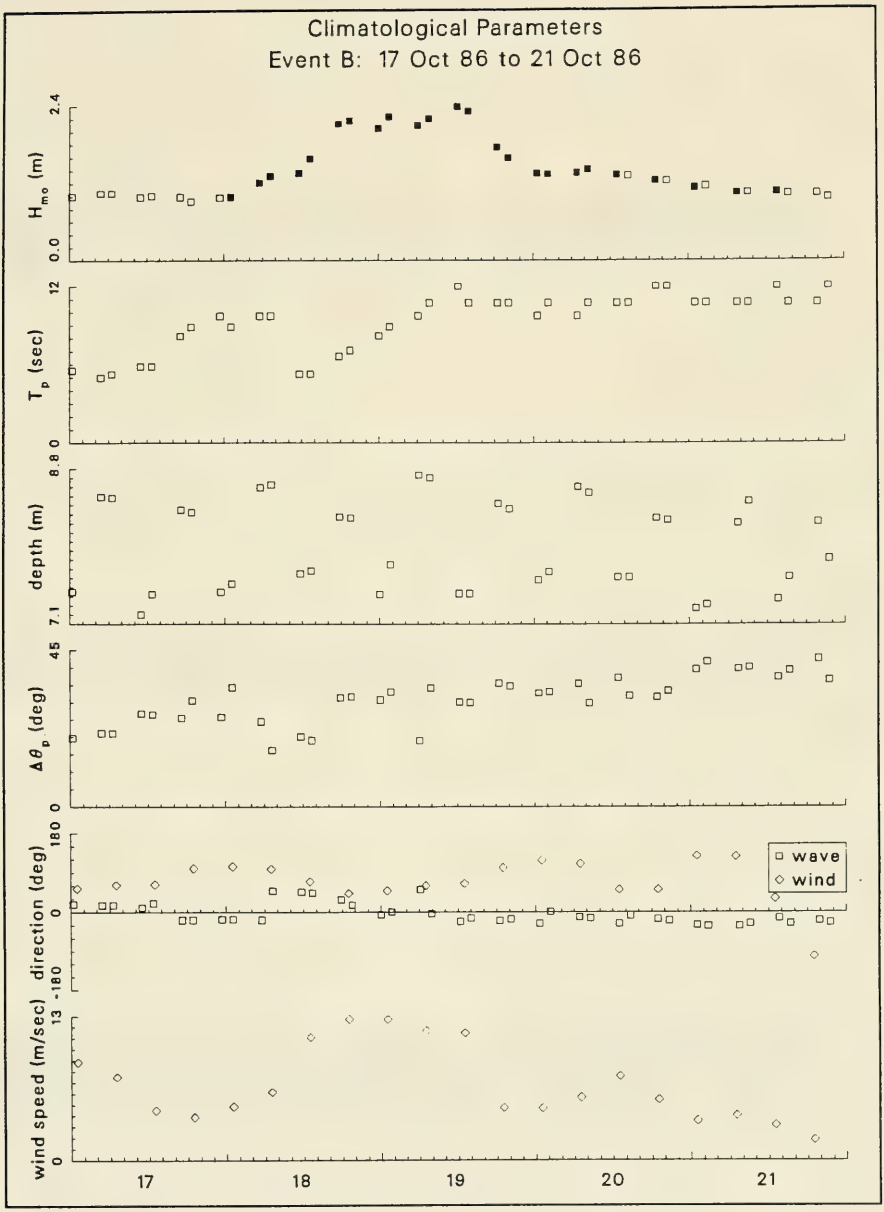
Climatological Parameters
Event B: 17 Oct 86 to 21 Oct 86
H_{mo} (m)
2.4
0.0
T_p (sec)
12
0
depth (m)
8.8
7.1
$\Delta\theta_p$ (deg)
45
0
direction (deg)
180
0
-180
wave
wind
wind speed (m/sec)
13
0
17
18
19
20
21

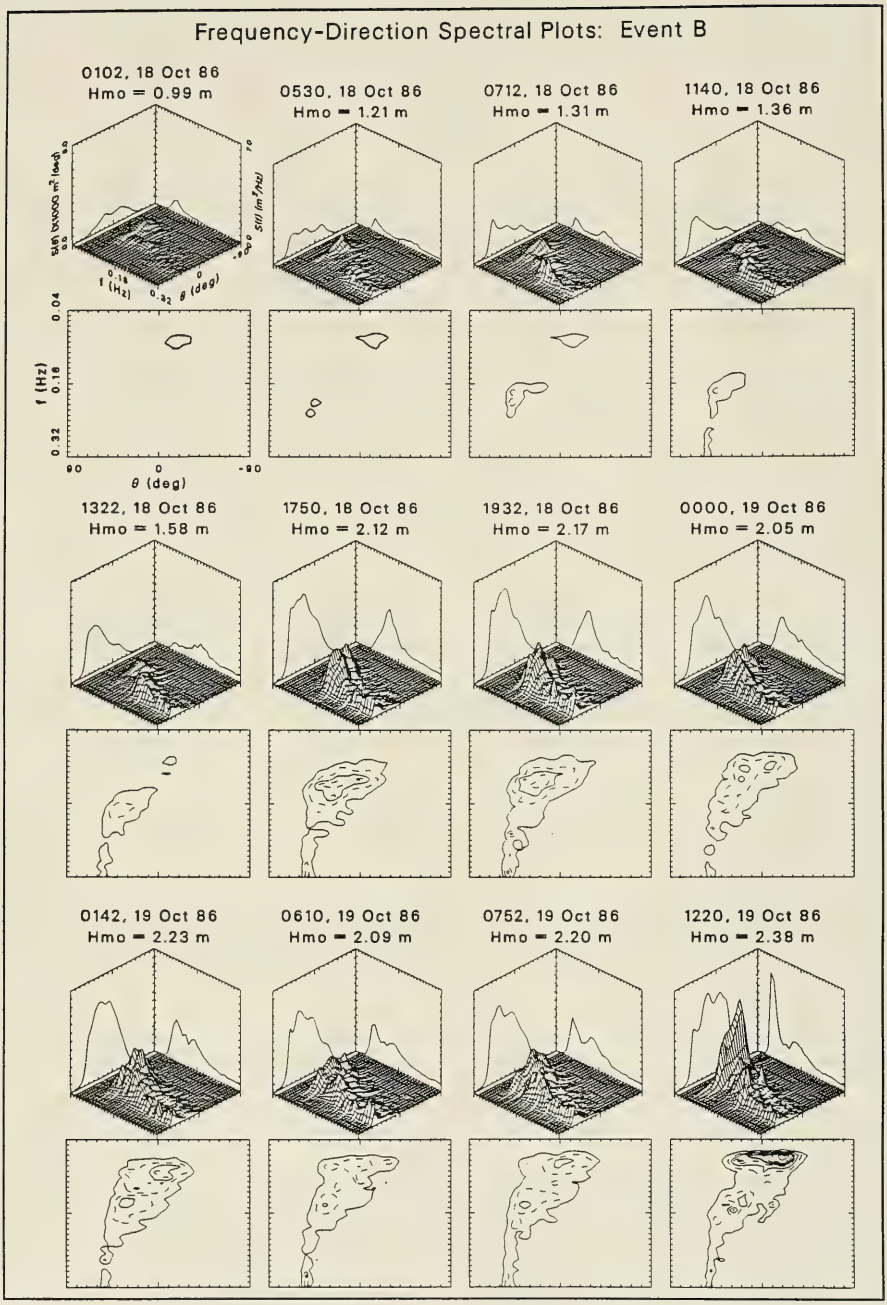
Frequency-Direction Spectral Plots: Event B
0102, 18 Oct 86
Hmo = 0.99 m
0530, 18 Oct 86
Hmo = 1.21 m
0712, 18 Oct 86
Hmo = 1.31 m
1140, 18 Oct 86
Hmo = 1.36 m
f (Hz)
0.04
0.16
0.32
90
0
-90
θ (deg)
1322, 18 Oct 86
Hmo = 1.58 m
1750, 18 Oct 86
Hmo = 2.12 m
1932, 18 Oct 86
Hmo = 2.17 m
0000, 19 Oct 86
Hmo = 2.05 m
0142, 19 Oct 86
Hmo = 2.23 m
0610, 19 Oct 86
Hmo = 2.09 m
0752, 19 Oct 86
Hmo = 2.20 m
1220, 19 Oct 86
Hmo = 2.38 m

Frequency-Direction Spectral Plots: Event B

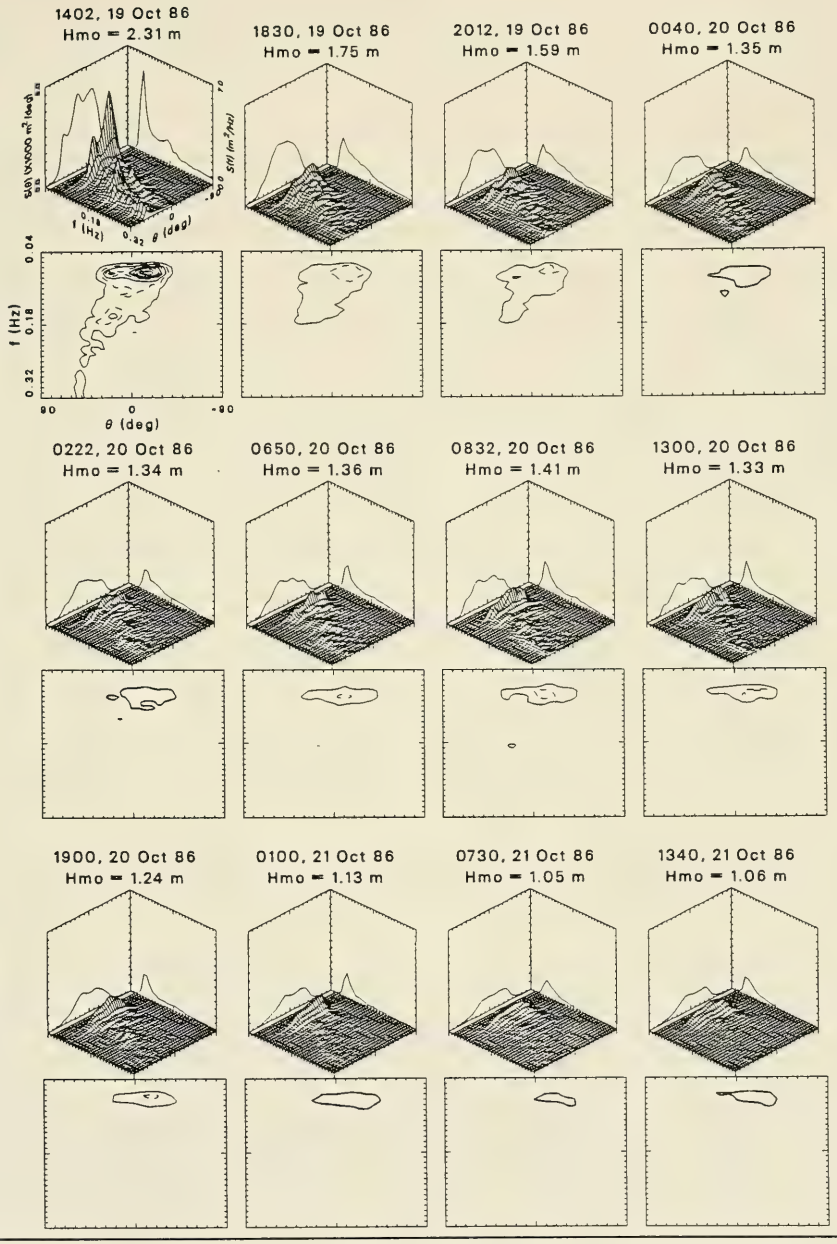

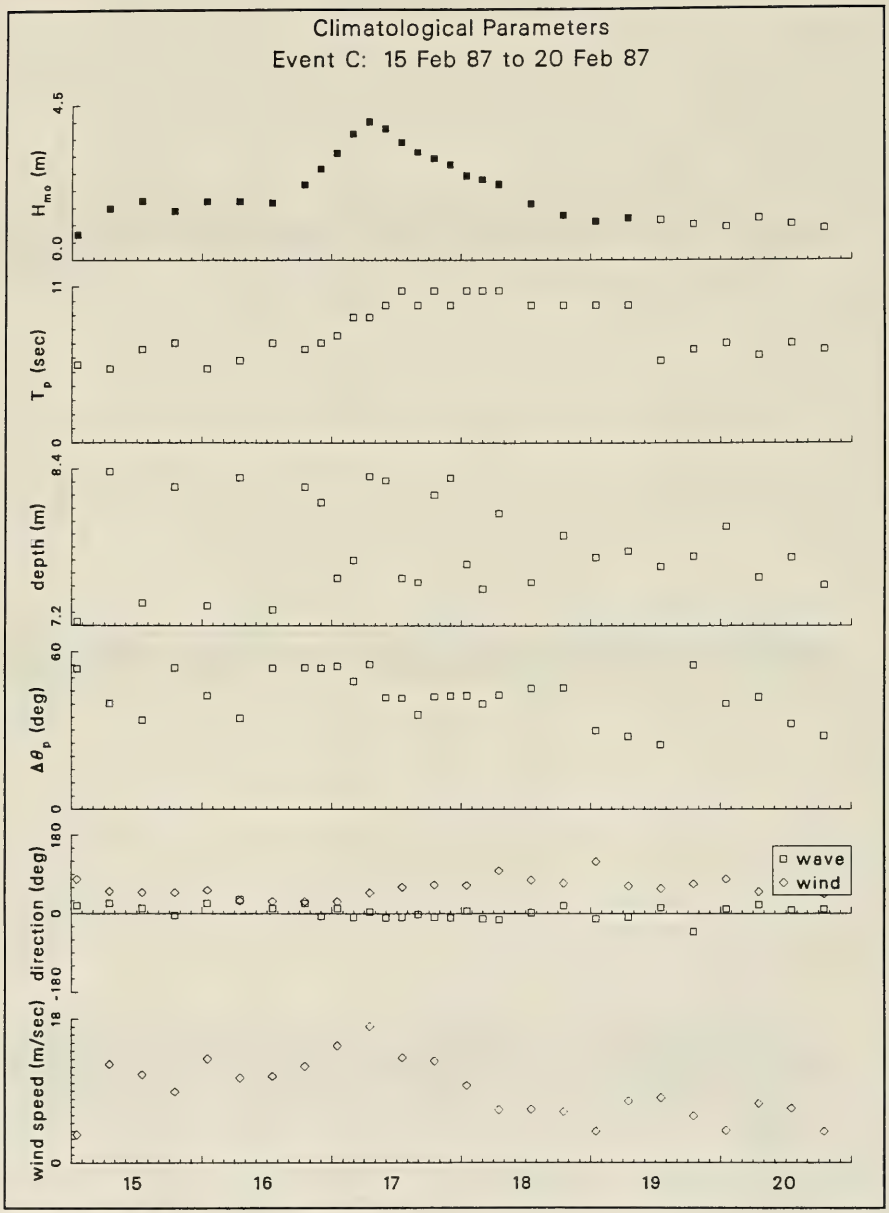
Climatological Parameters
Event C: 15 Feb 87 to 20 Feb 87
H_{mo} (m)
4.5
0.0
T_p (sec)
11
0
depth (m)
8.4 0
7.2
$\Delta\theta_p$ (deg)
60
0
direction (deg)
180
0
-180
wave
wind
wind speed (m/sec)
18
0
15
16
17
18
19
20

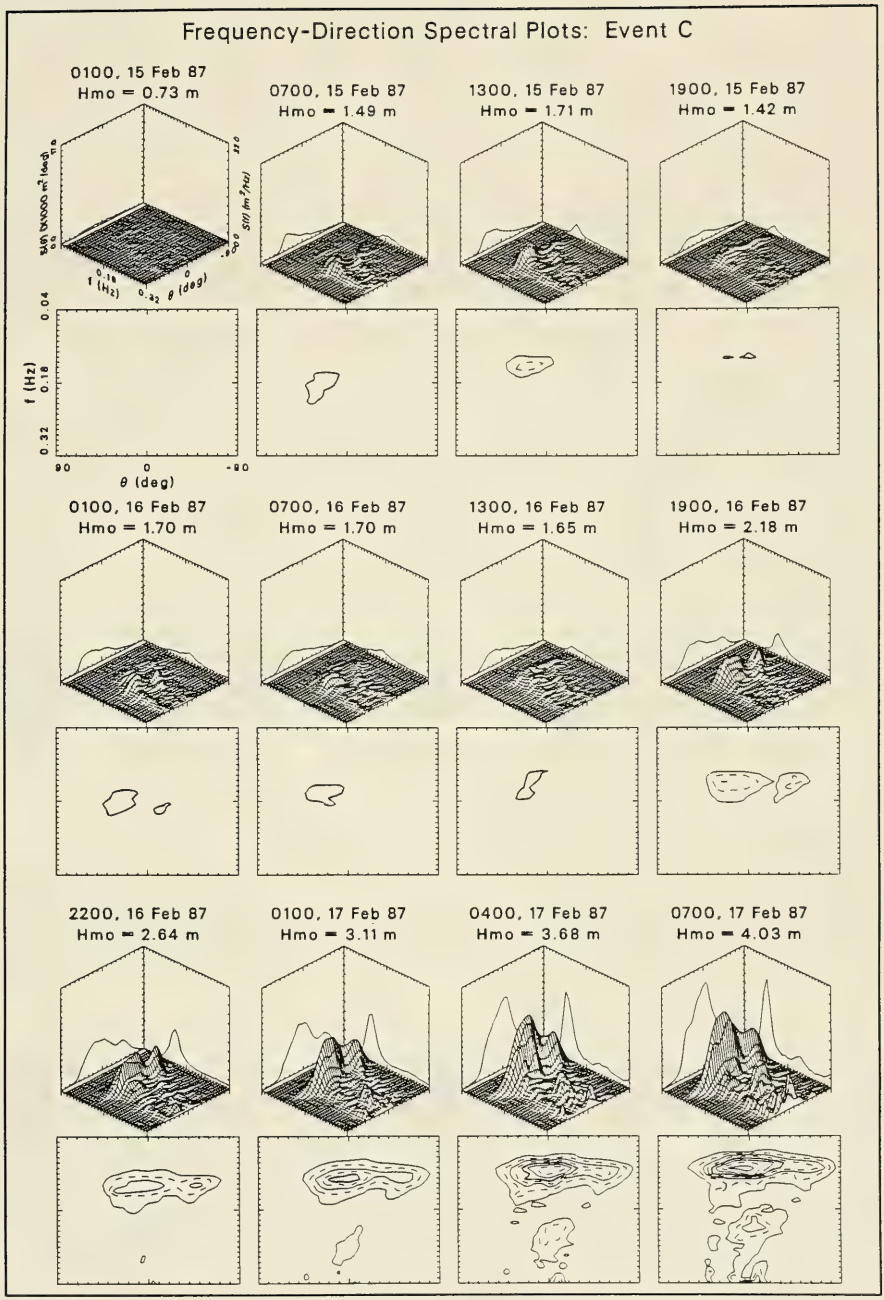
Frequency-Direction Spectral Plots: Event C
0100, 15 Feb 87
Hmo = 0.73 m
0700, 15 Feb 87
Hmo = 1.49 m
1300, 15 Feb 87
Hmo = 1.71 m
1900, 15 Feb 87
Hmo = 1.42 m
f (Hz)
θ (deg)
0100, 16 Feb 87
Hmo = 1.70 m
0700, 16 Feb 87
Hmo = 1.70 m
1300, 16 Feb 87
Hmo = 1.65 m
1900, 16 Feb 87
Hmo = 2.18 m
2200, 16 Feb 87
Hmo = 2.64 m
0100, 17 Feb 87
Hmo = 3.11 m
0400, 17 Feb 87
Hmo = 3.68 m
0700, 17 Feb 87
Hmo = 4.03 m

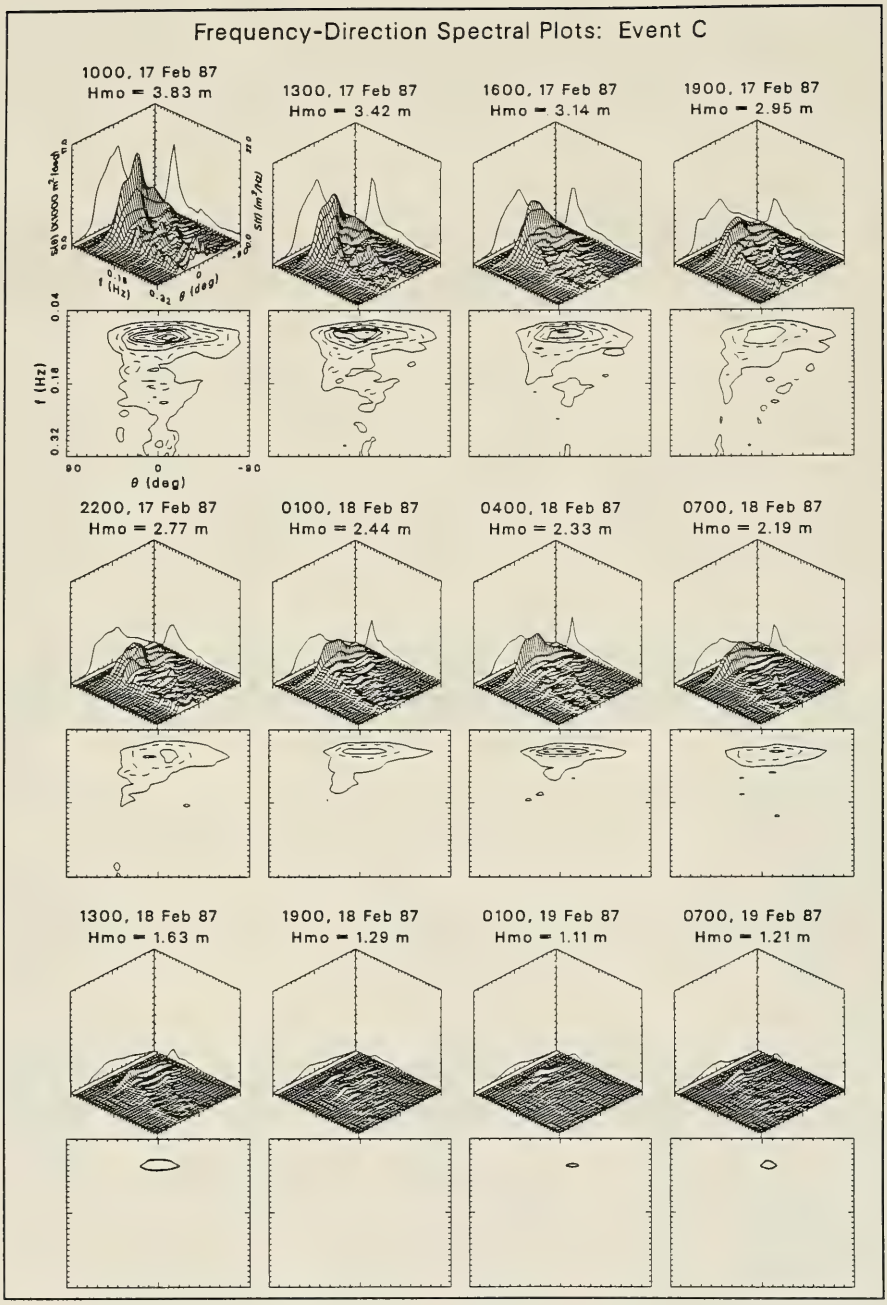
Frequency-Direction Spectral Plots: Event C
1000, 17 Feb 87
Hmo = 3.83 m
1300, 17 Feb 87
Hmo = 3.42 m
1600, 17 Feb 87
Hmo = 3.14 m
1900, 17 Feb 87
Hmo = 2.95 m
2200, 17 Feb 87
Hmo = 2.77 m
0100, 18 Feb 87
Hmo = 2.44 m
0400, 18 Feb 87
Hmo = 2.33 m
0700, 18 Feb 87
Hmo = 2.19 m
1300, 18 Feb 87
Hmo = 1.63 m
1900, 18 Feb 87
Hmo = 1.29 m
0100, 19 Feb 87
Hmo = 1.11 m
0700, 19 Feb 87
Hmo = 1.21 m
f (Hz)
θ (deg)

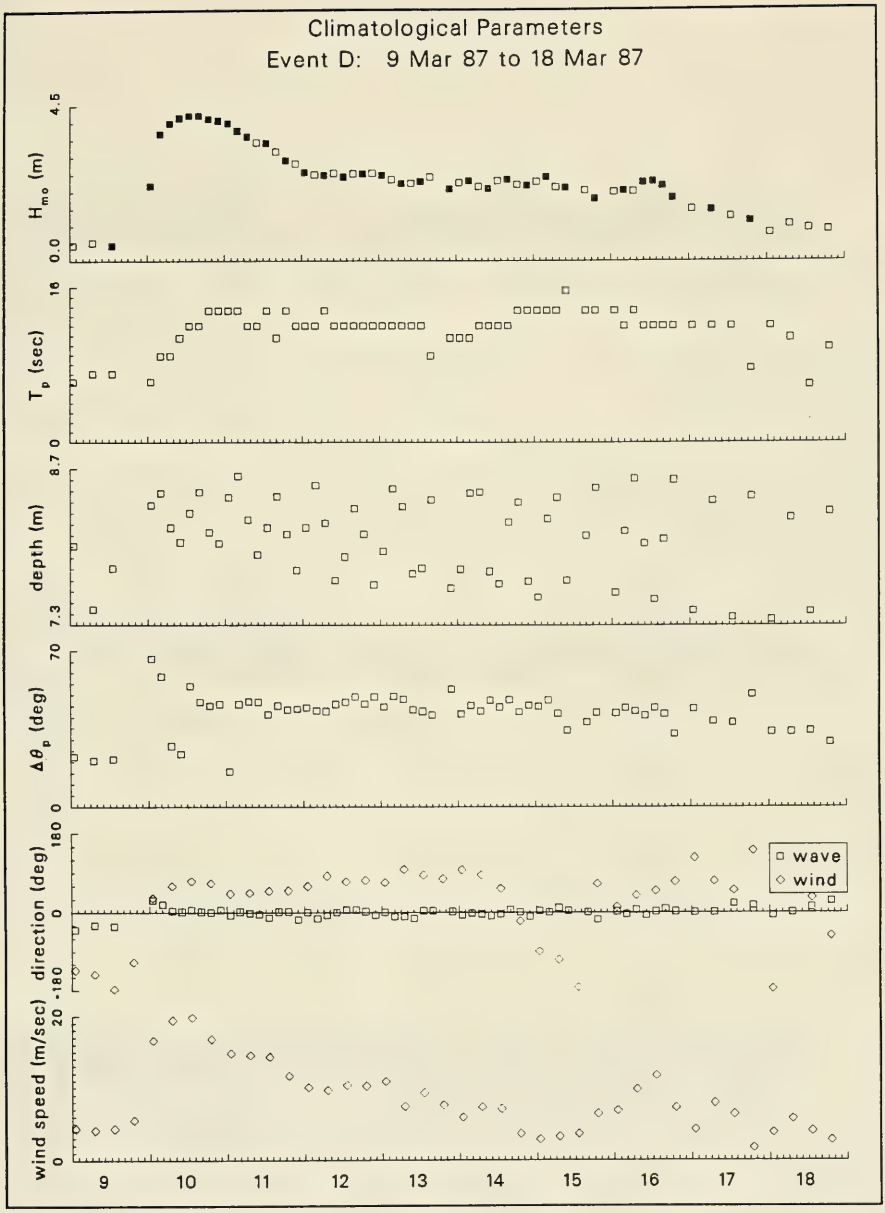
Climatological Parameters
Event D: 9 Mar 87 to 18 Mar 87
H_{mo} (m)
4.5
0.0
T_p (sec)
16
0
depth (m)
8.7
7.3
$\Delta\theta_p$ (deg)
70
0
wave direction (deg)
180
0
-180
wave
wind
wind speed (m/sec)
20
0
9
10
11
12
13
14
15
16
17
18

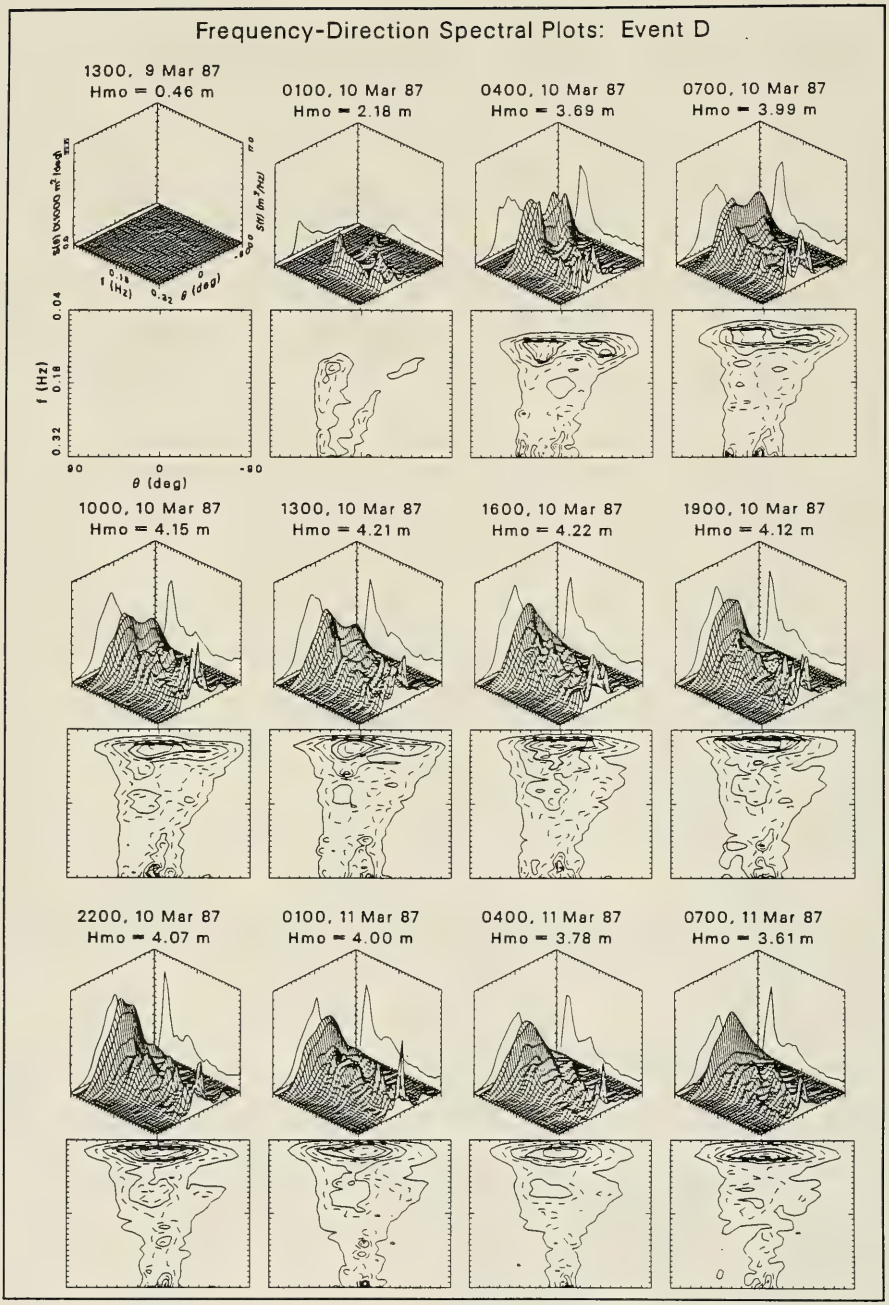
Frequency-Direction Spectral Plots: Event D
1300, 9 Mar 87
Hmo = 0.46 m
0100, 10 Mar 87
Hmo = 2.18 m
0400, 10 Mar 87
Hmo = 3.69 m
0700, 10 Mar 87
Hmo = 3.99 m
f (Hz)
θ (deg)
1000, 10 Mar 87
Hmo = 4.15 m
1300, 10 Mar 87
Hmo = 4.21 m
1600, 10 Mar 87
Hmo = 4.22 m
1900, 10 Mar 87
Hmo = 4.12 m
2200, 10 Mar 87
Hmo = 4.07 m
0100, 11 Mar 87
Hmo = 4.00 m
0400, 11 Mar 87
Hmo = 3.78 m
0700, 11 Mar 87
Hmo = 3.61 m

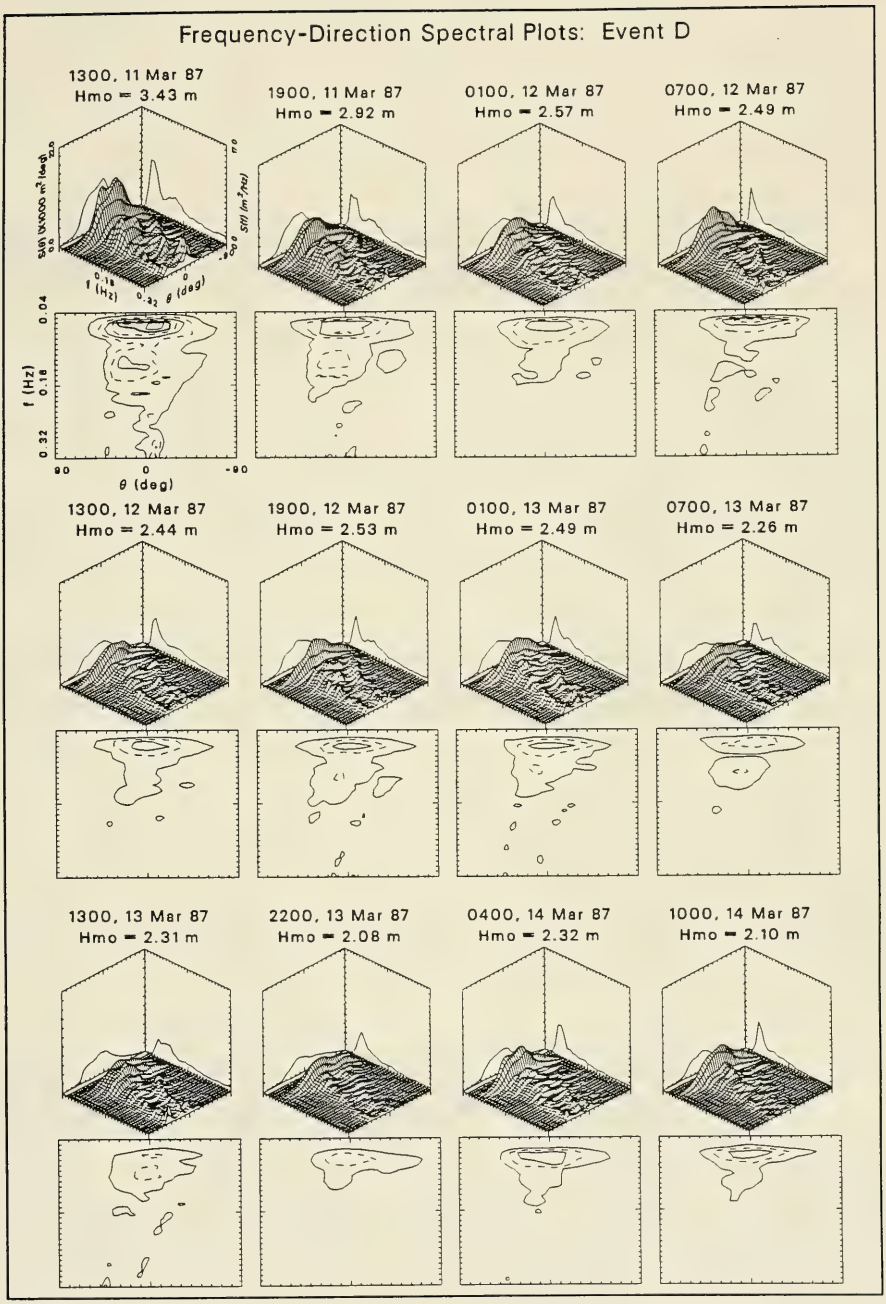
Frequency-Direction Spectral Plots: Event D
1300, 11 Mar 87
Hmo = 3.43 m
1900, 11 Mar 87
Hmo = 2.92 m
0100, 12 Mar 87
Hmo = 2.57 m
0700, 12 Mar 87
Hmo = 2.49 m
f (Hz)
0.04
0.18
0.32
90
0
-90
θ (deg)
1300, 12 Mar 87
Hmo = 2.44 m
1900, 12 Mar 87
Hmo = 2.53 m
0100, 13 Mar 87
Hmo = 2.49 m
0700, 13 Mar 87
Hmo = 2.26 m
1300, 13 Mar 87
Hmo = 2.31 m
2200, 13 Mar 87
Hmo = 2.08 m
0400, 14 Mar 87
Hmo = 2.32 m
1000, 14 Mar 87
Hmo = 2.10 m

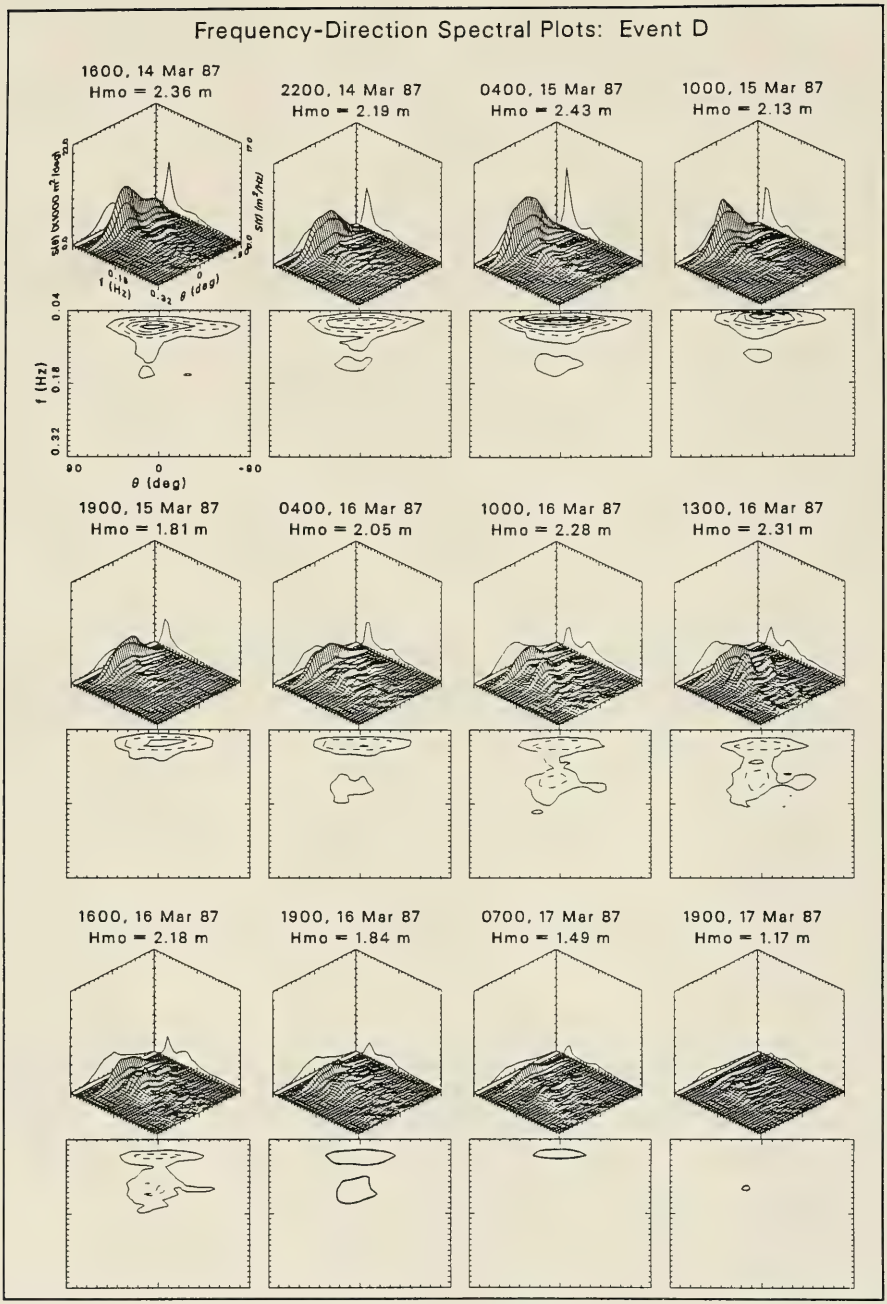
Frequency-Direction Spectral Plots: Event D
1600, 14 Mar 87
Hmo = 2.36 m
2200, 14 Mar 87
Hmo = 2.19 m
0400, 15 Mar 87
Hmo = 2.43 m
1000, 15 Mar 87
Hmo = 2.13 m
1900, 15 Mar 87
Hmo = 1.81 m
0400, 16 Mar 87
Hmo = 2.05 m
1000, 16 Mar 87
Hmo = 2.28 m
1300, 16 Mar 87
Hmo = 2.31 m
1600, 16 Mar 87
Hmo = 2.18 m
1900, 16 Mar 87
Hmo = 1.84 m
0700, 17 Mar 87
Hmo = 1.49 m
1900, 17 Mar 87
Hmo = 1.17 m
f (Hz)
0.04
0.18
0.32
90
0
-90
θ (deg)

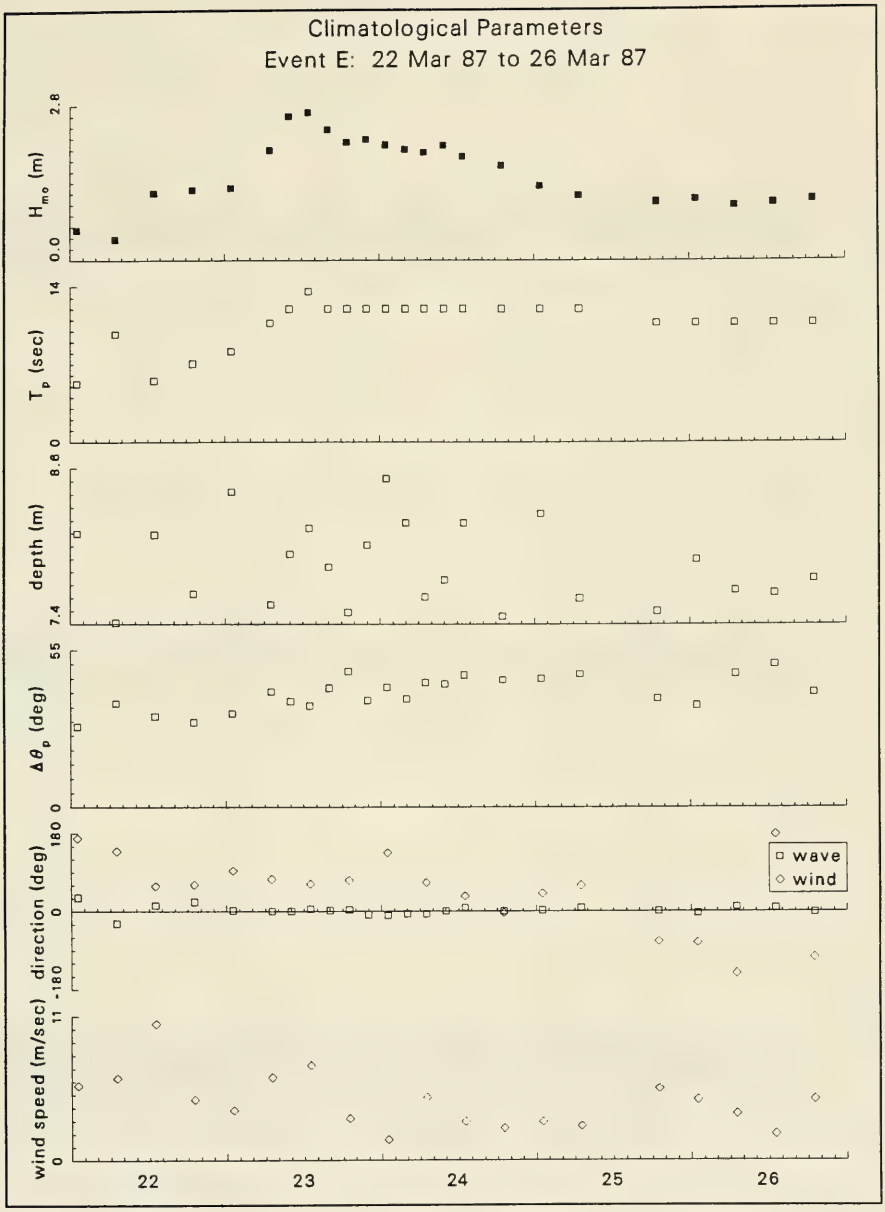
Climatological Parameters
Event E: 22 Mar 87 to 26 Mar 87
H_{mo} (m)
2.8
0.0
T_p (sec)
14
0
depth (m)
8.6
7.4
$\Delta\theta_p$ (deg)
55
0
direction (deg)
180
0
-180
wave
wind
wind speed (m/sec)
11
0
22
23
24
25
26

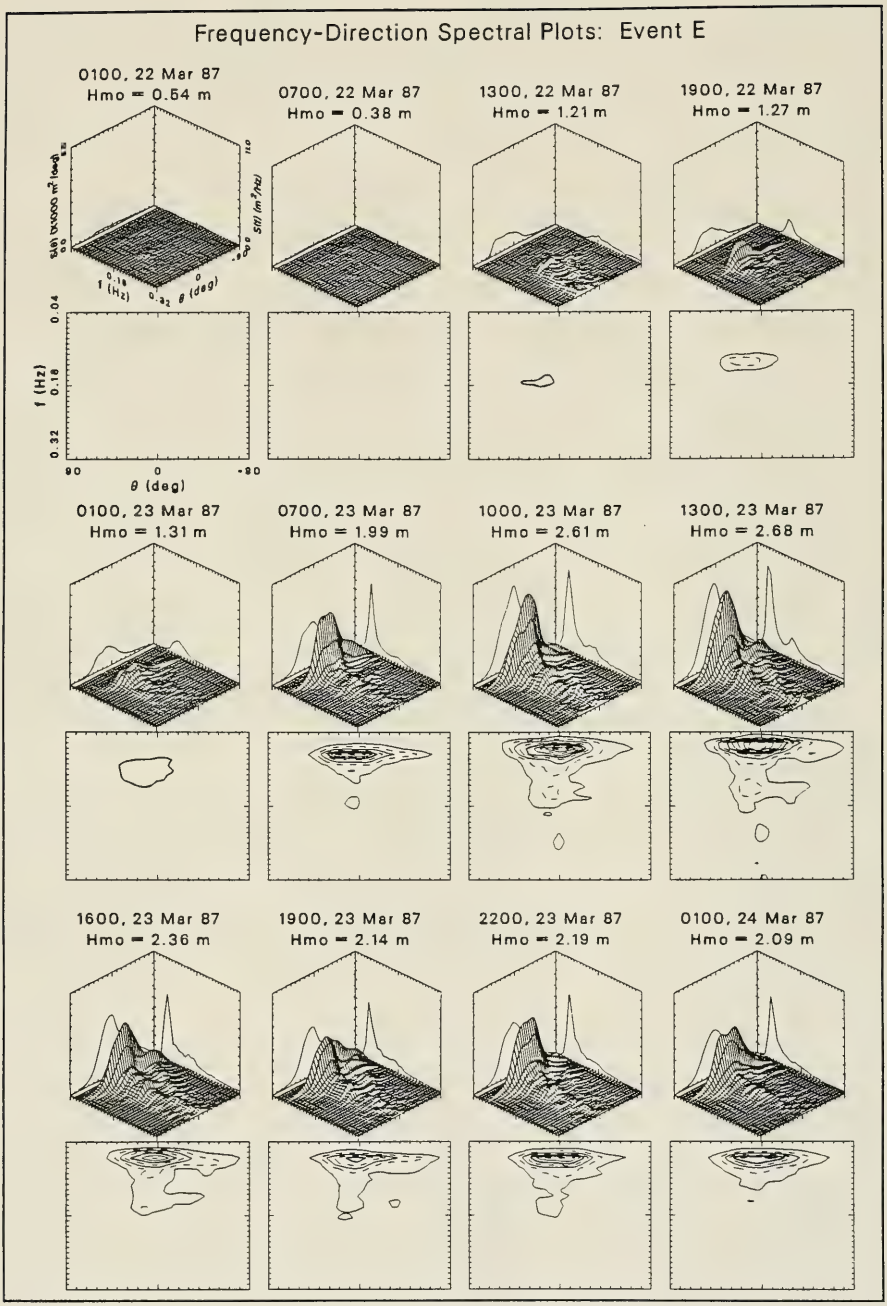
Frequency-Direction Spectral Plots: Event E
0100, 22 Mar 87
Hmo = 0.54 m
0700, 22 Mar 87
Hmo = 0.38 m
1300, 22 Mar 87
Hmo = 1.21 m
1900, 22 Mar 87
Hmo = 1.27 m
f (Hz)
0.04
0.18
0.32
90
0
-90
θ (deg)
0100, 23 Mar 87
Hmo = 1.31 m
0700, 23 Mar 87
Hmo = 1.99 m
1000, 23 Mar 87
Hmo = 2.61 m
1300, 23 Mar 87
Hmo = 2.68 m
1600, 23 Mar 87
Hmo = 2.36 m
1900, 23 Mar 87
Hmo = 2.14 m
2200, 23 Mar 87
Hmo = 2.19 m
0100, 24 Mar 87
Hmo = 2.09 m

Frequency-Direction Spectral Plots: Event E

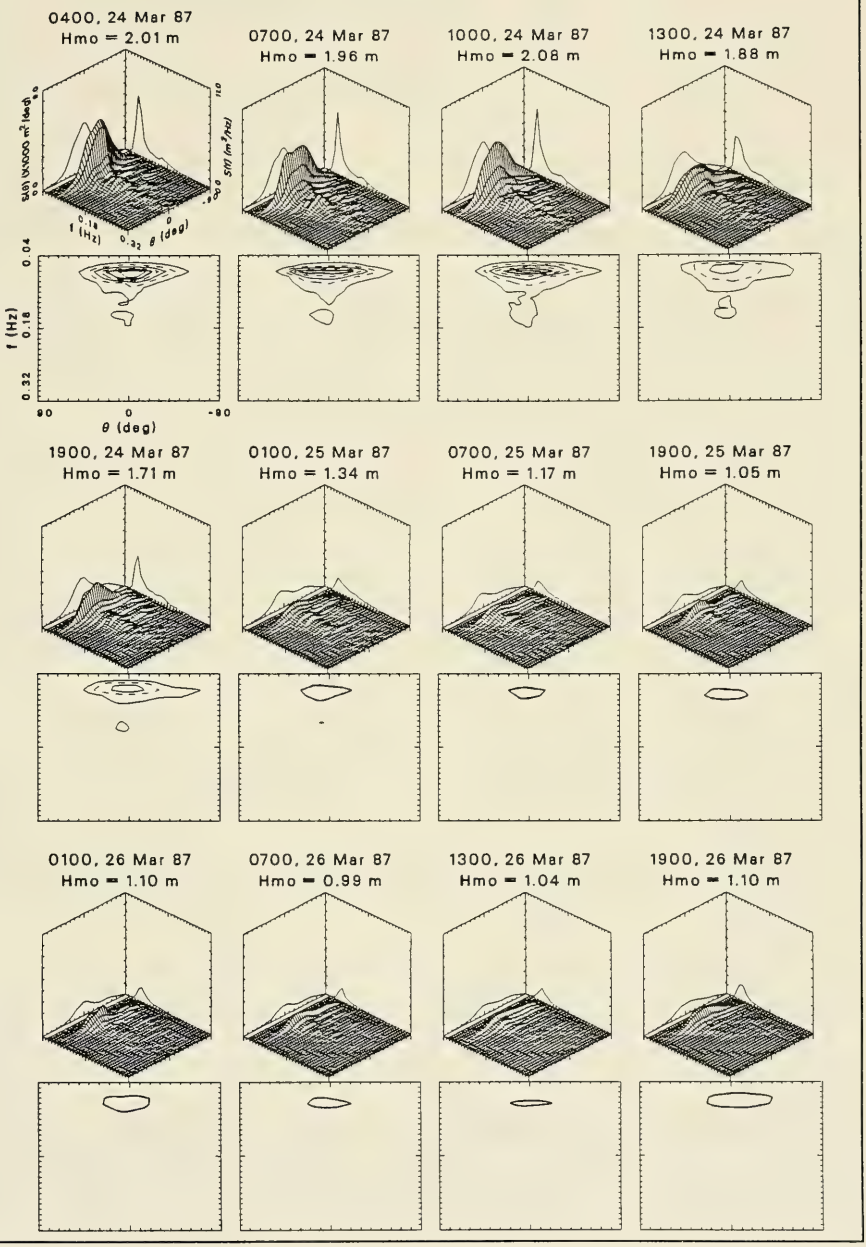

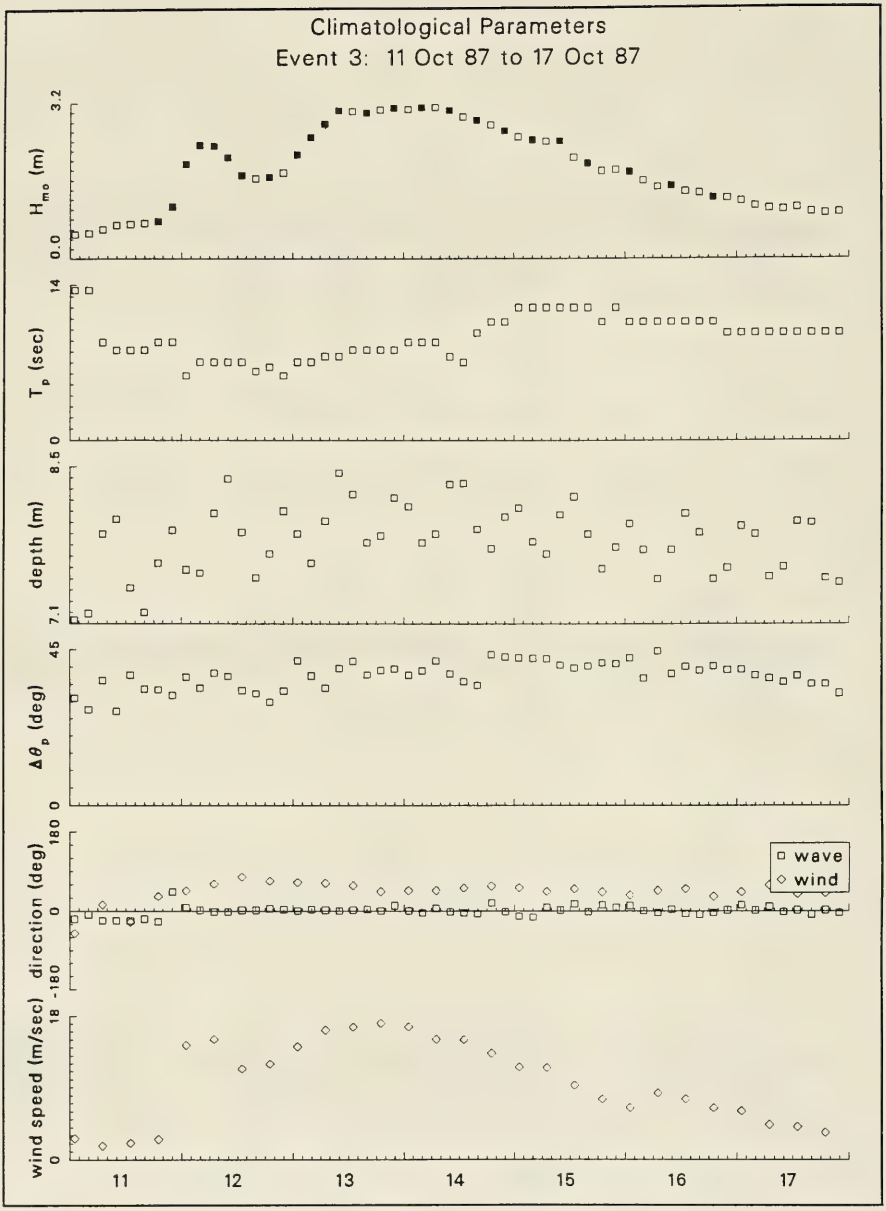
Climatological Parameters
Event 3: 11 Oct 87 to 17 Oct 87
H_{mo} (m)
3.2
0.0
T_p (sec)
14
0
depth (m)
8.5
7.1
$\Delta\theta_p$ (deg)
45
0
direction (deg)
180
0
-180
wave
wind
wind speed (m/sec)
18
0
11
12
13
14
15
16
17

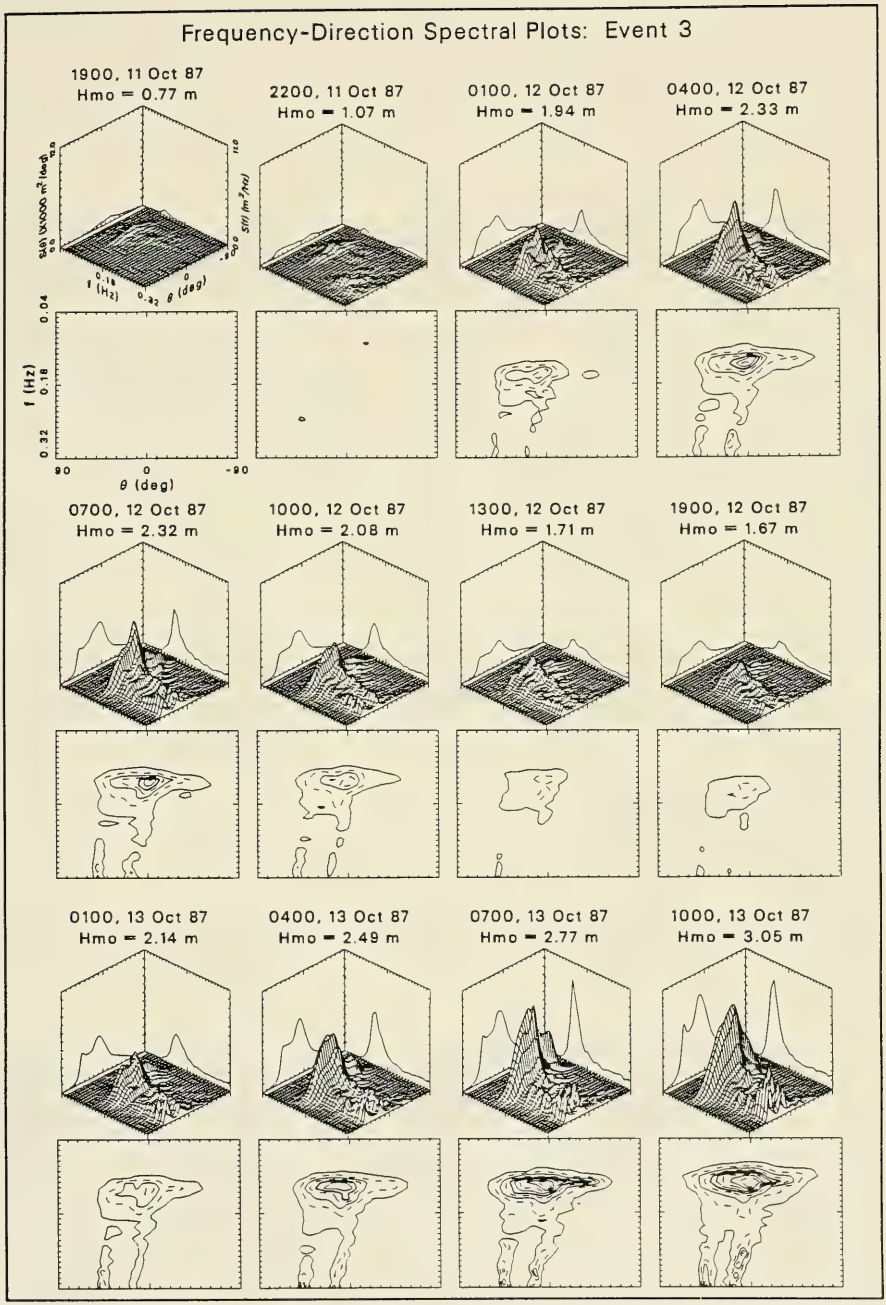
Frequency-Direction Spectral Plots: Event 3
1900, 11 Oct 87
Hmo = 0.77 m
2200, 11 Oct 87
Hmo = 1.07 m
0100, 12 Oct 87
Hmo = 1.94 m
0400, 12 Oct 87
Hmo = 2.33 m
f (Hz)
θ (deg)
0700, 12 Oct 87
Hmo = 2.32 m
1000, 12 Oct 87
Hmo = 2.08 m
1300, 12 Oct 87
Hmo = 1.71 m
1900, 12 Oct 87
Hmo = 1.67 m
0100, 13 Oct 87
Hmo = 2.14 m
0400, 13 Oct 87
Hmo = 2.49 m
0700, 13 Oct 87
Hmo = 2.77 m
1000, 13 Oct 87
Hmo = 3.05 m

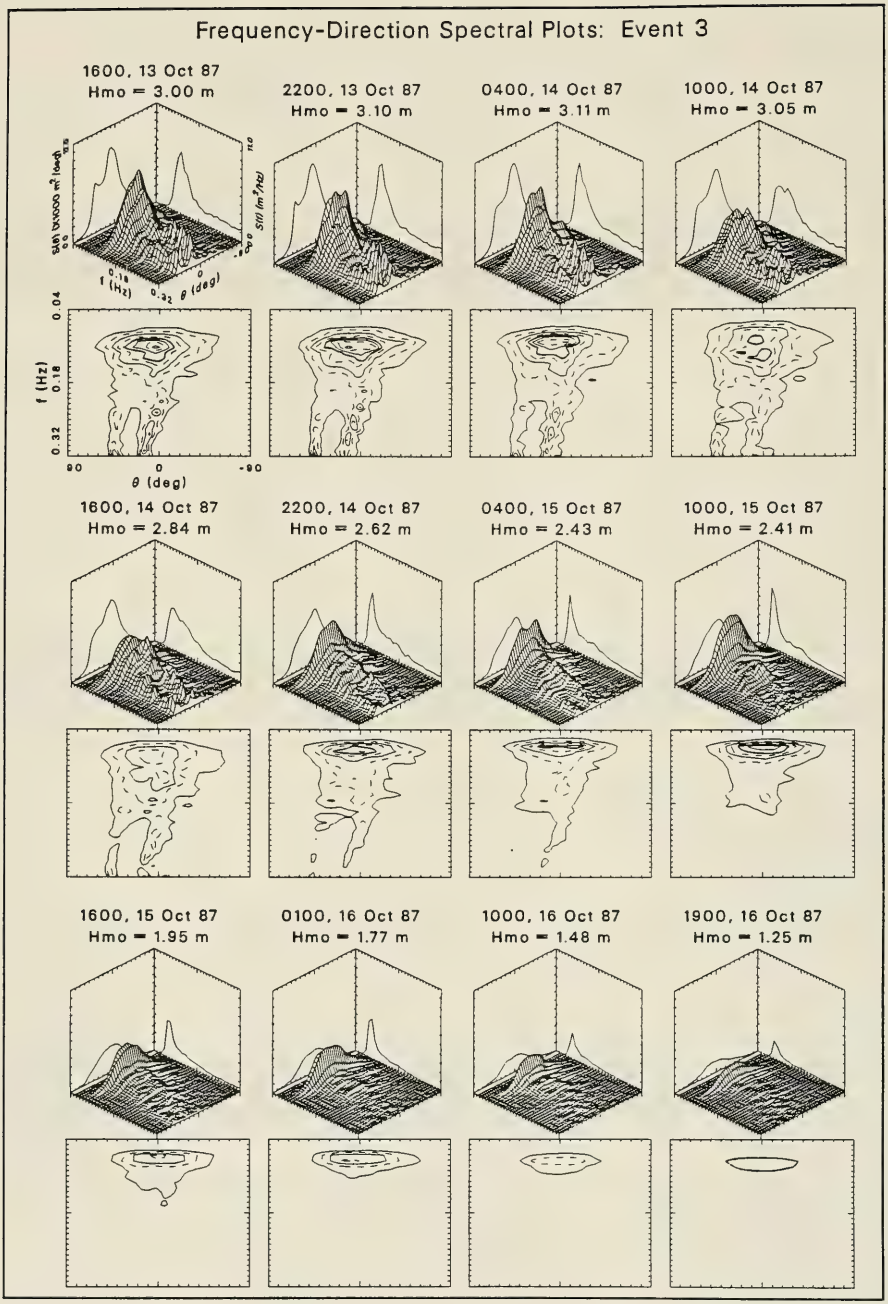
Frequency-Direction Spectral Plots: Event 3
1600, 13 Oct 87
Hmo = 3.00 m
2200, 13 Oct 87
Hmo = 3.10 m
0400, 14 Oct 87
Hmo = 3.11 m
1000, 14 Oct 87
Hmo = 3.05 m
f (Hz)
0.04
0.18
0.32
90
0
-90
θ (deg)
1600, 14 Oct 87
Hmo = 2.84 m
2200, 14 Oct 87
Hmo = 2.62 m
0400, 15 Oct 87
Hmo = 2.43 m
1000, 15 Oct 87
Hmo = 2.41 m
1600, 15 Oct 87
Hmo = 1.95 m
0100, 16 Oct 87
Hmo = 1.77 m
1000, 16 Oct 87
Hmo = 1.48 m
1900, 16 Oct 87
Hmo = 1.25 m

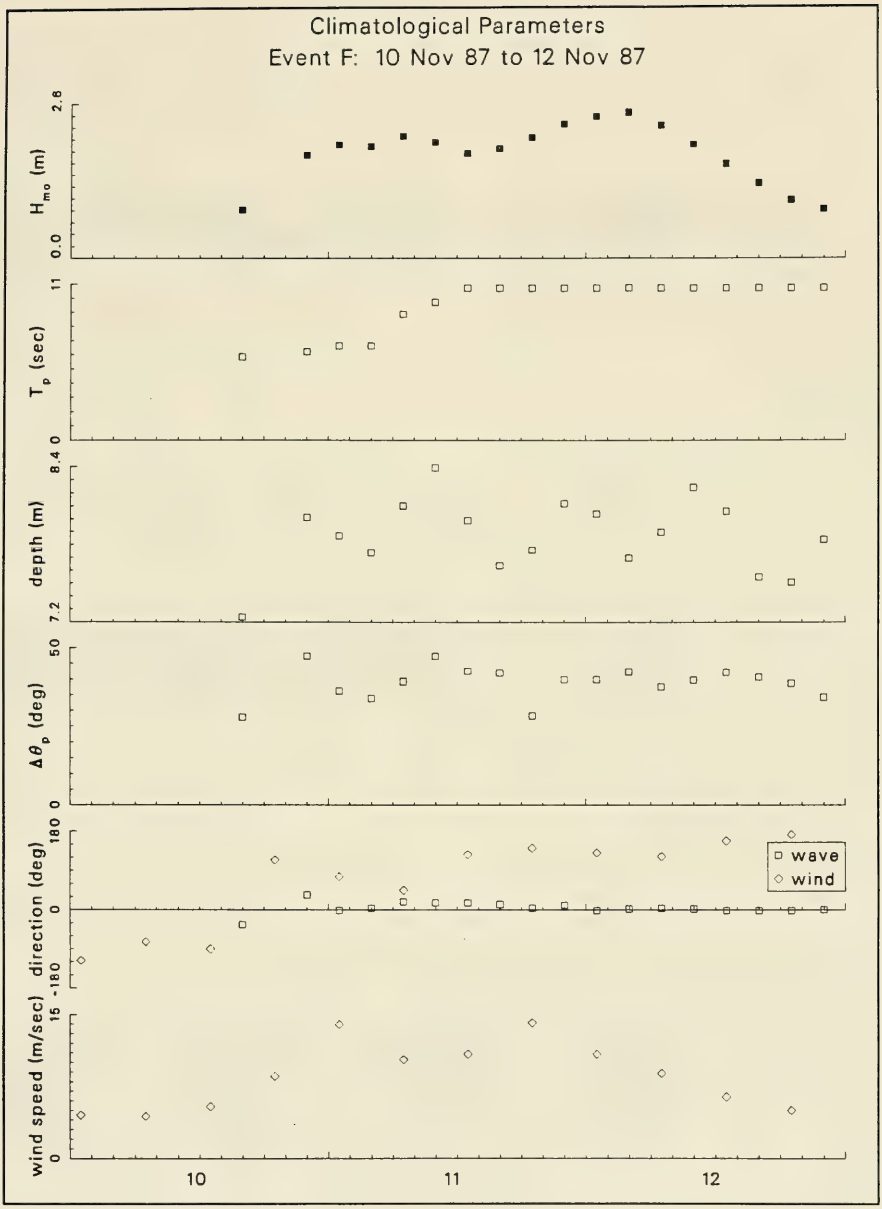
Climatological Parameters
Event F: 10 Nov 87 to 12 Nov 87
H_{mo} (m)
2.8
0.0
T_p (sec)
11
0
depth (m)
8.4
7.2
$\Delta\theta_p$ (deg)
50
0
direction (deg)
180
0
-180
wave
wind
wind speed (m/sec)
15
0
10
11
12

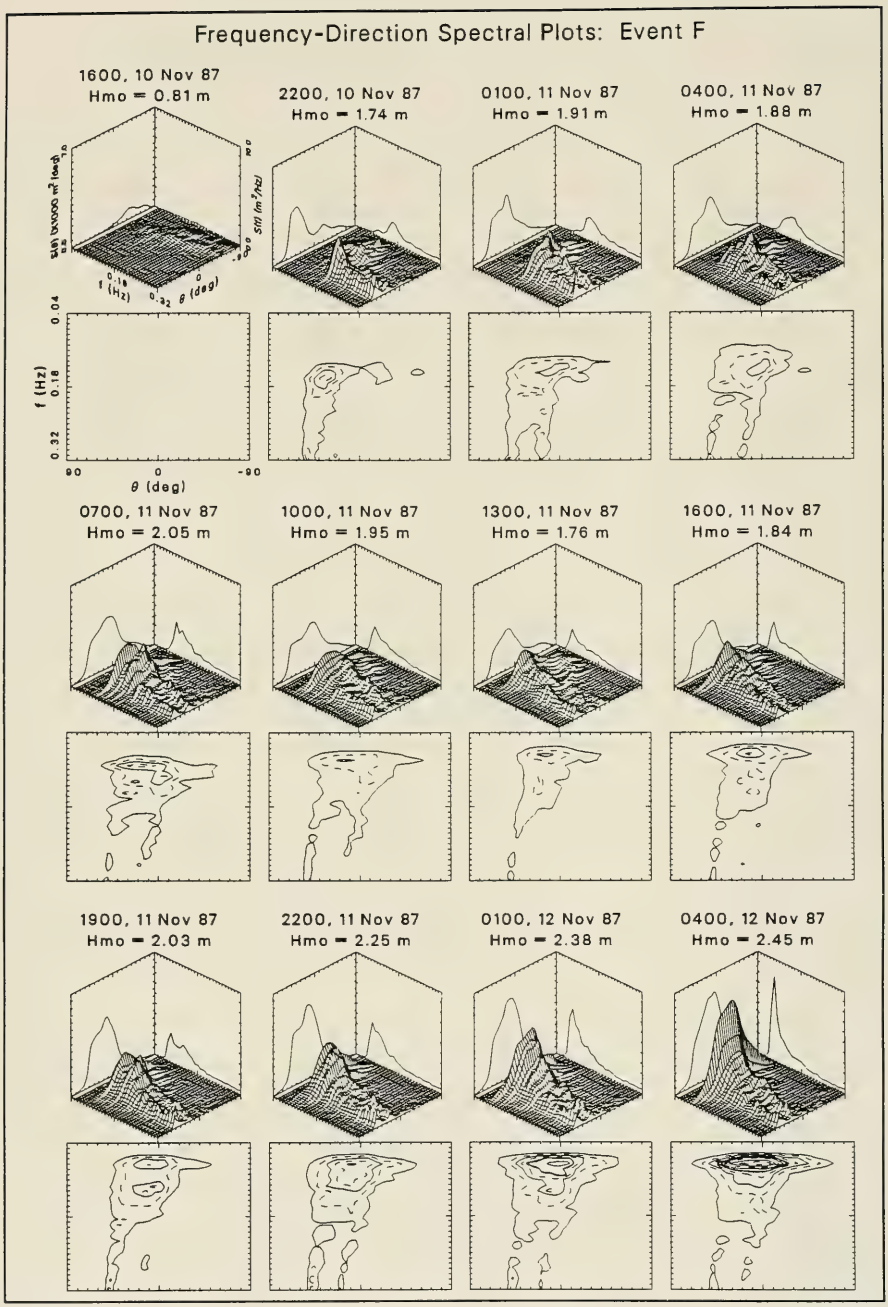
Frequency-Direction Spectral Plots: Event F
1600, 10 Nov 87
Hmo = 0.81 m
2200, 10 Nov 87
Hmo = 1.74 m
0100, 11 Nov 87
Hmo = 1.91 m
0400, 11 Nov 87
Hmo = 1.88 m
f (Hz)
θ (deg)
0700, 11 Nov 87
Hmo = 2.05 m
1000, 11 Nov 87
Hmo = 1.95 m
1300, 11 Nov 87
Hmo = 1.76 m
1600, 11 Nov 87
Hmo = 1.84 m
1900, 11 Nov 87
Hmo = 2.03 m
2200, 11 Nov 87
Hmo = 2.25 m
0100, 12 Nov 87
Hmo = 2.38 m
0400, 12 Nov 87
Hmo = 2.45 m

Frequency-Direction Spectral Plots: Event F

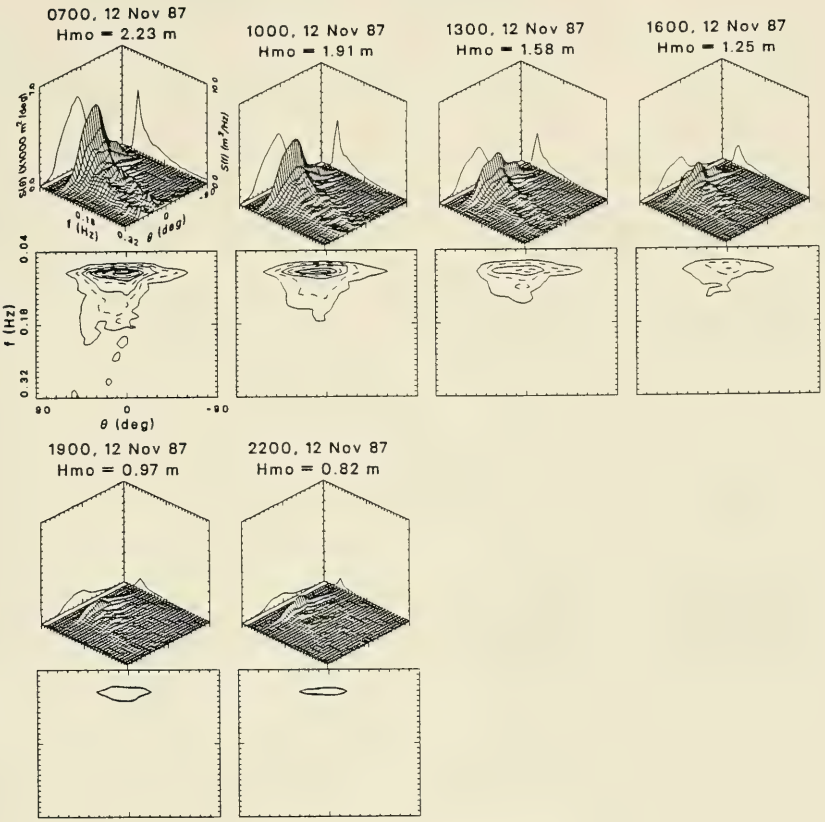

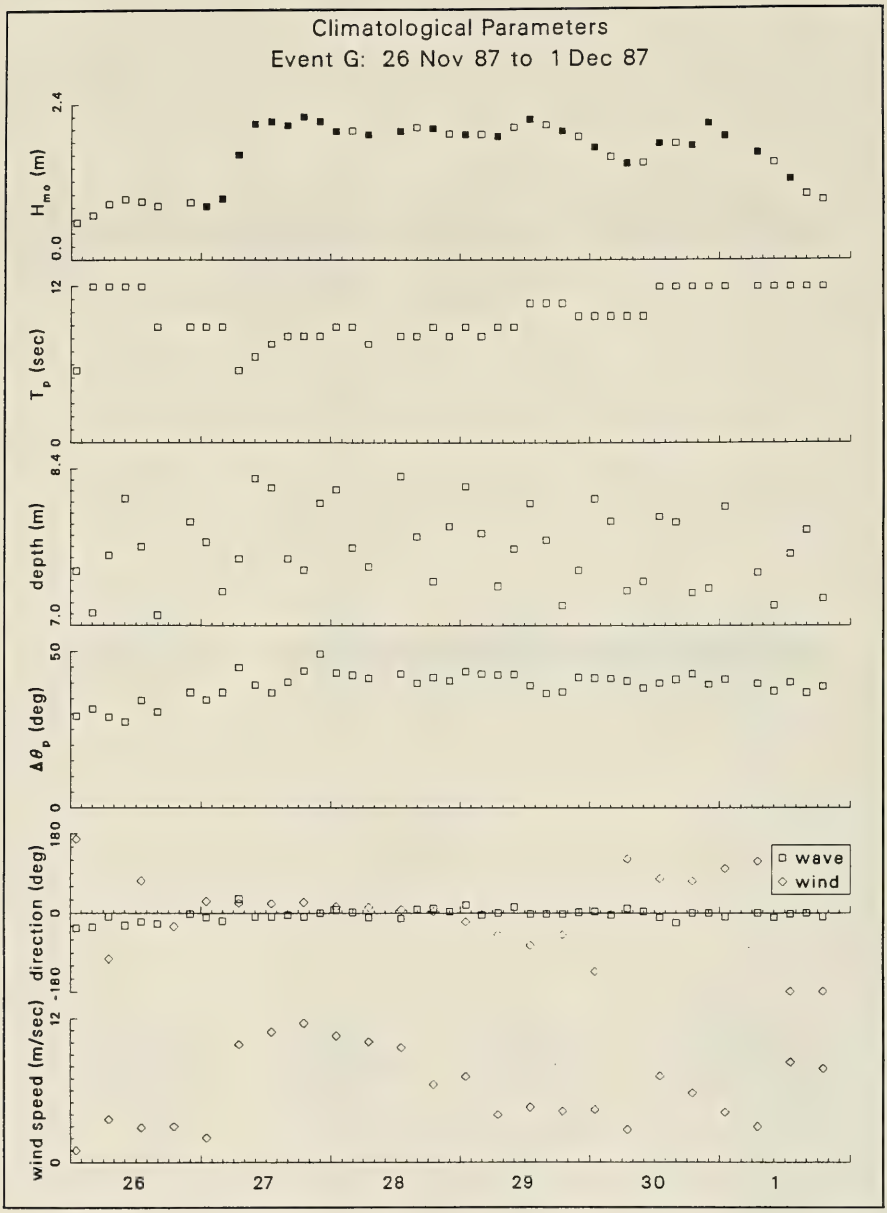
Climatological Parameters
Event G: 26 Nov 87 to 1 Dec 87
H_{mo} (m)
2.4
0.0
T_p (sec)
12
0
depth (m)
8.4
7.0
$\Delta\theta_p$ (deg)
50
0
direction (deg)
180
0
-180
wave
wind
wind speed (m/sec)
12
0
26
27
28
29
30
1

Frequency-Direction Spectral Plots: Event G

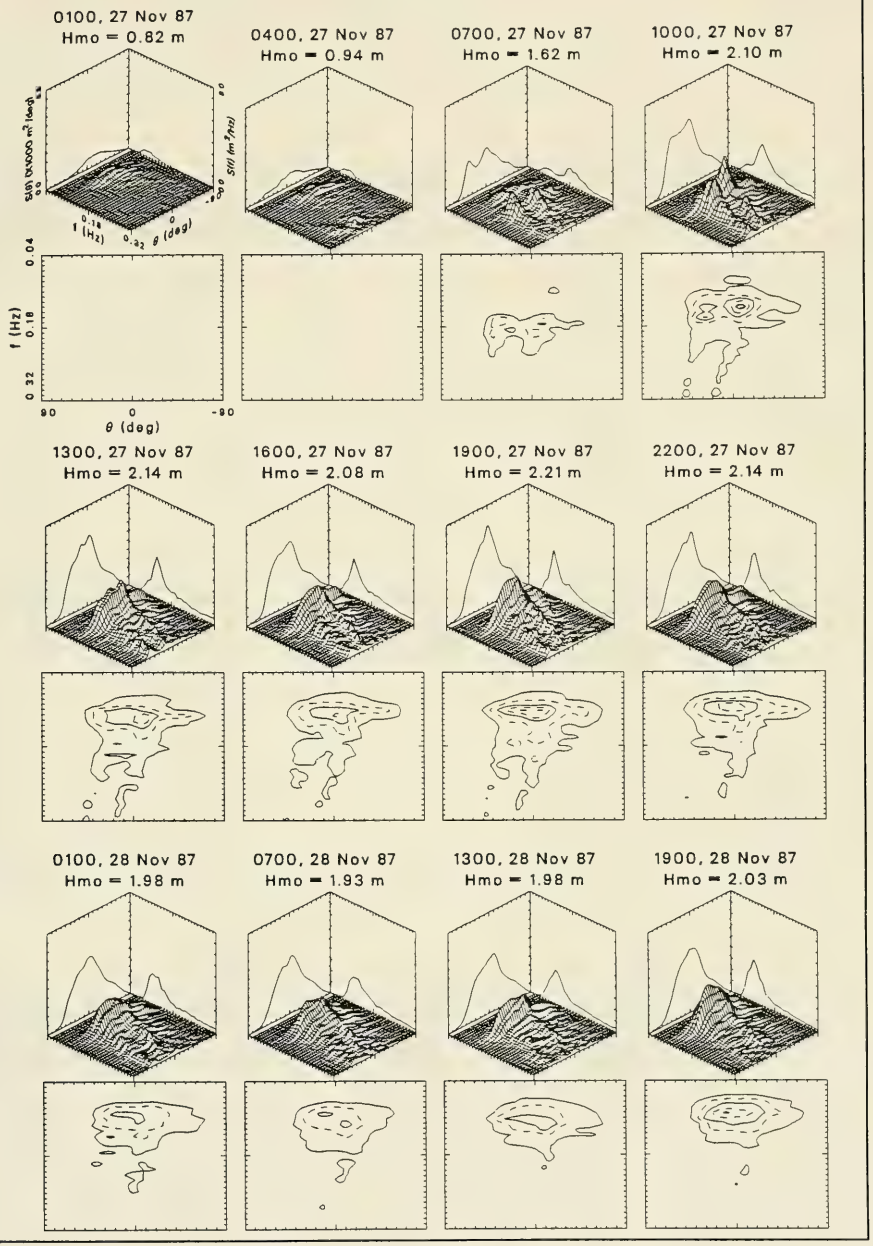

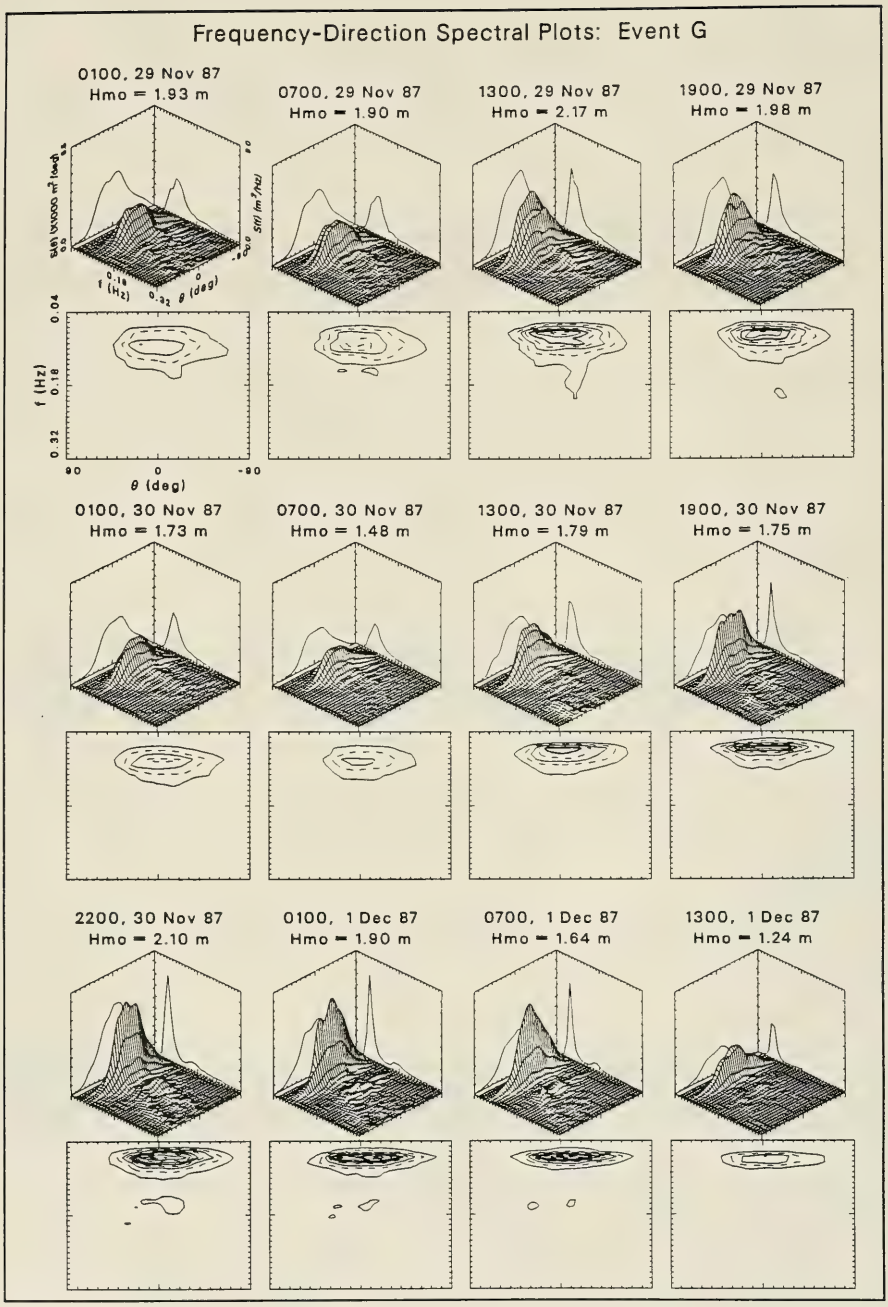
Frequency-Direction Spectral Plots: Event G
0100, 29 Nov 87
Hmo = 1.93 m
0700, 29 Nov 87
Hmo = 1.90 m
1300, 29 Nov 87
Hmo = 2.17 m
1900, 29 Nov 87
Hmo = 1.98 m
f (Hz)
0.04
0.18
0.32
90
0
-90
θ (deg)
0100, 30 Nov 87
Hmo = 1.73 m
0700, 30 Nov 87
Hmo = 1.48 m
1300, 30 Nov 87
Hmo = 1.79 m
1900, 30 Nov 87
Hmo = 1.75 m
2200, 30 Nov 87
Hmo = 2.10 m
0100, 1 Dec 87
Hmo = 1.90 m
0700, 1 Dec 87
Hmo = 1.64 m
1300, 1 Dec 87
Hmo = 1.24 m

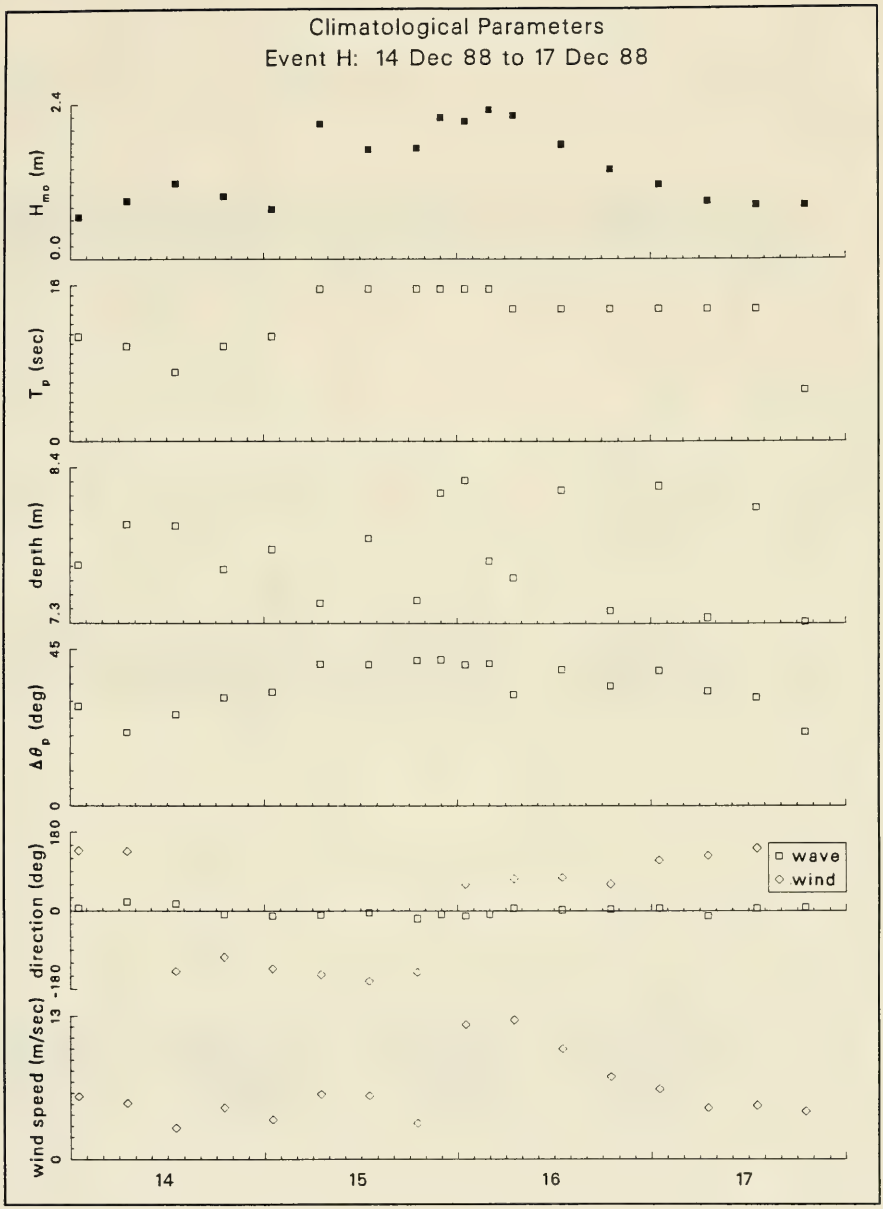
Climatological Parameters
Event H: 14 Dec 88 to 17 Dec 88
H_{mo} (m)
2.4
0.0
T_p (sec)
16
0
depth (m)
8.4
7.3
$\Delta\theta_p$ (deg)
45
0
direction (deg)
180
0
-180
wave
wind
wind speed (m/sec)
13
0
14
15
16
17

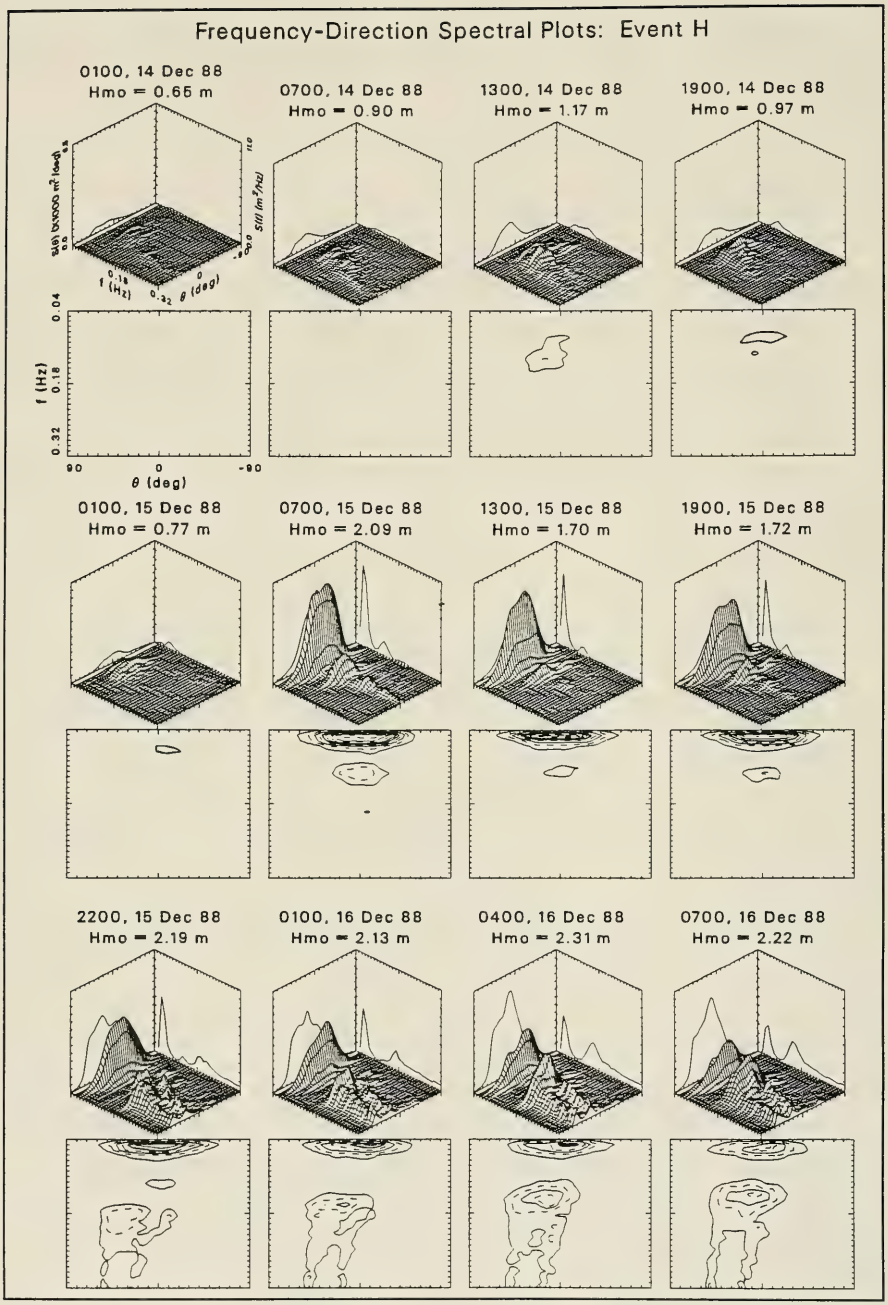
Frequency-Direction Spectral Plots: Event H
0100, 14 Dec 88
Hmo = 0.65 m
0700, 14 Dec 88
Hmo = 0.90 m
1300, 14 Dec 88
Hmo = 1.17 m
1900, 14 Dec 88
Hmo = 0.97 m
f (Hz)
0.04
0.18
0.32
90
0
-90
θ (deg)
0100, 15 Dec 88
Hmo = 0.77 m
0700, 15 Dec 88
Hmo = 2.09 m
1300, 15 Dec 88
Hmo = 1.70 m
1900, 15 Dec 88
Hmo = 1.72 m
2200, 15 Dec 88
Hmo = 2.19 m
0100, 16 Dec 88
Hmo = 2.13 m
0400, 16 Dec 88
Hmo = 2.31 m
0700, 16 Dec 88
Hmo = 2.22 m

Frequency-Direction Spectral Plots: Event H

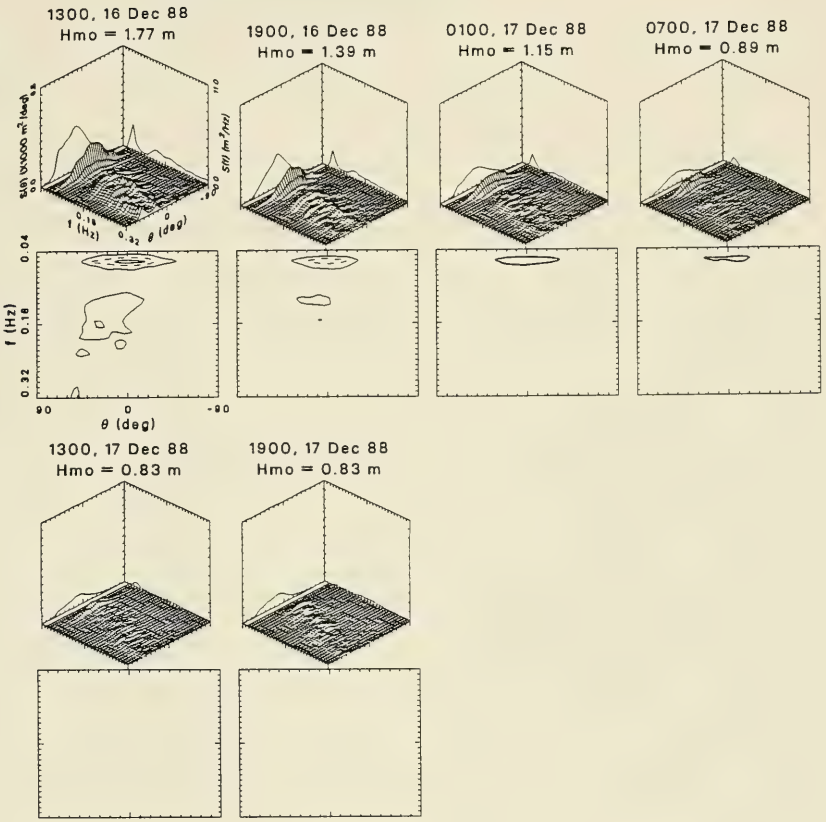

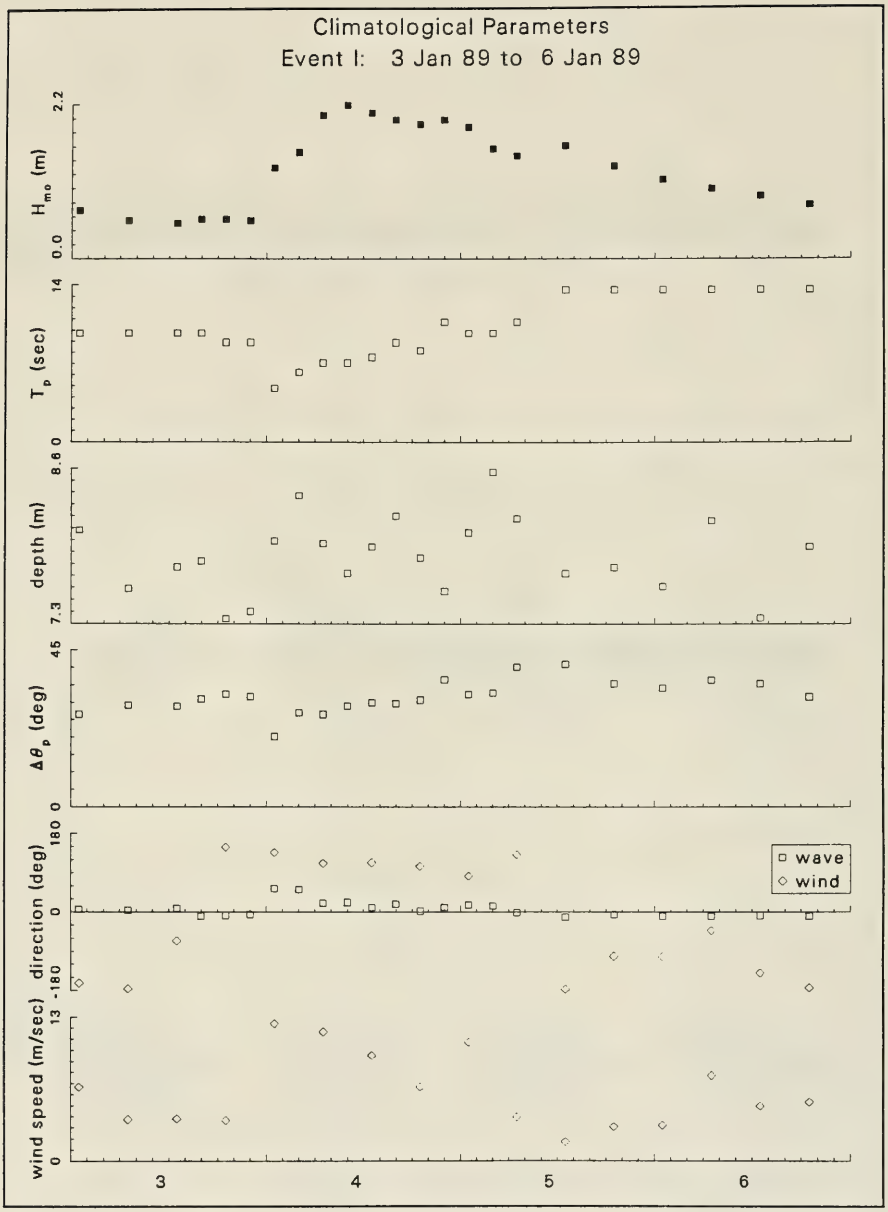
Climatological Parameters
Event I: 3 Jan 89 to 6 Jan 89
H_{mo} (m)
2.2
0.0
T_p (sec)
14
0
depth (m)
8.6
7.3
$\Delta\theta_p$ (deg)
45
0
direction (deg)
180
0
-180
wave
wind
wind speed (m/sec)
13
0
3
4
5
6

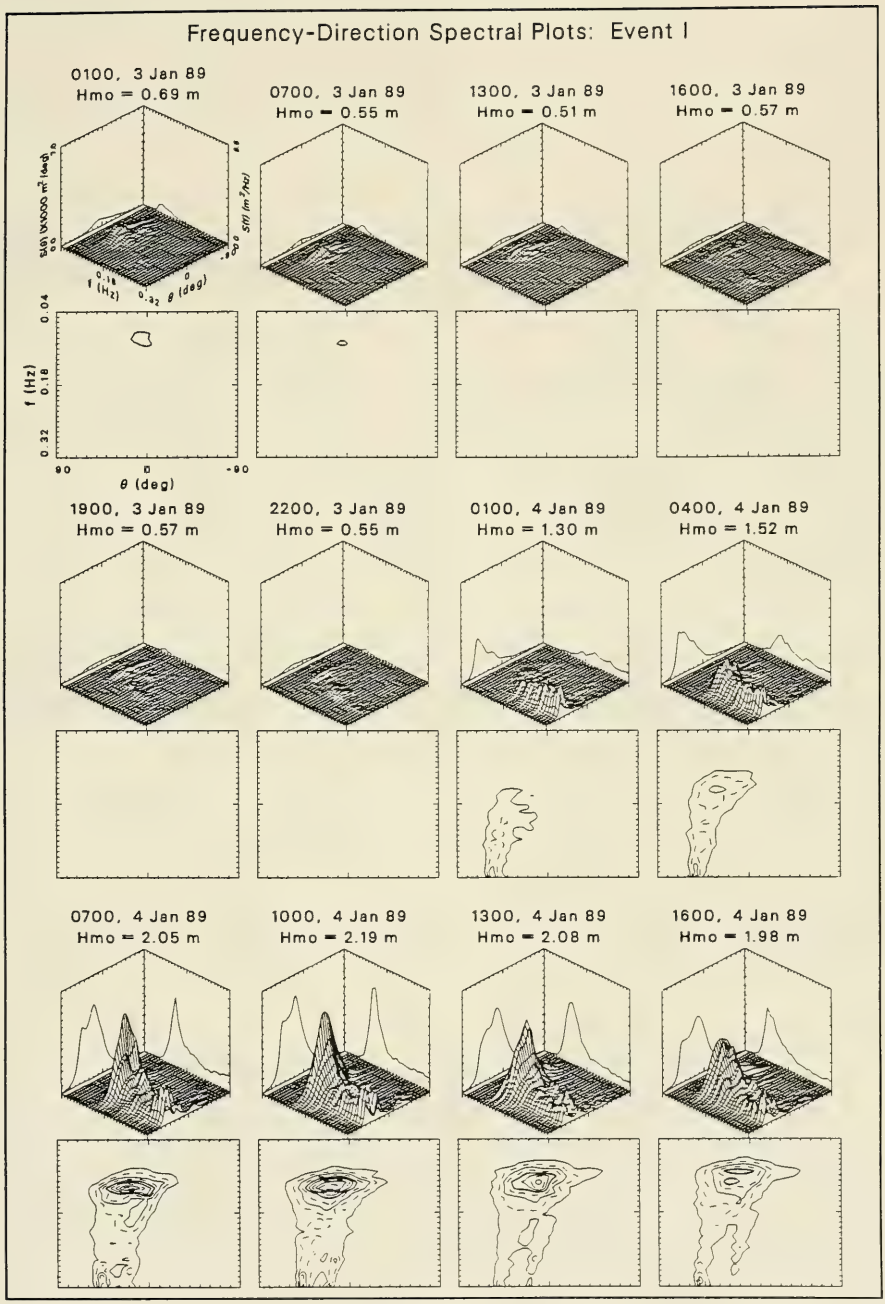
Frequency-Direction Spectral Plots: Event I
0100, 3 Jan 89
Hmo = 0.69 m
0700, 3 Jan 89
Hmo = 0.55 m
1300, 3 Jan 89
Hmo = 0.51 m
1600, 3 Jan 89
Hmo = 0.57 m
f (Hz)
θ (deg)
1900, 3 Jan 89
Hmo = 0.57 m
2200, 3 Jan 89
Hmo = 0.55 m
0100, 4 Jan 89
Hmo = 1.30 m
0400, 4 Jan 89
Hmo = 1.52 m
0700, 4 Jan 89
Hmo = 2.05 m
1000, 4 Jan 89
Hmo = 2.19 m
1300, 4 Jan 89
Hmo = 2.08 m
1600, 4 Jan 89
Hmo = 1.98 m

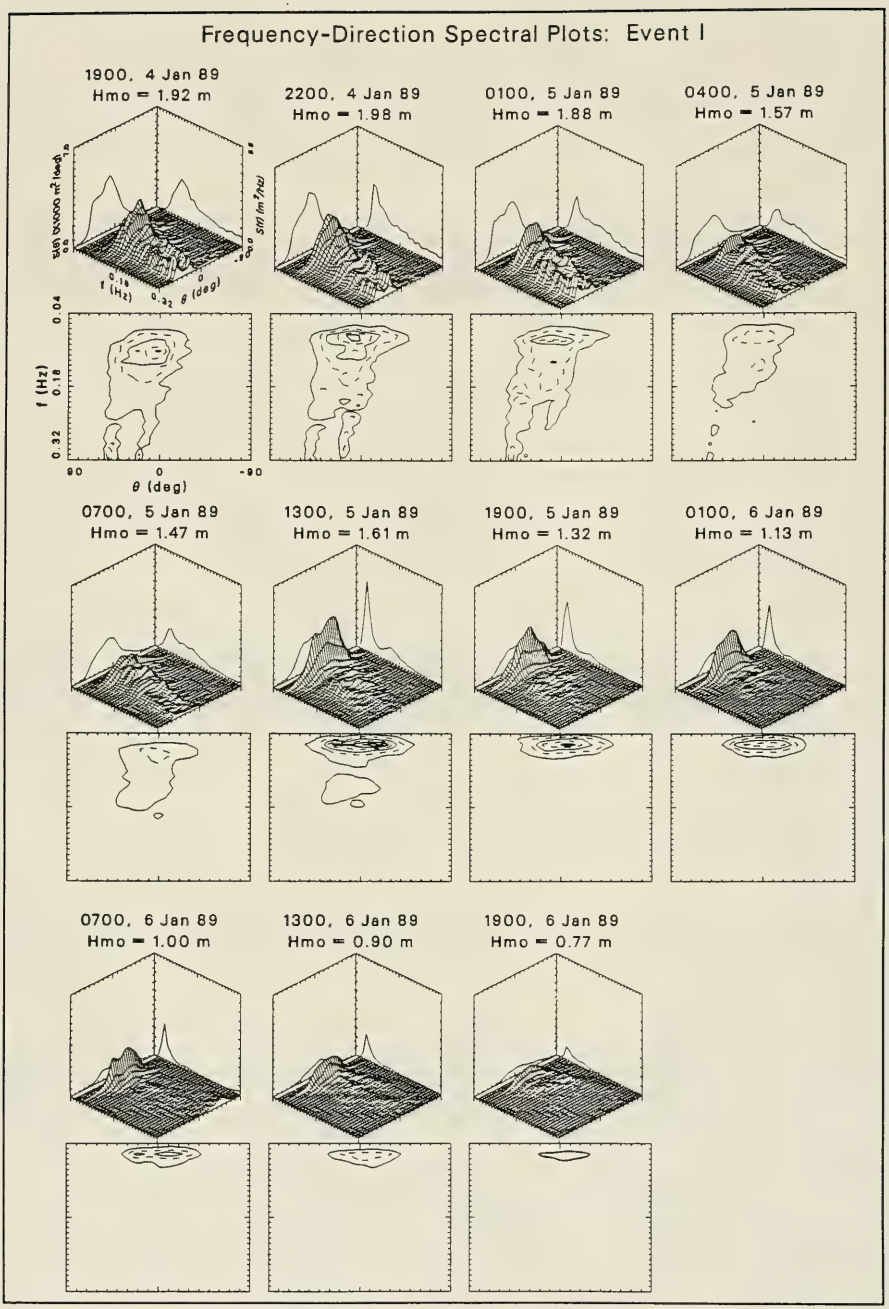
Frequency-Direction Spectral Plots: Event I
1900, 4 Jan 89
Hmo = 1.92 m
2200, 4 Jan 89
Hmo = 1.98 m
0100, 5 Jan 89
Hmo = 1.88 m
0400, 5 Jan 89
Hmo = 1.57 m
f (Hz)
0.04
0.16
0.32
θ (deg)
90
0
-90
0700, 5 Jan 89
Hmo = 1.47 m
1300, 5 Jan 89
Hmo = 1.61 m
1900, 5 Jan 89
Hmo = 1.32 m
0100, 6 Jan 89
Hmo = 1.13 m
0700, 6 Jan 89
Hmo = 1.00 m
1300, 6 Jan 89
Hmo = 0.90 m
1900, 6 Jan 89
Hmo = 0.77 m

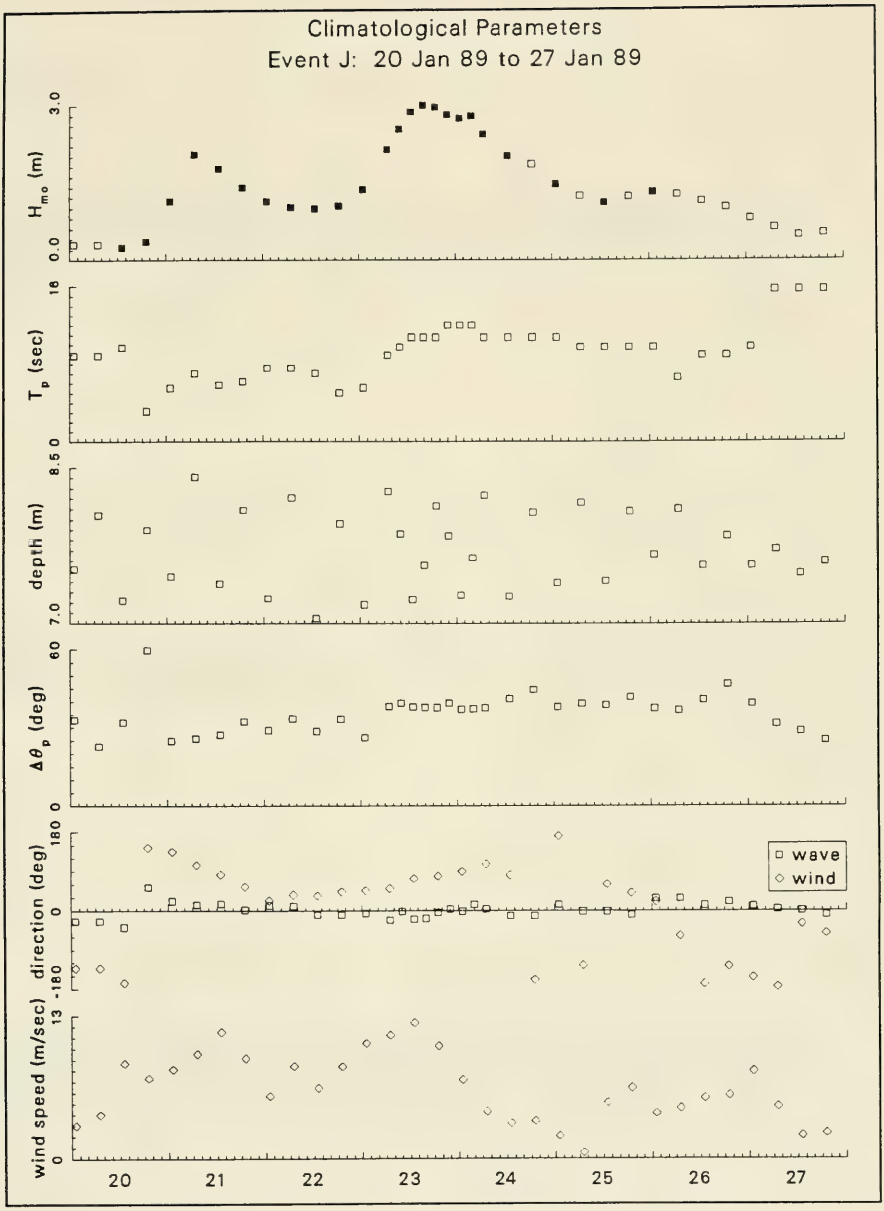
Climatological Parameters
Event J: 20 Jan 89 to 27 Jan 89
H_{mo} (m)
3.0
0.0
T_p (sec)
16
0
depth (m)
8.5
7.0
$\Delta\theta_p$ (deg)
60
0
direction (deg)
180
0
-180
wave
wind
wind speed (m/sec)
13
0
20
21
22
23
24
25
26
27

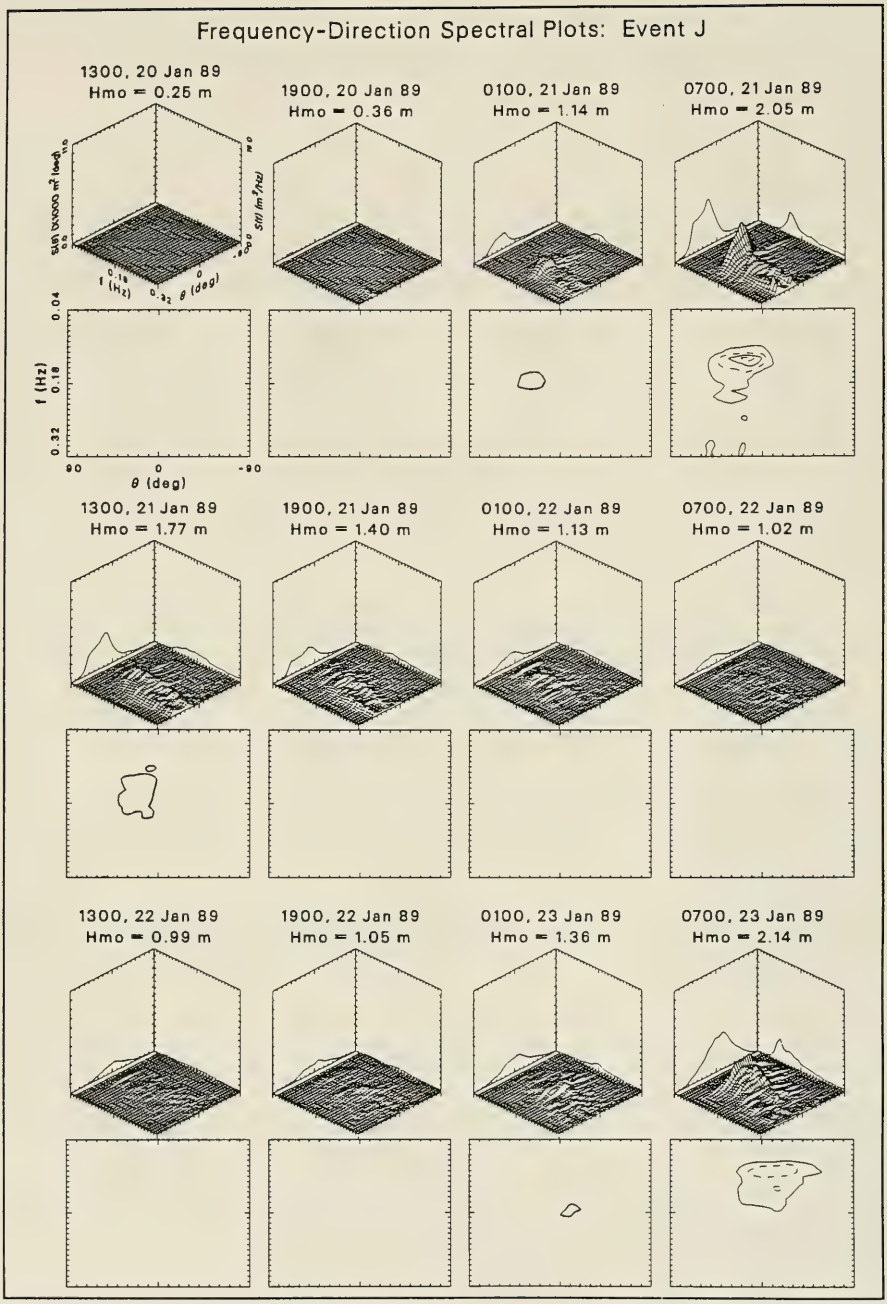
Frequency-Direction Spectral Plots: Event J
1300, 20 Jan 89
Hmo = 0.25 m
1900, 20 Jan 89
Hmo = 0.36 m
0100, 21 Jan 89
Hmo = 1.14 m
0700, 21 Jan 89
Hmo = 2.05 m
f (Hz)
θ (deg)
1300, 21 Jan 89
Hmo = 1.77 m
1900, 21 Jan 89
Hmo = 1.40 m
0100, 22 Jan 89
Hmo = 1.13 m
0700, 22 Jan 89
Hmo = 1.02 m
1300, 22 Jan 89
Hmo = 0.99 m
1900, 22 Jan 89
Hmo = 1.05 m
0100, 23 Jan 89
Hmo = 1.36 m
0700, 23 Jan 89
Hmo = 2.14 m

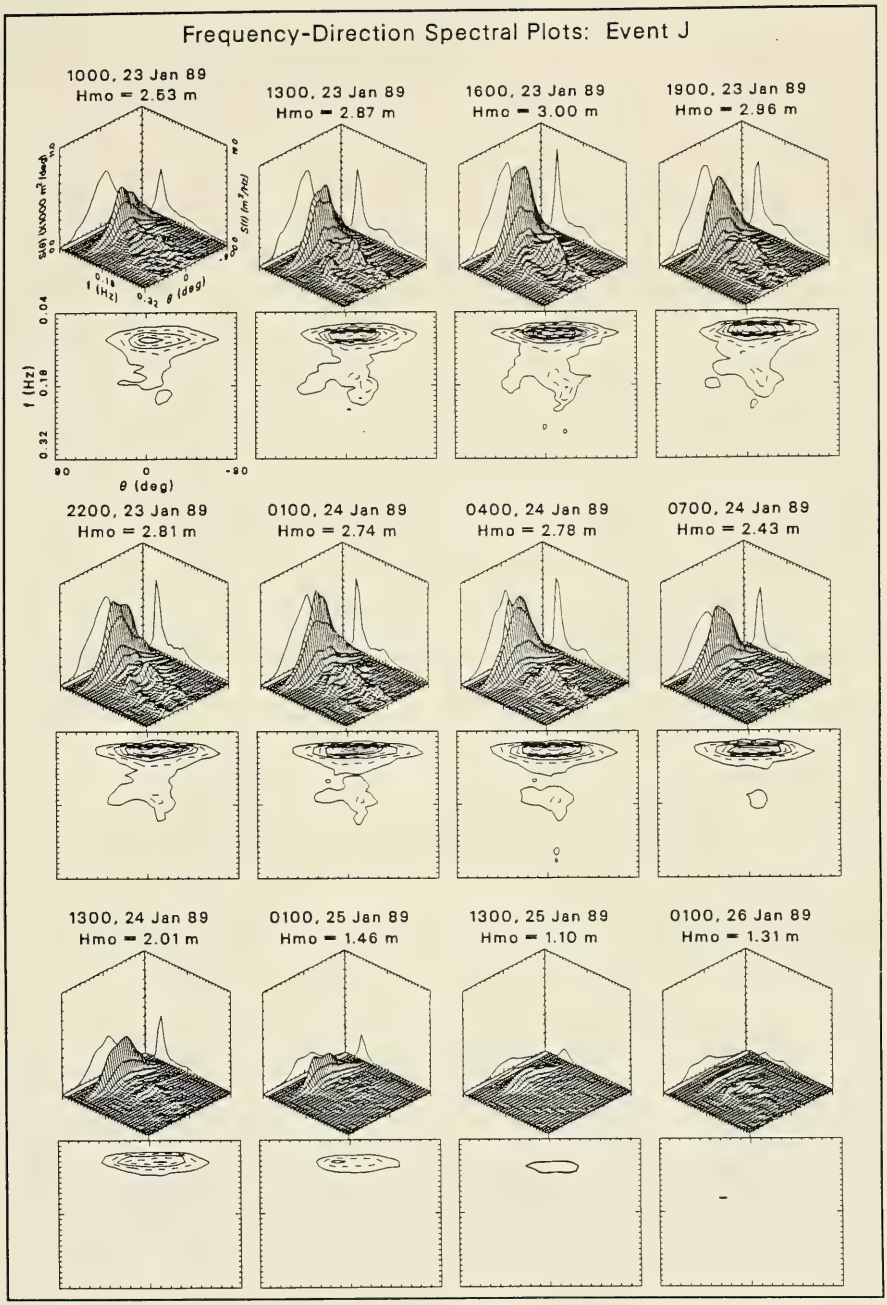
Frequency-Direction Spectral Plots: Event J
1000, 23 Jan 89
Hmo = 2.53 m
1300, 23 Jan 89
Hmo = 2.87 m
1600, 23 Jan 89
Hmo = 3.00 m
1900, 23 Jan 89
Hmo = 2.96 m
2200, 23 Jan 89
Hmo = 2.81 m
0100, 24 Jan 89
Hmo = 2.74 m
0400, 24 Jan 89
Hmo = 2.78 m
0700, 24 Jan 89
Hmo = 2.43 m
1300, 24 Jan 89
Hmo = 2.01 m
0100, 25 Jan 89
Hmo = 1.46 m
1300, 25 Jan 89
Hmo = 1.10 m
0100, 26 Jan 89
Hmo = 1.31 m
f (Hz)
0.04
0.18
0.32
90
0
-90
θ (deg)

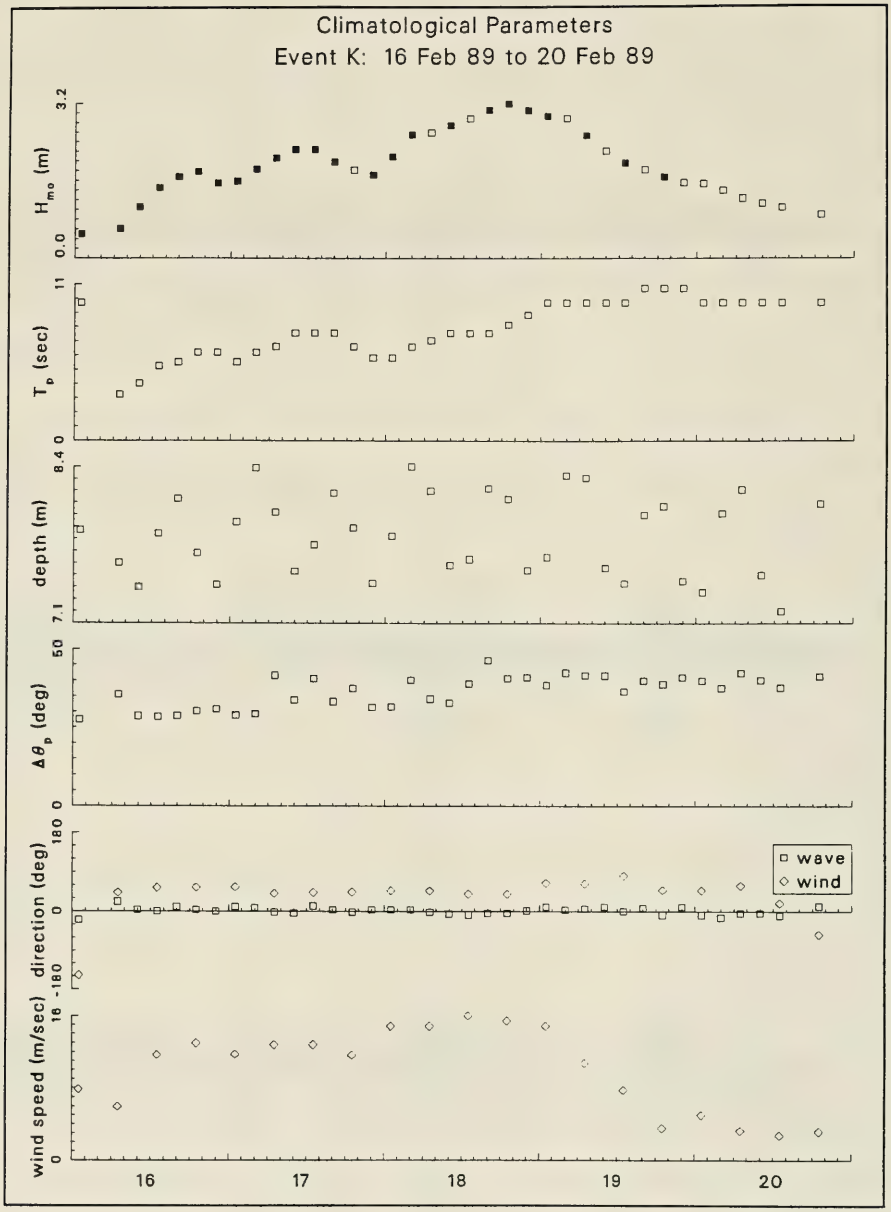
Climatological Parameters
Event K: 16 Feb 89 to 20 Feb 89
H_{mo} (m)
3.2
0.0
T_p (sec)
11
0
depth (m)
8.4
7.1
$\Delta\theta_p$ (deg)
50
0
direction (deg)
180
0
-180
wave
wind
wind speed (m/sec)
16
0
16
17
18
19
20

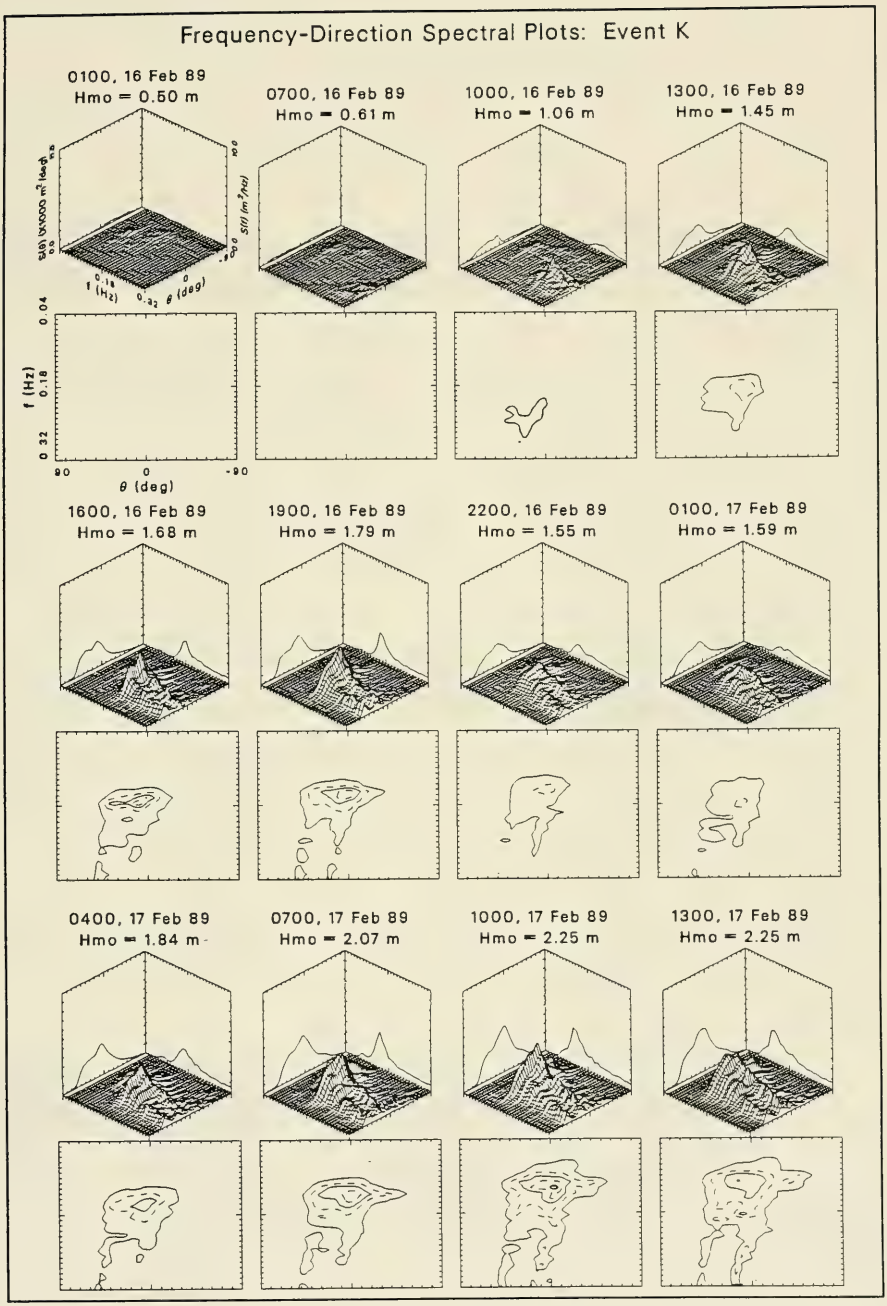
Frequency-Direction Spectral Plots: Event K
0100, 16 Feb 89
Hmo = 0.50 m
0700, 16 Feb 89
Hmo = 0.61 m
1000, 16 Feb 89
Hmo = 1.06 m
1300, 16 Feb 89
Hmo = 1.45 m
f (Hz)
0.04
0.18
0.32
90
0
-90
θ (deg)
1600, 16 Feb 89
Hmo = 1.68 m
1900, 16 Feb 89
Hmo = 1.79 m
2200, 16 Feb 89
Hmo = 1.55 m
0100, 17 Feb 89
Hmo = 1.59 m
0400, 17 Feb 89
Hmo = 1.84 m
0700, 17 Feb 89
Hmo = 2.07 m
1000, 17 Feb 89
Hmo = 2.25 m
1300, 17 Feb 89
Hmo = 2.25 m

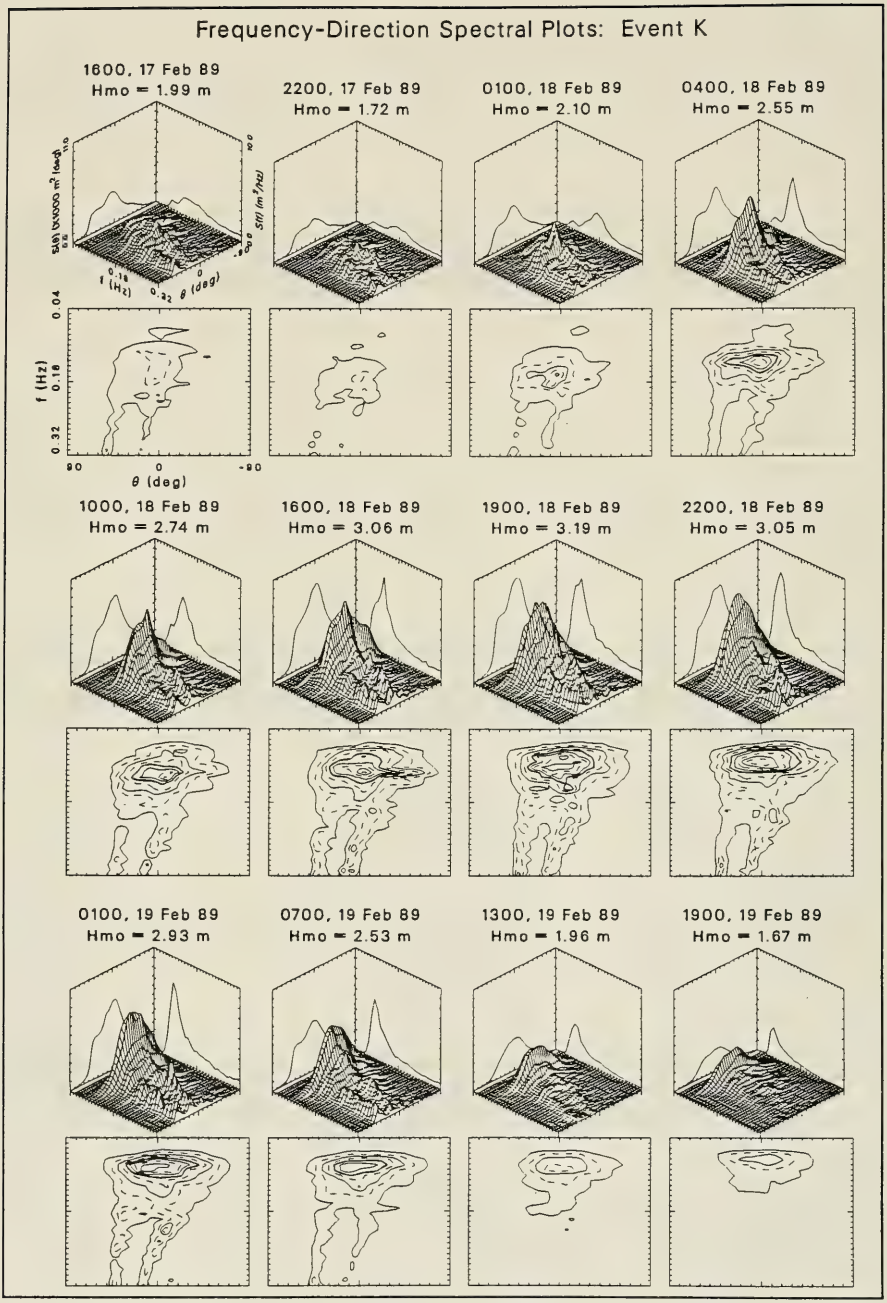
Frequency-Direction Spectral Plots: Event K
1600, 17 Feb 89
Hmo = 1.99 m
2200, 17 Feb 89
Hmo = 1.72 m
0100, 18 Feb 89
Hmo = 2.10 m
0400, 18 Feb 89
Hmo = 2.55 m
1000, 18 Feb 89
Hmo = 2.74 m
1600, 18 Feb 89
Hmo = 3.06 m
1900, 18 Feb 89
Hmo = 3.19 m
2200, 18 Feb 89
Hmo = 3.05 m
0100, 19 Feb 89
Hmo = 2.93 m
0700, 19 Feb 89
Hmo = 2.53 m
1300, 19 Feb 89
Hmo = 1.96 m
1900, 19 Feb 89
Hmo = 1.67 m
f (Hz)
0.04
0.16
0.32
90
0
-90
θ (deg)

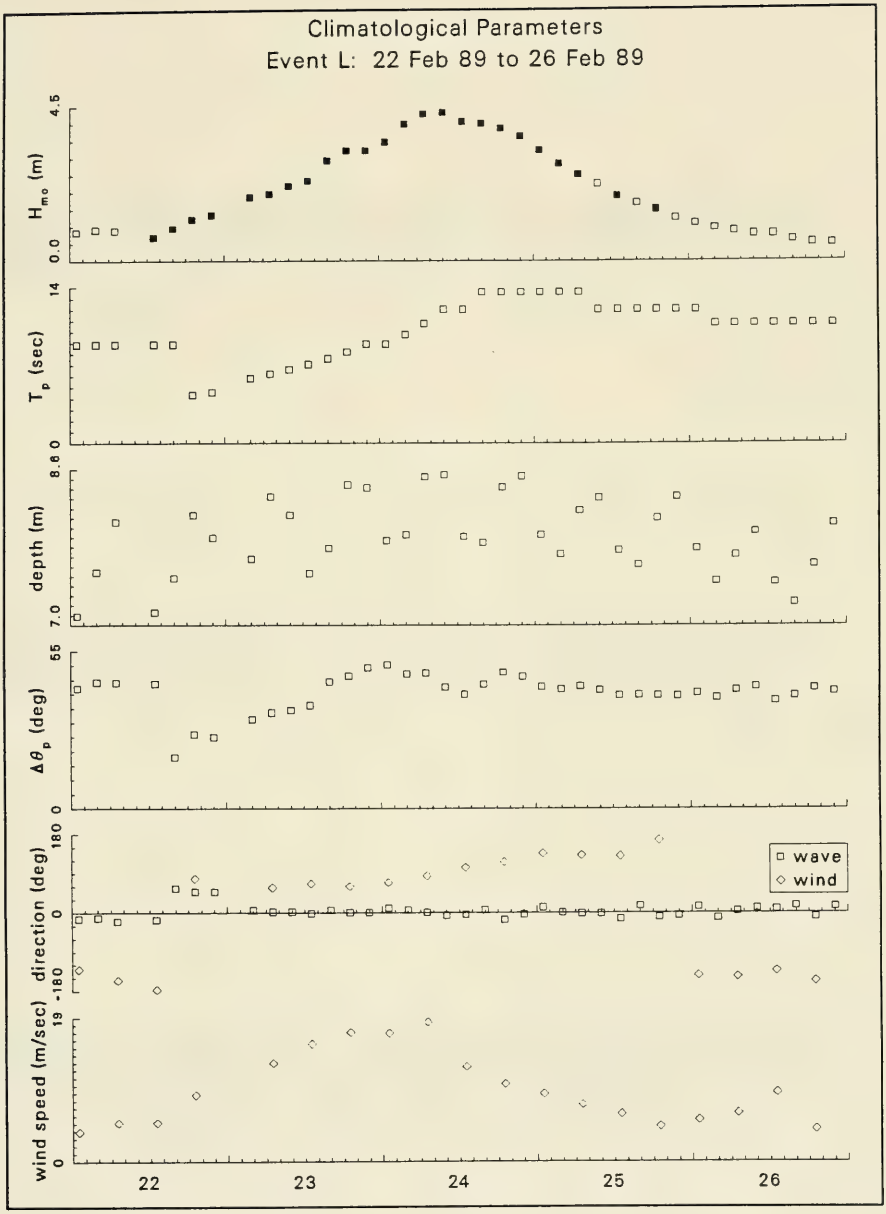
Climatological Parameters
Event L: 22 Feb 89 to 26 Feb 89
H_{m_0} (m)
4.5
0.0
T_p (sec)
14
0
depth (m)
8.0
7.0
$\Delta\theta_p$ (deg)
55
0
direction (deg)
180
0
-180
wave
wind
wind speed (m/sec)
19
0
22
23
24
25
26

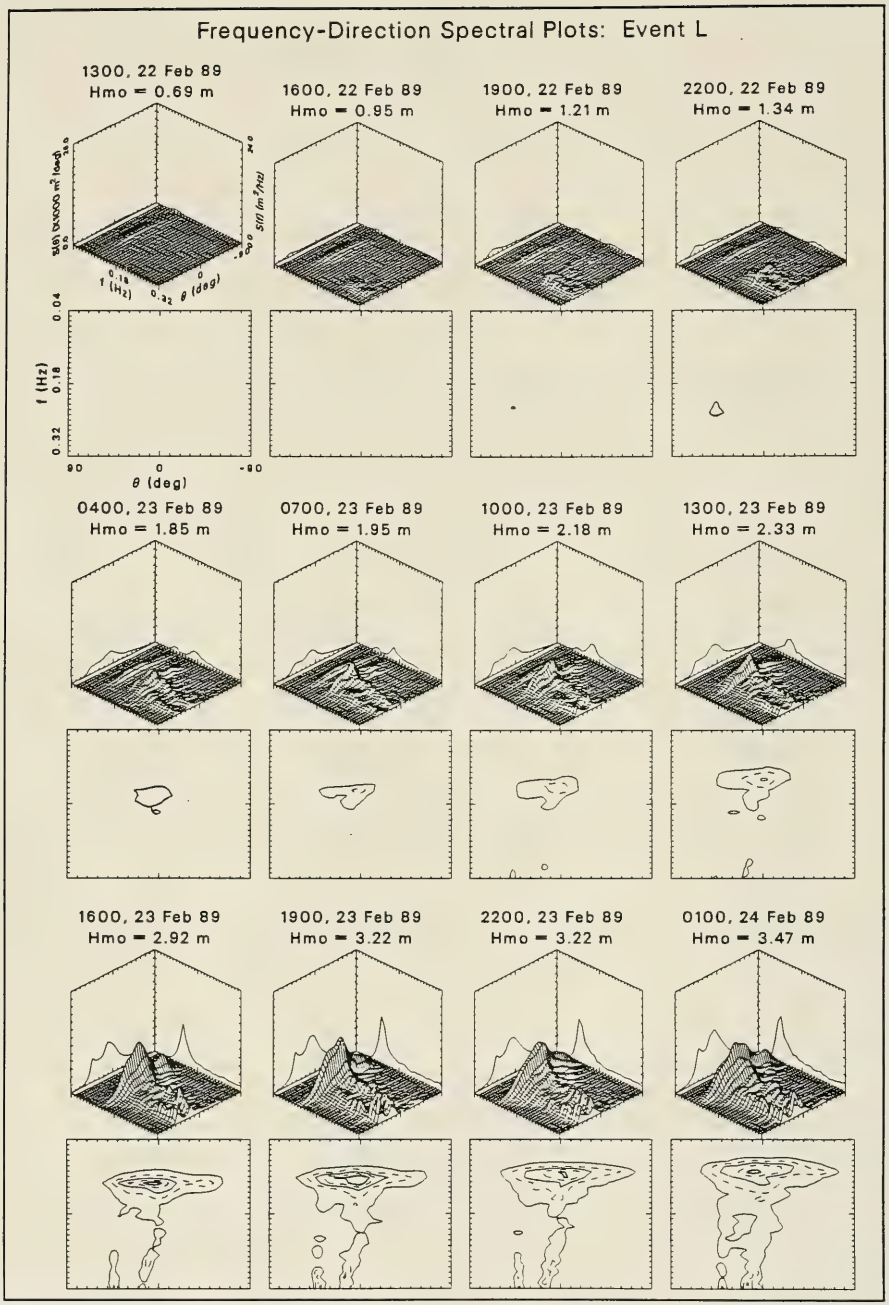
Frequency-Direction Spectral Plots: Event L
1300, 22 Feb 89
Hmo = 0.69 m
1600, 22 Feb 89
Hmo = 0.95 m
1900, 22 Feb 89
Hmo = 1.21 m
2200, 22 Feb 89
Hmo = 1.34 m
f (Hz)
0.04
0.18
0.32
90
0
-90
θ (deg)
0400, 23 Feb 89
Hmo = 1.85 m
0700, 23 Feb 89
Hmo = 1.95 m
1000, 23 Feb 89
Hmo = 2.18 m
1300, 23 Feb 89
Hmo = 2.33 m
1600, 23 Feb 89
Hmo = 2.92 m
1900, 23 Feb 89
Hmo = 3.22 m
2200, 23 Feb 89
Hmo = 3.22 m
0100, 24 Feb 89
Hmo = 3.47 m

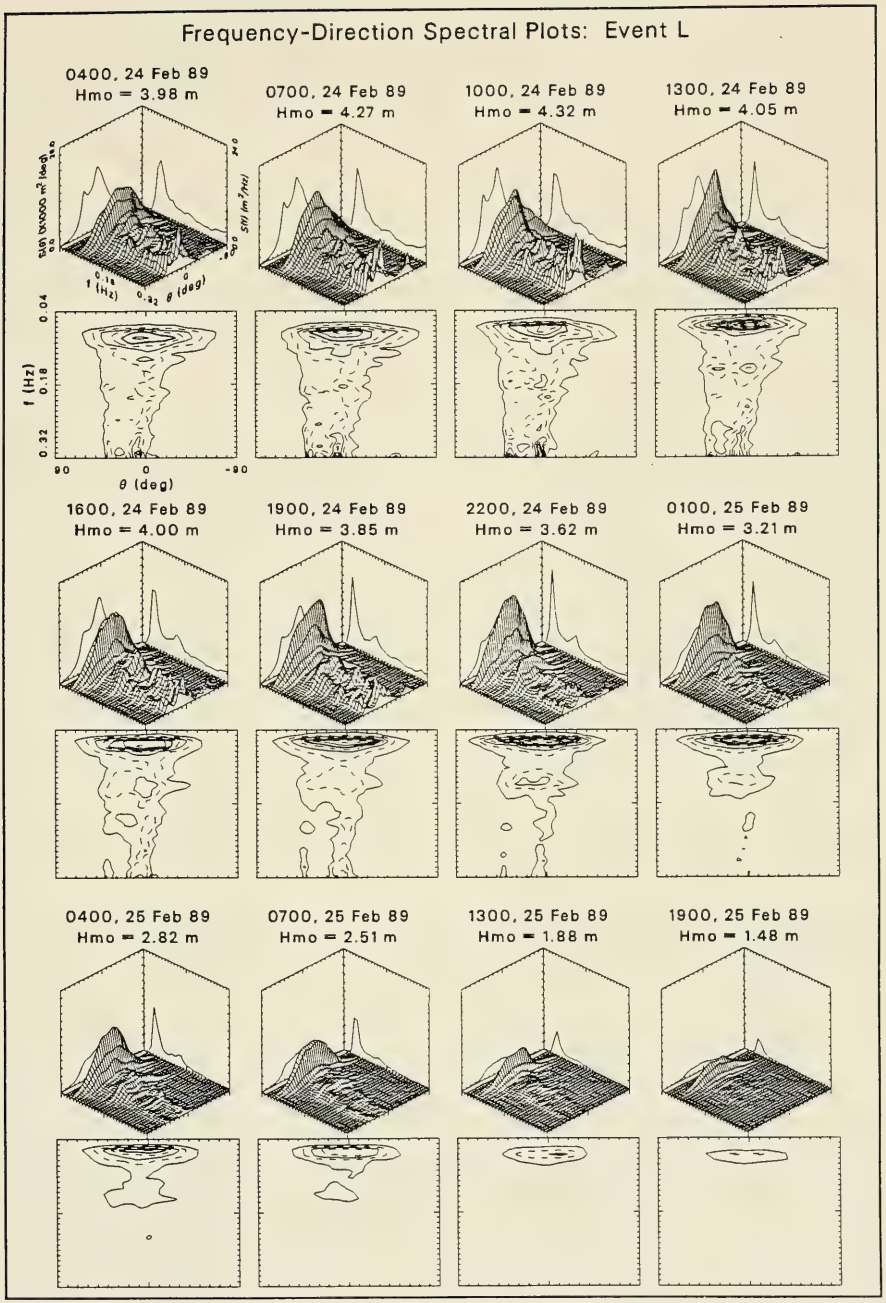
Frequency-Direction Spectral Plots: Event L
0400, 24 Feb 89
Hmo = 3.98 m
0700, 24 Feb 89
Hmo = 4.27 m
1000, 24 Feb 89
Hmo = 4.32 m
1300, 24 Feb 89
Hmo = 4.05 m
1600, 24 Feb 89
Hmo = 4.00 m
1900, 24 Feb 89
Hmo = 3.85 m
2200, 24 Feb 89
Hmo = 3.62 m
0100, 25 Feb 89
Hmo = 3.21 m
0400, 25 Feb 89
Hmo = 2.82 m
0700, 25 Feb 89
Hmo = 2.51 m
1300, 25 Feb 89
Hmo = 1.88 m
1900, 25 Feb 89
Hmo = 1.48 m
f (Hz)
θ (deg)

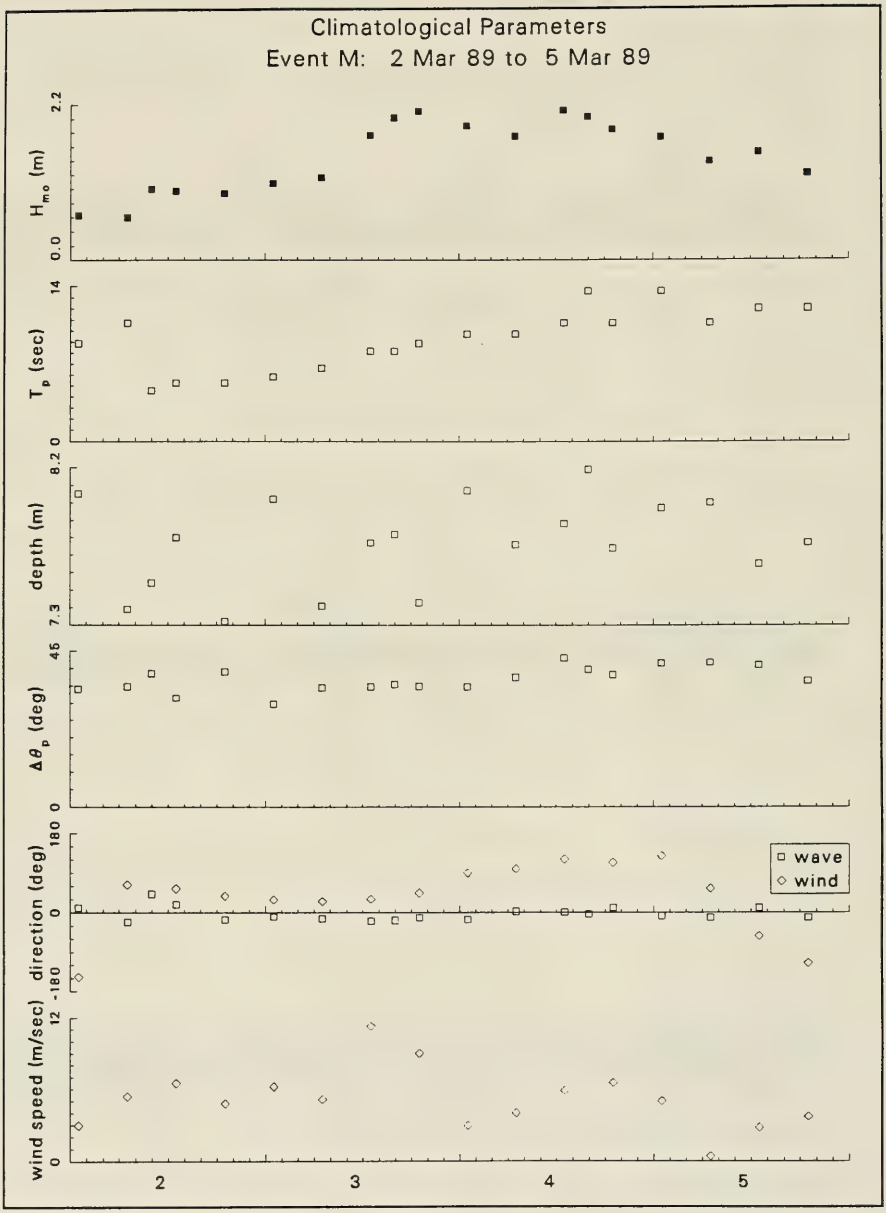
Climatological Parameters
Event M: 2 Mar 89 to 5 Mar 89
H_{m0} (m)
2.2
0.0
T_p (sec)
14
0
depth (m)
8.2
7.3
$\Delta\theta_p$ (deg)
45
0
direction (deg)
180
0
-180
wave
wind
wind speed (m/sec)
12
0
2
3
4
5

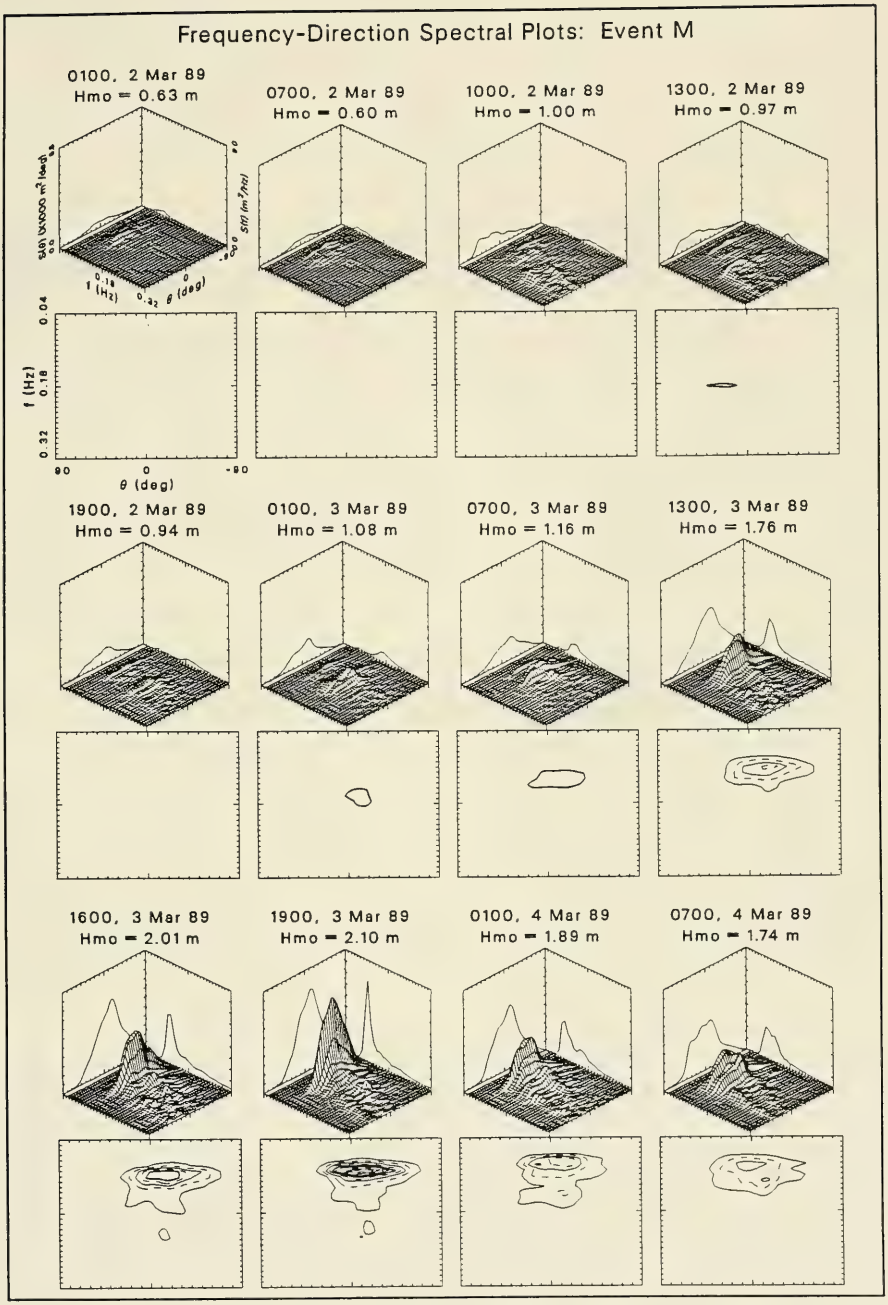
Frequency-Direction Spectral Plots: Event M
0100, 2 Mar 89
Hmo = 0.63 m
0700, 2 Mar 89
Hmo = 0.60 m
1000, 2 Mar 89
Hmo = 1.00 m
1300, 2 Mar 89
Hmo = 0.97 m
f (Hz)
θ (deg)
1900, 2 Mar 89
Hmo = 0.94 m
0100, 3 Mar 89
Hmo = 1.08 m
0700, 3 Mar 89
Hmo = 1.16 m
1300, 3 Mar 89
Hmo = 1.76 m
1600, 3 Mar 89
Hmo = 2.01 m
1900, 3 Mar 89
Hmo = 2.10 m
0100, 4 Mar 89
Hmo = 1.89 m
0700, 4 Mar 89
Hmo = 1.74 m

Frequency-Direction Spectral Plots: Event M

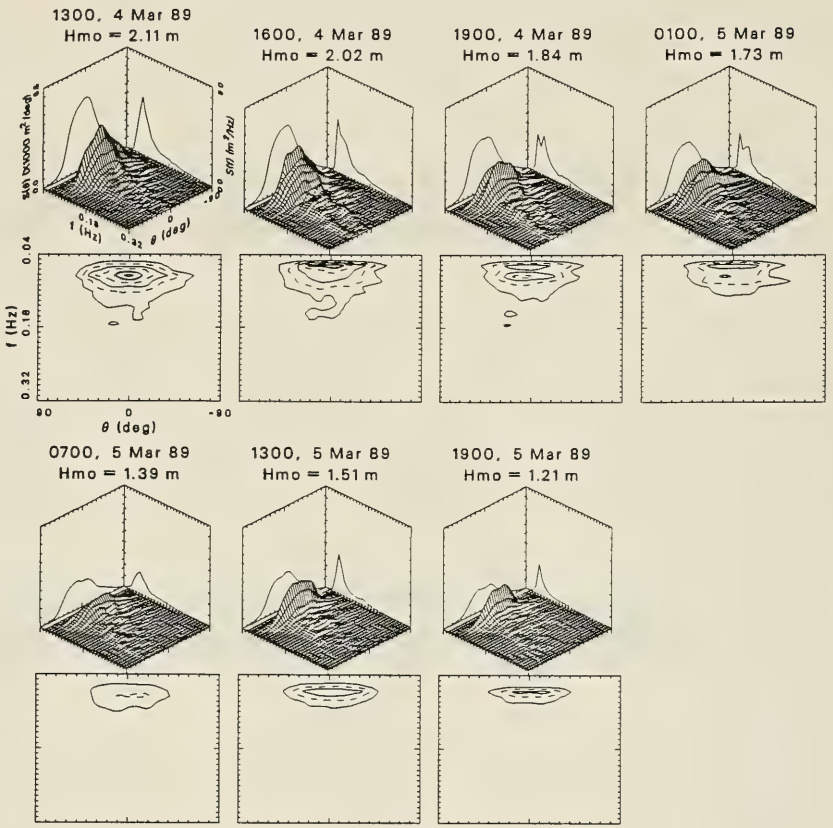

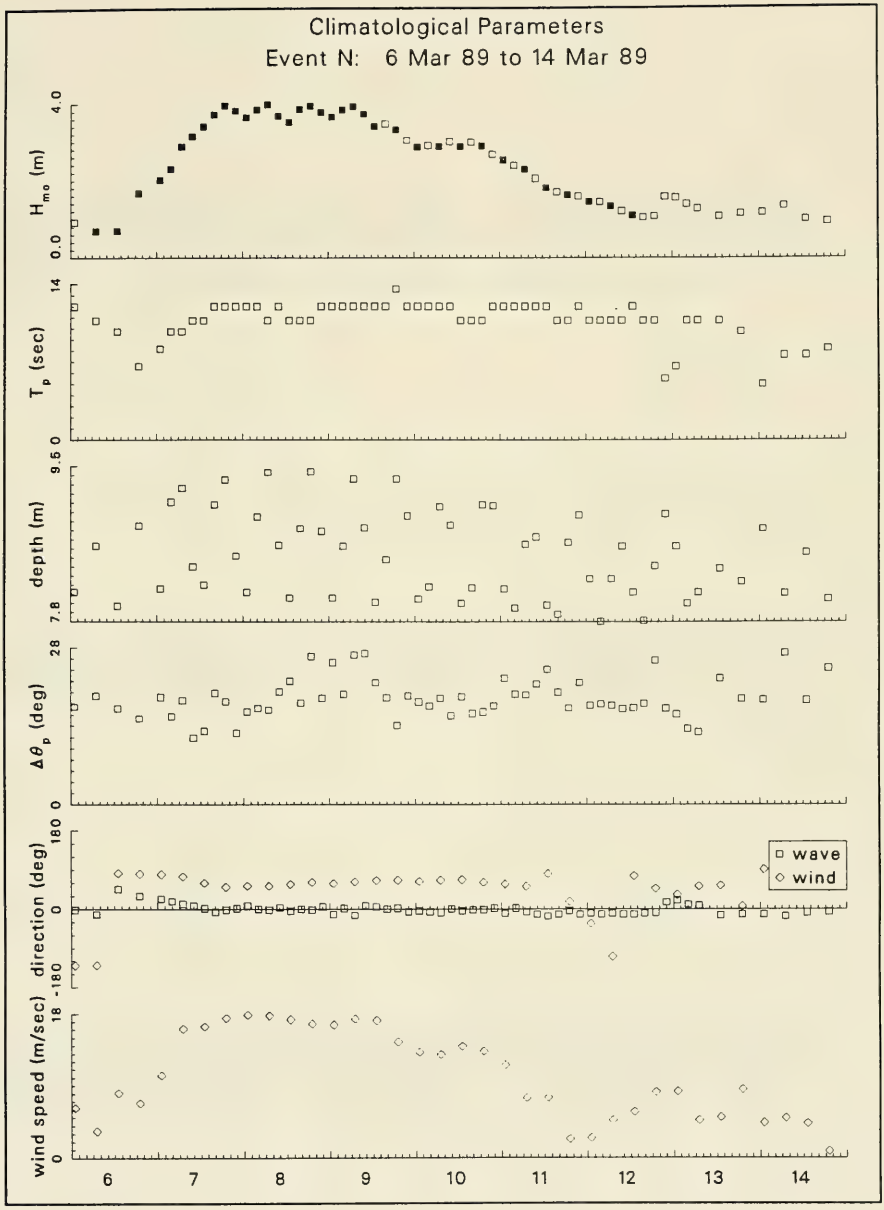
Climatological Parameters
Event N: 6 Mar 89 to 14 Mar 89
H_{mo} (m)
4.0
0.0
T_p (sec)
14
0
depth (m)
9.6
7.8
$\Delta\theta_p$ (deg)
28
0
direction (deg)
180
0
-180
wave
wind
wind speed (m/sec)
18
0
6
7
8
9
10
11
12
13
14

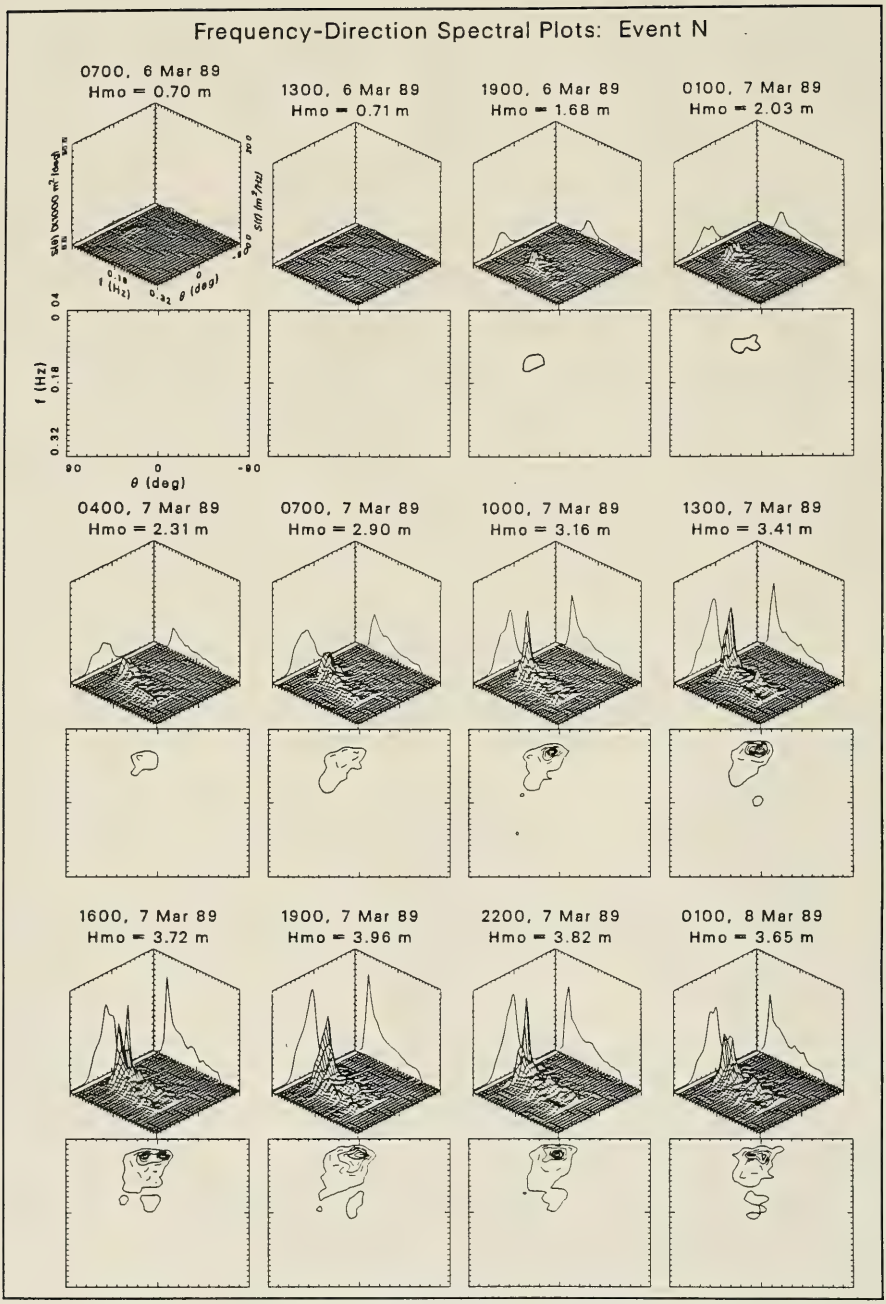
Frequency-Direction Spectral Plots: Event N
0700, 6 Mar 89
Hmo = 0.70 m
1300, 6 Mar 89
Hmo = 0.71 m
1900, 6 Mar 89
Hmo = 1.68 m
0100, 7 Mar 89
Hmo = 2.03 m
f (Hz)
0.04
0.16
0.32
90
0
-90
θ (deg)
0400, 7 Mar 89
Hmo = 2.31 m
0700, 7 Mar 89
Hmo = 2.90 m
1000, 7 Mar 89
Hmo = 3.16 m
1300, 7 Mar 89
Hmo = 3.41 m
1600, 7 Mar 89
Hmo = 3.72 m
1900, 7 Mar 89
Hmo = 3.96 m
2200, 7 Mar 89
Hmo = 3.82 m
0100, 8 Mar 89
Hmo = 3.65 m

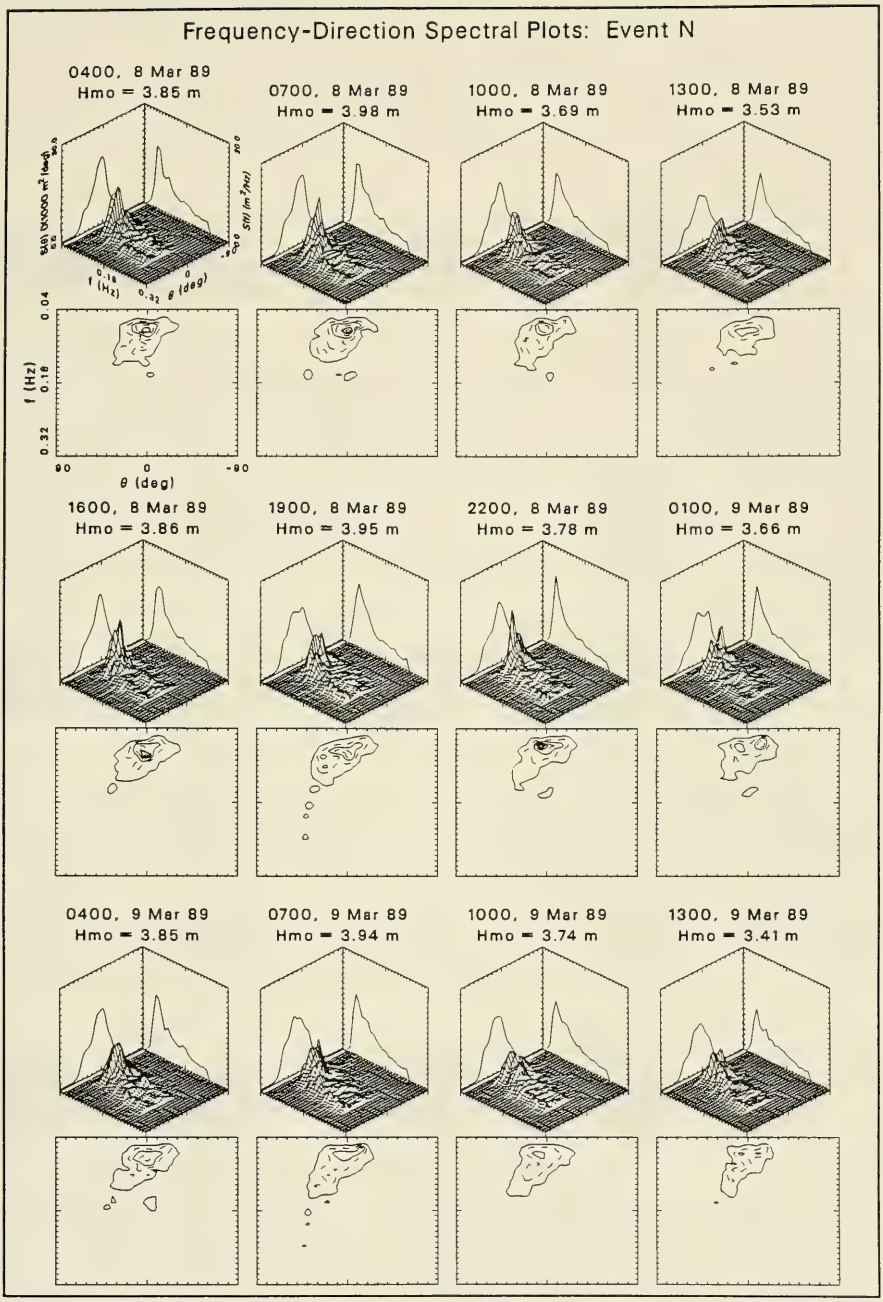
Frequency-Direction Spectral Plots: Event N
0400, 8 Mar 89
Hmo = 3.85 m
0700, 8 Mar 89
Hmo = 3.98 m
1000, 8 Mar 89
Hmo = 3.69 m
1300, 8 Mar 89
Hmo = 3.53 m
1600, 8 Mar 89
Hmo = 3.86 m
1900, 8 Mar 89
Hmo = 3.95 m
2200, 8 Mar 89
Hmo = 3.78 m
0100, 9 Mar 89
Hmo = 3.66 m
0400, 9 Mar 89
Hmo = 3.85 m
0700, 9 Mar 89
Hmo = 3.94 m
1000, 9 Mar 89
Hmo = 3.74 m
1300, 9 Mar 89
Hmo = 3.41 m
f (Hz)
0.04
0.18
0.32
90
0
-90
θ (deg)

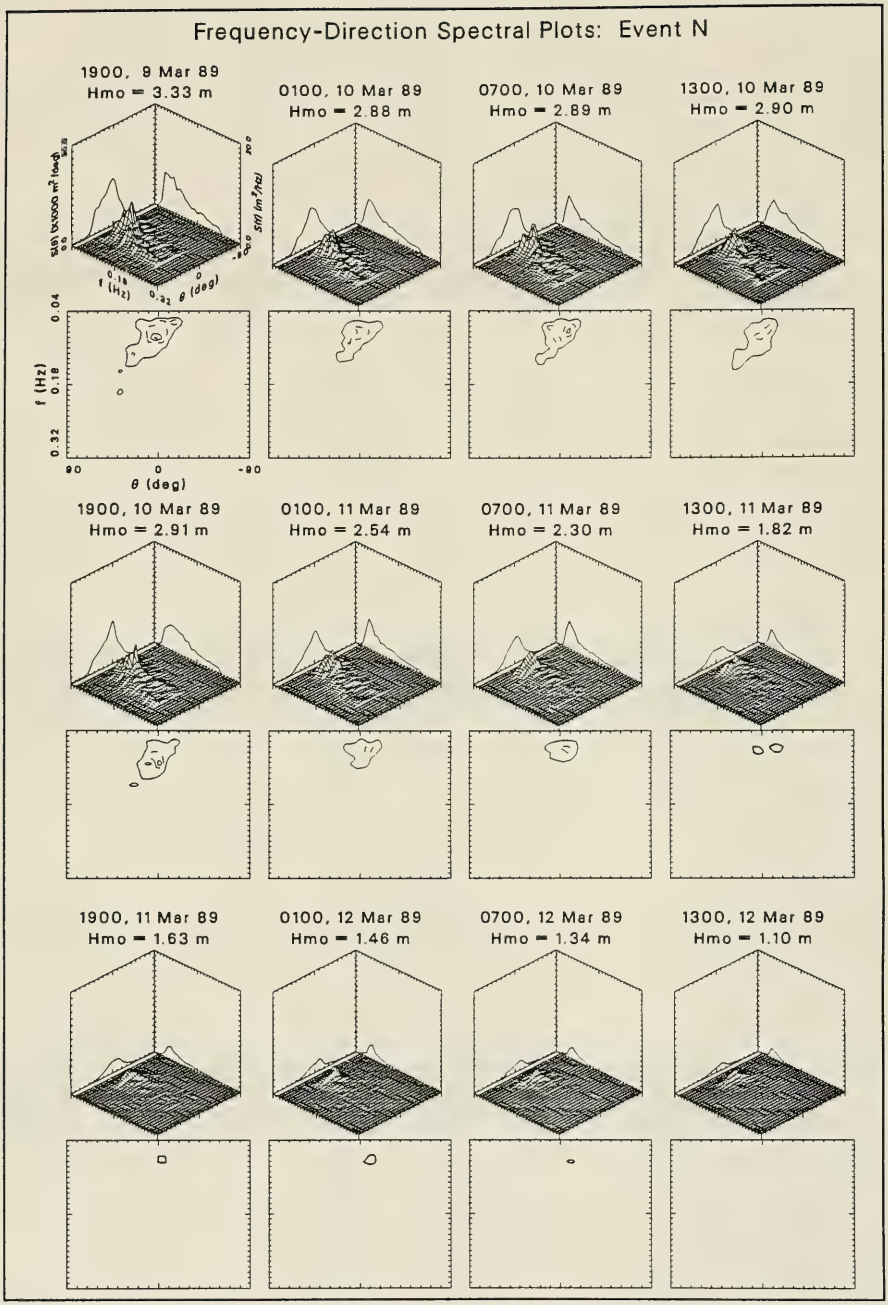
Frequency-Direction Spectral Plots: Event N
1900, 9 Mar 89
Hmo = 3.33 m
0100, 10 Mar 89
Hmo = 2.88 m
0700, 10 Mar 89
Hmo = 2.89 m
1300, 10 Mar 89
Hmo = 2.90 m
f (Hz)
0.04
0.18
0.32
90
0
-90
θ (deg)
1900, 10 Mar 89
Hmo = 2.91 m
0100, 11 Mar 89
Hmo = 2.54 m
0700, 11 Mar 89
Hmo = 2.30 m
1300, 11 Mar 89
Hmo = 1.82 m
1900, 11 Mar 89
Hmo = 1.63 m
0100, 12 Mar 89
Hmo = 1.46 m
0700, 12 Mar 89
Hmo = 1.34 m
1300, 12 Mar 89
Hmo = 1.10 m

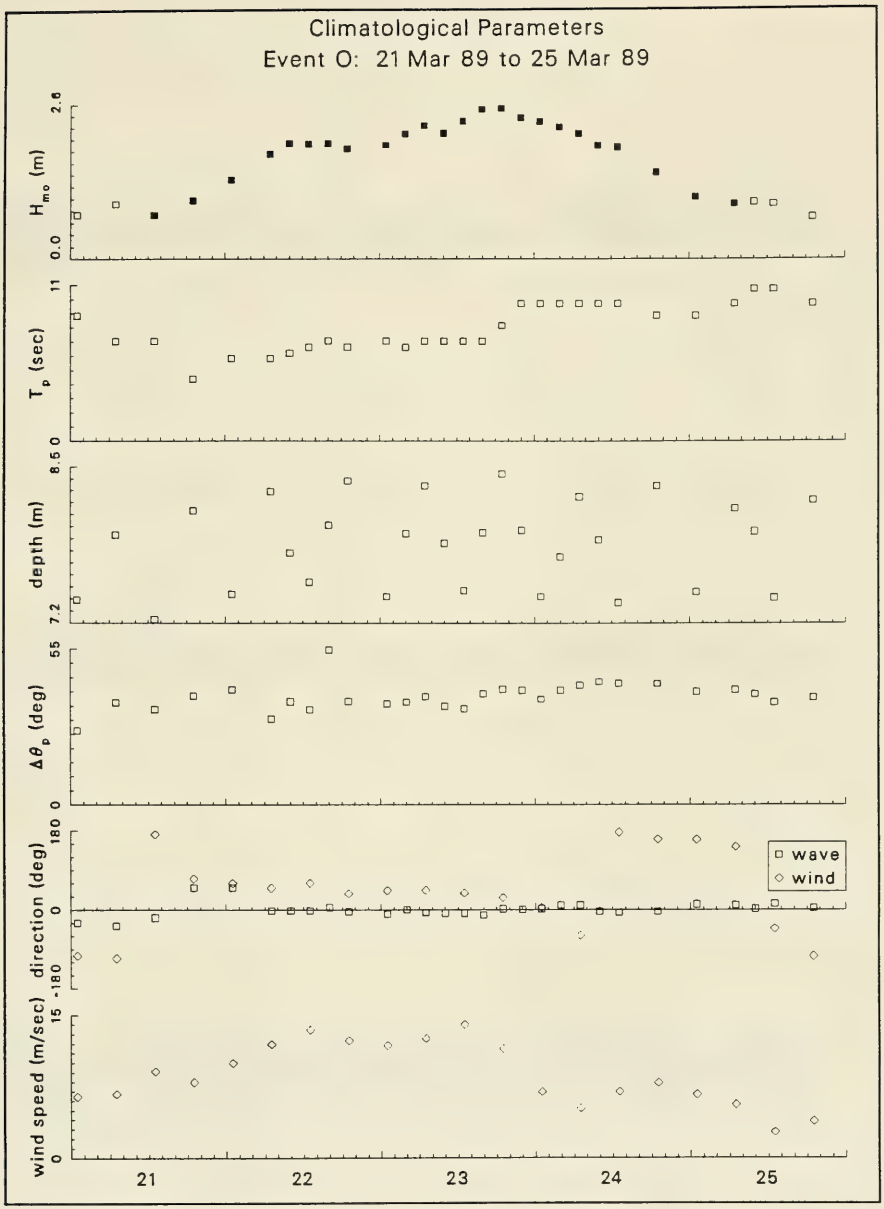
Climatological Parameters
Event O: 21 Mar 89 to 25 Mar 89
H_{mo} (m)
2.6
0.0
T_p (sec)
11
0
depth (m)
8.5
7.2
$\Delta\theta_p$ (deg)
55
0
direction (deg)
180
0
-180
wave
wind
wind speed (m/sec)
15
0
21
22
23
24
25

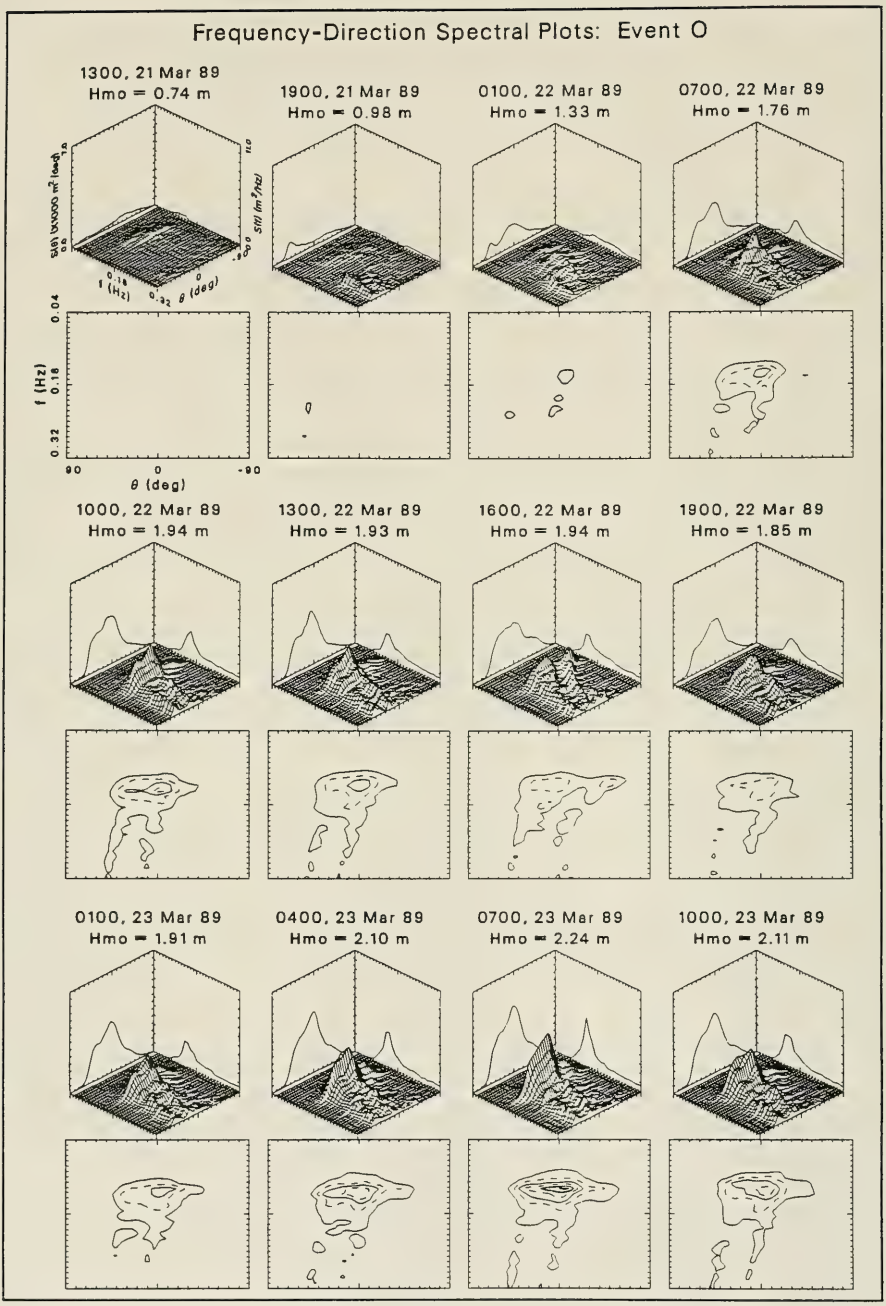
Frequency-Direction Spectral Plots: Event O
1300, 21 Mar 89
Hmo = 0.74 m
1900, 21 Mar 89
Hmo = 0.98 m
0100, 22 Mar 89
Hmo = 1.33 m
0700, 22 Mar 89
Hmo = 1.76 m
f (Hz)
0.04
0.18
0.32
90
0
-90
θ (deg)
1000, 22 Mar 89
Hmo = 1.94 m
1300, 22 Mar 89
Hmo = 1.93 m
1600, 22 Mar 89
Hmo = 1.94 m
1900, 22 Mar 89
Hmo = 1.85 m
0100, 23 Mar 89
Hmo = 1.91 m
0400, 23 Mar 89
Hmo = 2.10 m
0700, 23 Mar 89
Hmo = 2.24 m
1000, 23 Mar 89
Hmo = 2.11 m

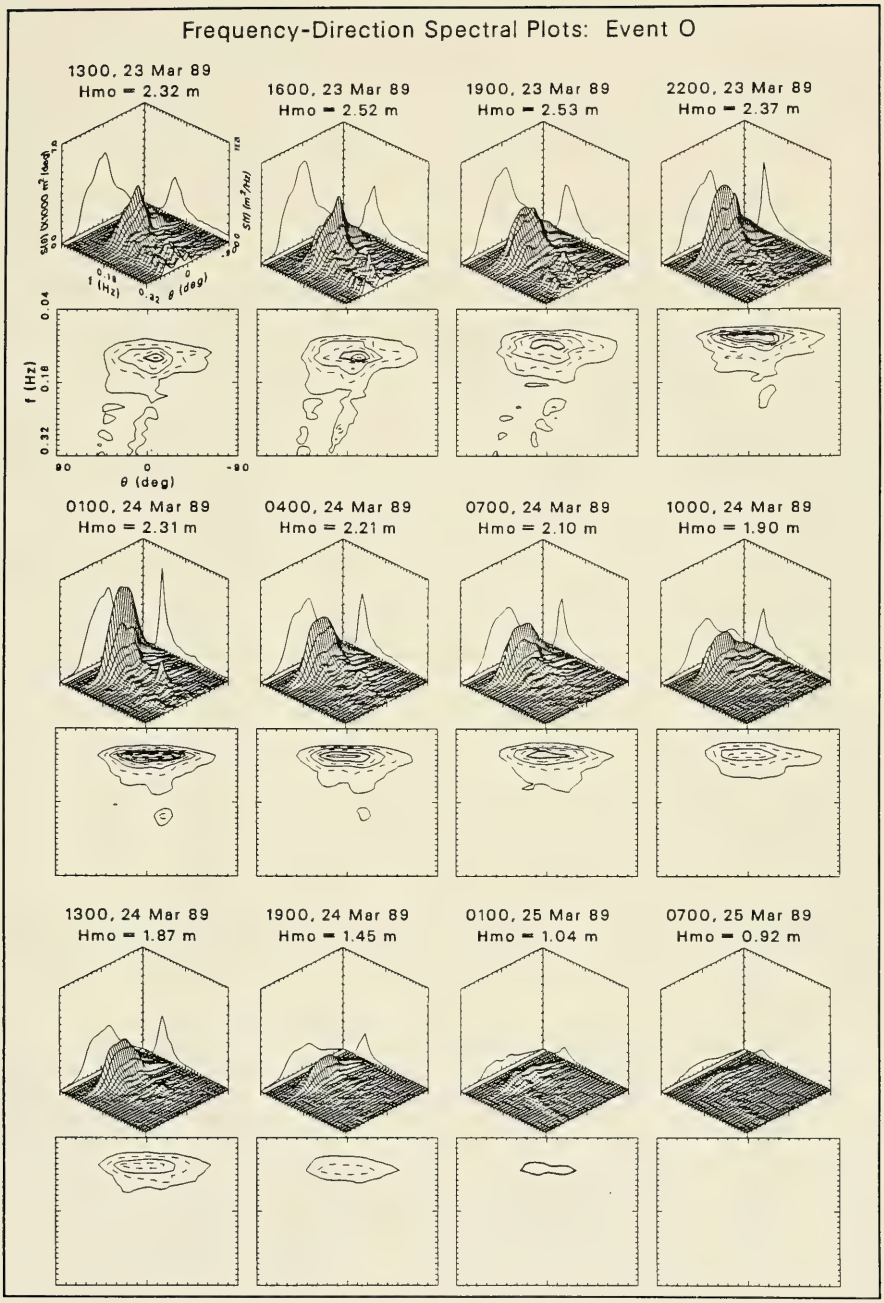
Frequency-Direction Spectral Plots: Event O
1300, 23 Mar 89
Hmo = 2.32 m
1600, 23 Mar 89
Hmo = 2.52 m
1900, 23 Mar 89
Hmo = 2.53 m
2200, 23 Mar 89
Hmo = 2.37 m
f (Hz)
θ (deg)
0100, 24 Mar 89
Hmo = 2.31 m
0400, 24 Mar 89
Hmo = 2.21 m
0700, 24 Mar 89
Hmo = 2.10 m
1000, 24 Mar 89
Hmo = 1.90 m
1300, 24 Mar 89
Hmo = 1.87 m
1900, 24 Mar 89
Hmo = 1.45 m
0100, 25 Mar 89
Hmo = 1.04 m
0700, 25 Mar 89
Hmo = 0.92 m

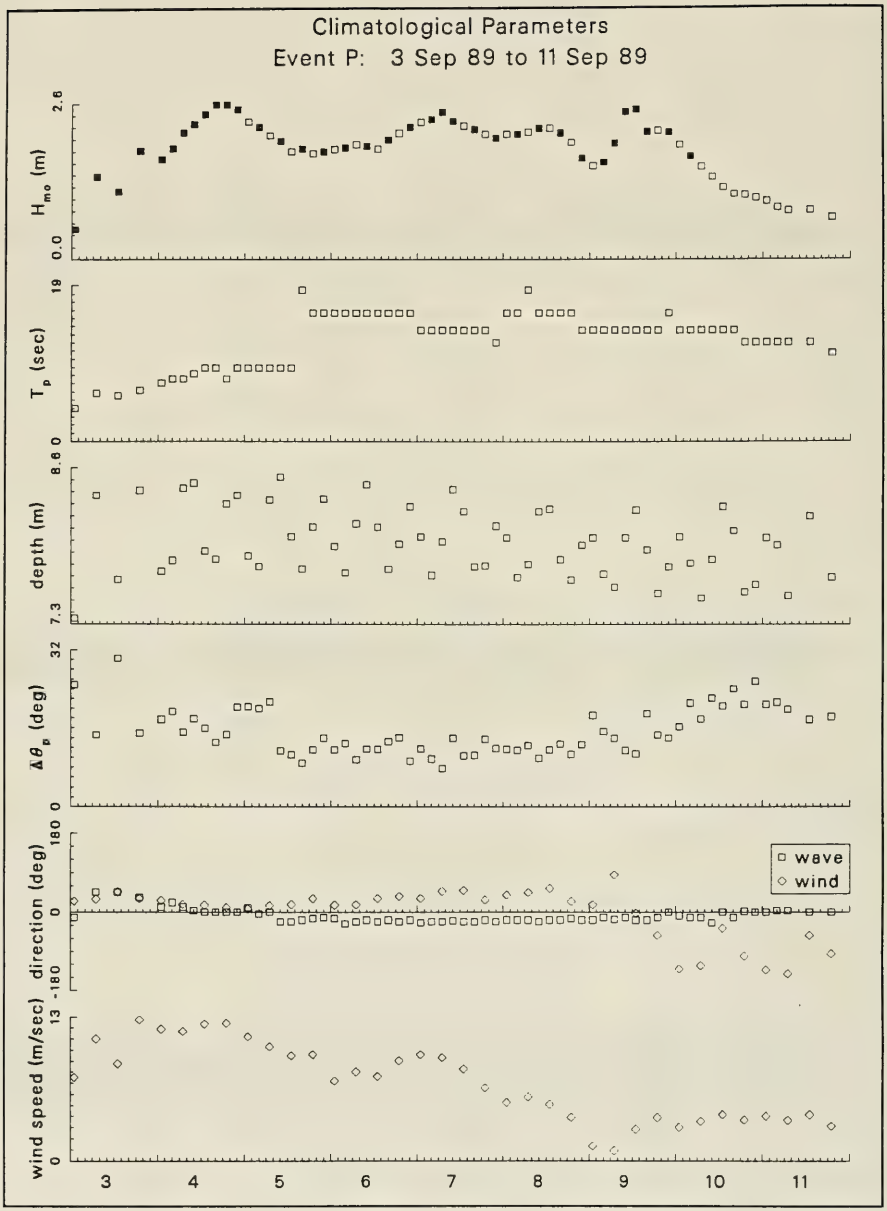
Climatological Parameters
Event P: 3 Sep 89 to 11 Sep 89
H_{mo} (m)
2.6
0.0
T_p (sec)
19
0
depth (m)
8.6
7.3
$\Delta\theta_p$ (deg)
32
0
direction (deg)
180
0
-180
wave
wind
wind speed (m/sec)
13
0
3
4
5
6
7
8
9
10
11

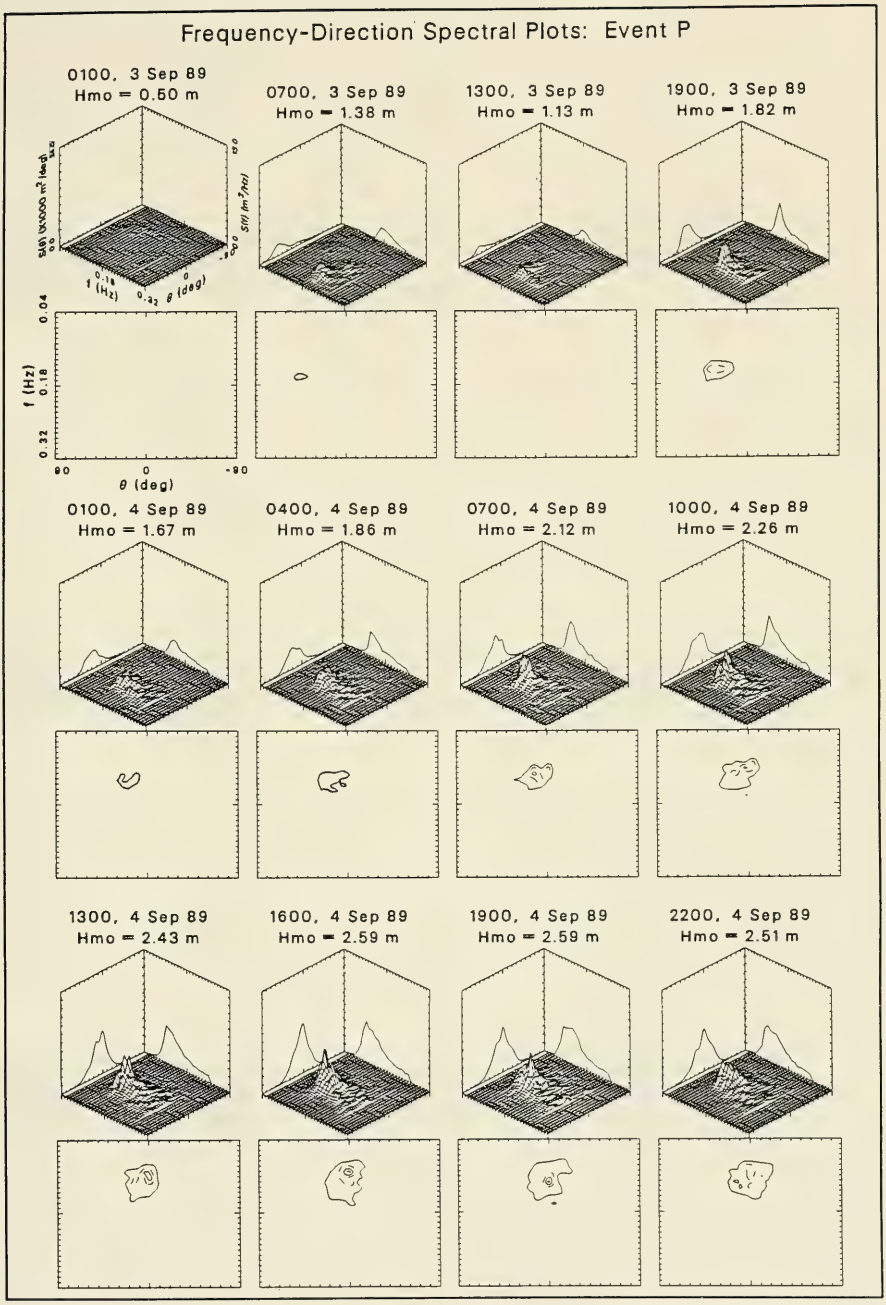
Frequency-Direction Spectral Plots: Event P
0100, 3 Sep 89
Hmo = 0.50 m
0700, 3 Sep 89
Hmo = 1.38 m
1300, 3 Sep 89
Hmo = 1.13 m
1900, 3 Sep 89
Hmo = 1.82 m
f (Hz)
0.04
0.18
0.32
90
0
-90
θ (deg)
0100, 4 Sep 89
Hmo = 1.67 m
0400, 4 Sep 89
Hmo = 1.86 m
0700, 4 Sep 89
Hmo = 2.12 m
1000, 4 Sep 89
Hmo = 2.26 m
1300, 4 Sep 89
Hmo = 2.43 m
1600, 4 Sep 89
Hmo = 2.59 m
1900, 4 Sep 89
Hmo = 2.59 m
2200, 4 Sep 89
Hmo = 2.51 m

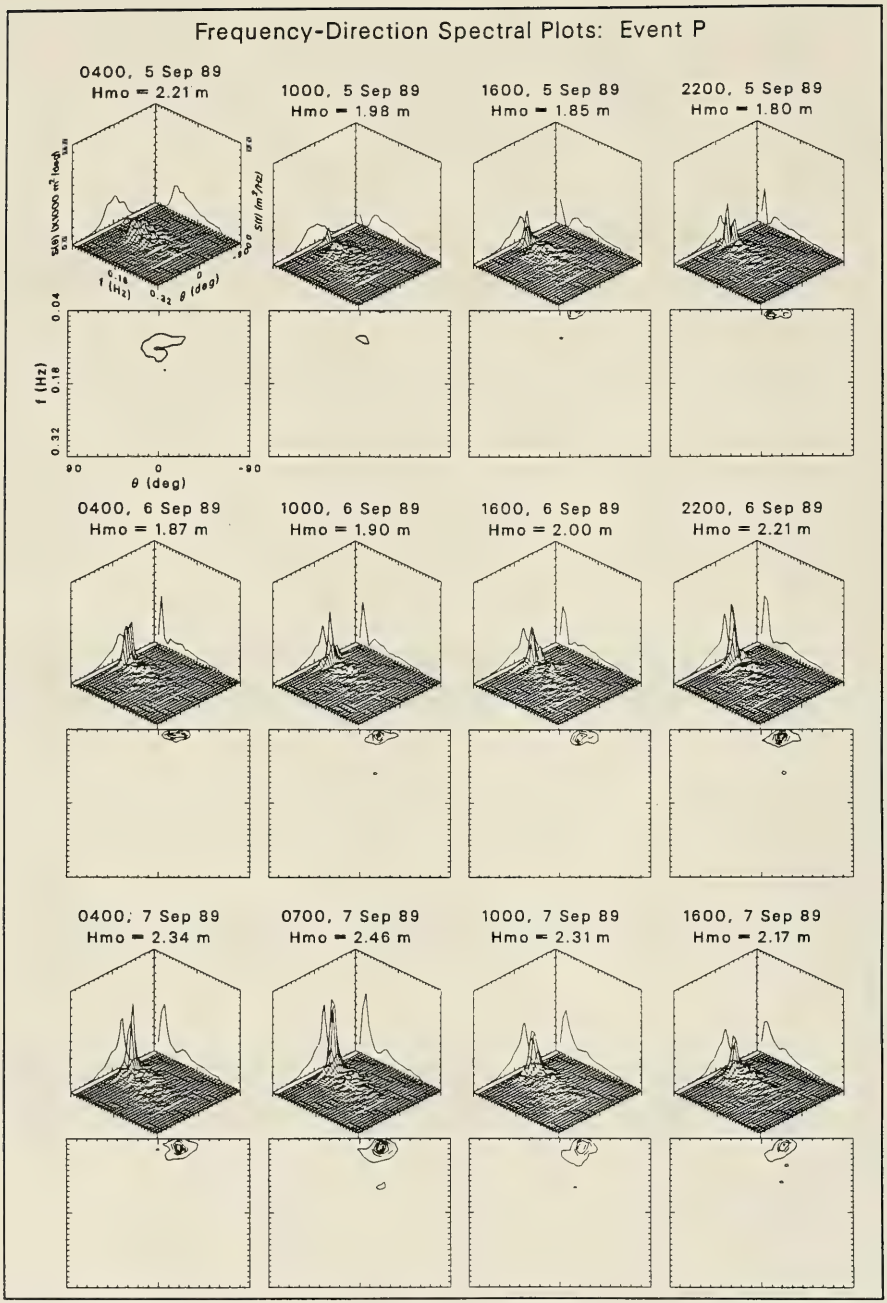
Frequency-Direction Spectral Plots: Event P
0400, 5 Sep 89
Hmo = 2.21 m
1000, 5 Sep 89
Hmo = 1.98 m
1600, 5 Sep 89
Hmo = 1.85 m
2200, 5 Sep 89
Hmo = 1.80 m
f (Hz)
0.04
0.18
0.32
90
0
-90
θ (deg)
0400, 6 Sep 89
Hmo = 1.87 m
1000, 6 Sep 89
Hmo = 1.90 m
1600, 6 Sep 89
Hmo = 2.00 m
2200, 6 Sep 89
Hmo = 2.21 m
0400, 7 Sep 89
Hmo = 2.34 m
0700, 7 Sep 89
Hmo = 2.46 m
1000, 7 Sep 89
Hmo = 2.31 m
1600, 7 Sep 89
Hmo = 2.17 m

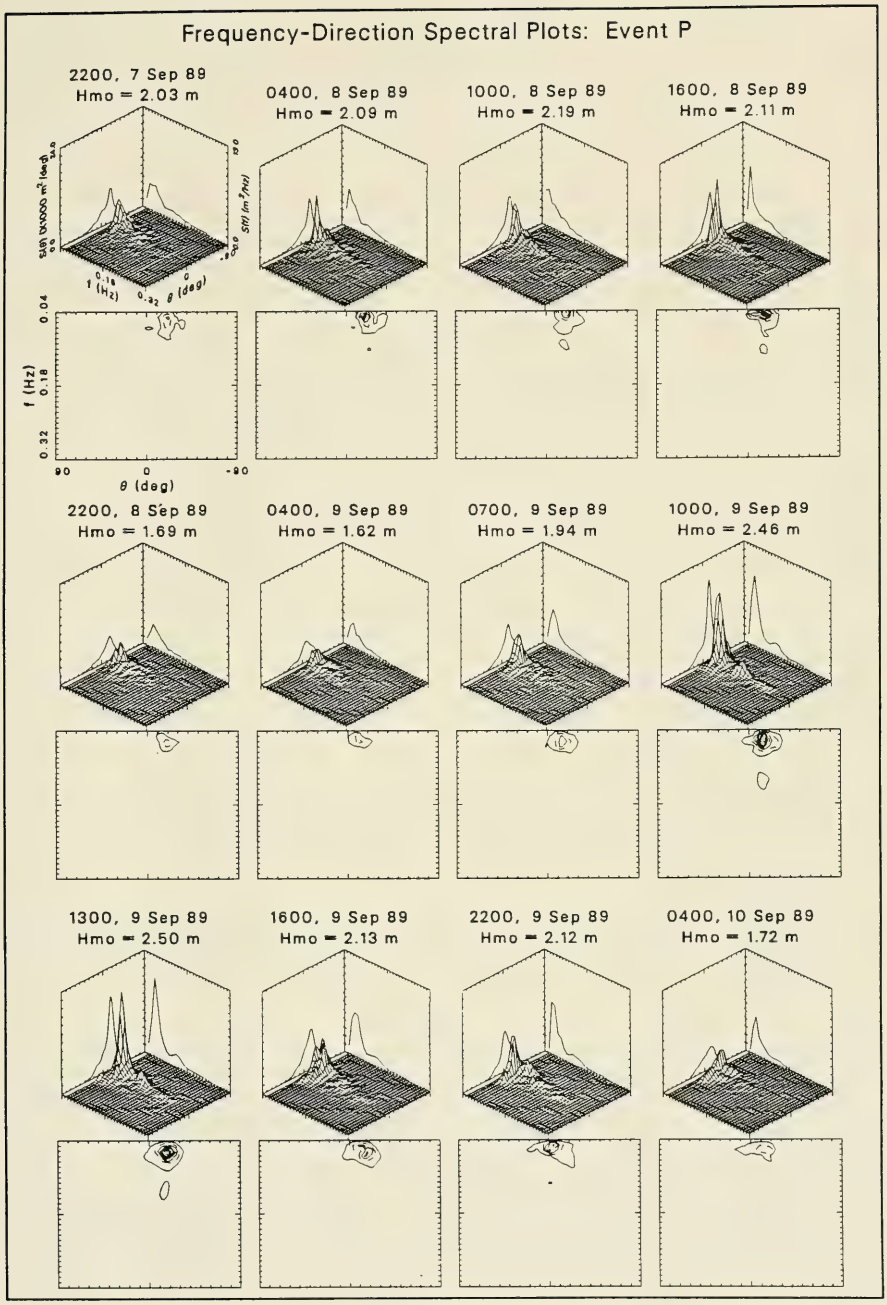
Frequency-Direction Spectral Plots: Event P
2200, 7 Sep 89
Hmo = 2.03 m
0400, 8 Sep 89
Hmo = 2.09 m
1000, 8 Sep 89
Hmo = 2.19 m
1600, 8 Sep 89
Hmo = 2.11 m
2200, 8 Sep 89
Hmo = 1.69 m
0400, 9 Sep 89
Hmo = 1.62 m
0700, 9 Sep 89
Hmo = 1.94 m
1000, 9 Sep 89
Hmo = 2.46 m
1300, 9 Sep 89
Hmo = 2.50 m
1600, 9 Sep 89
Hmo = 2.13 m
2200, 9 Sep 89
Hmo = 2.12 m
0400, 10 Sep 89
Hmo = 1.72 m
f (Hz)
0.04
0.18
0.32
90
0
-90
θ (deg)

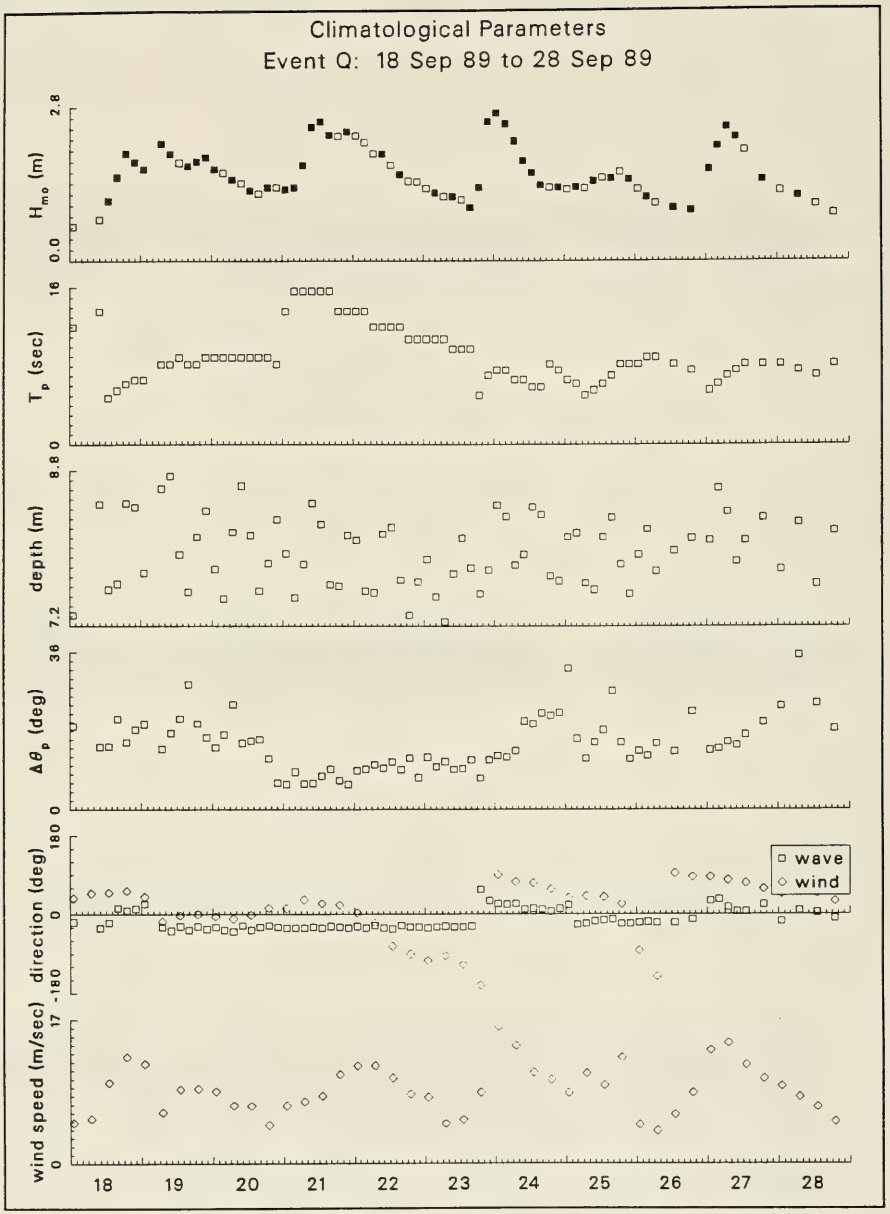
Climatological Parameters
Event Q: 18 Sep 89 to 28 Sep 89
H_{mo} (m)
2.8
0.0
T_p (sec)
16
0
depth (m)
8.8
7.2
$\Delta\theta_p$ (deg)
36
0
direction (deg)
180
0
-180
wave
wind
wind speed (m/sec)
17
0
18
19
20
21
22
23
24
25
26
27
28

Frequency-Direction Spectral Plots: Event Q

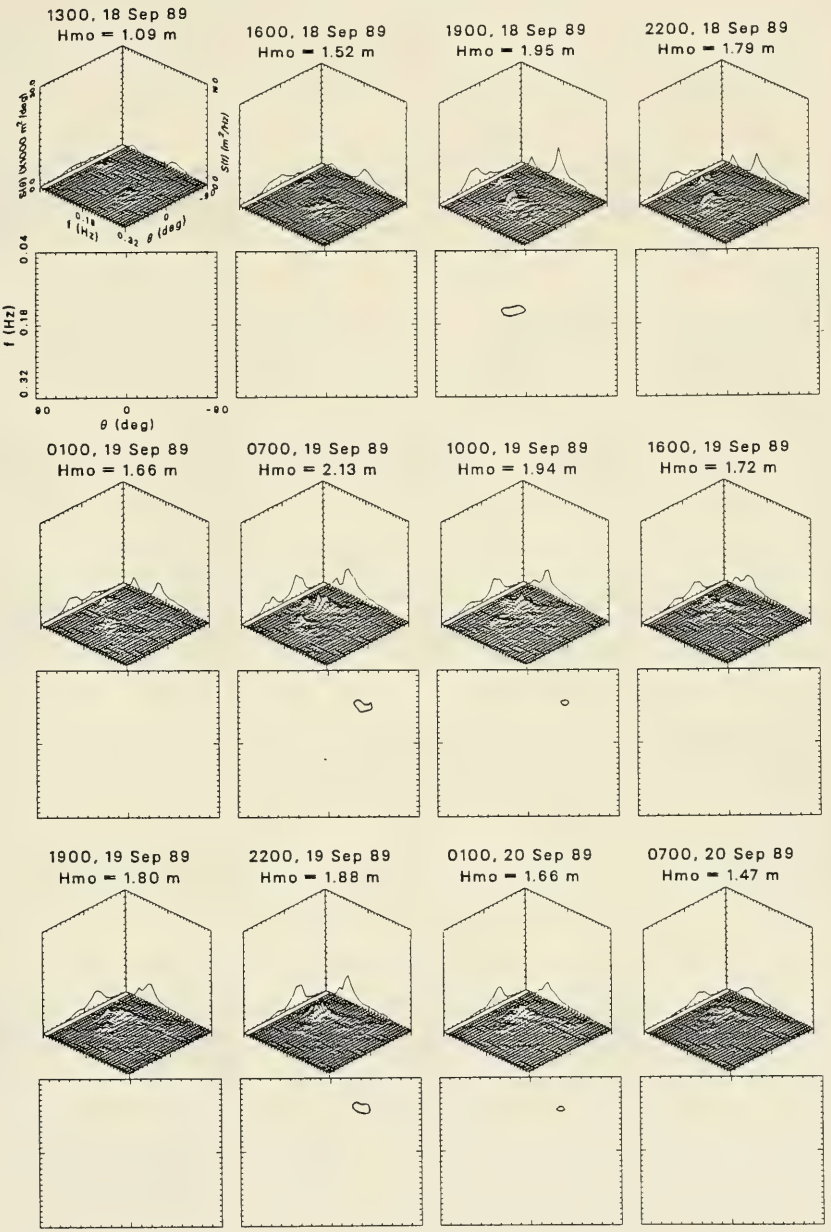

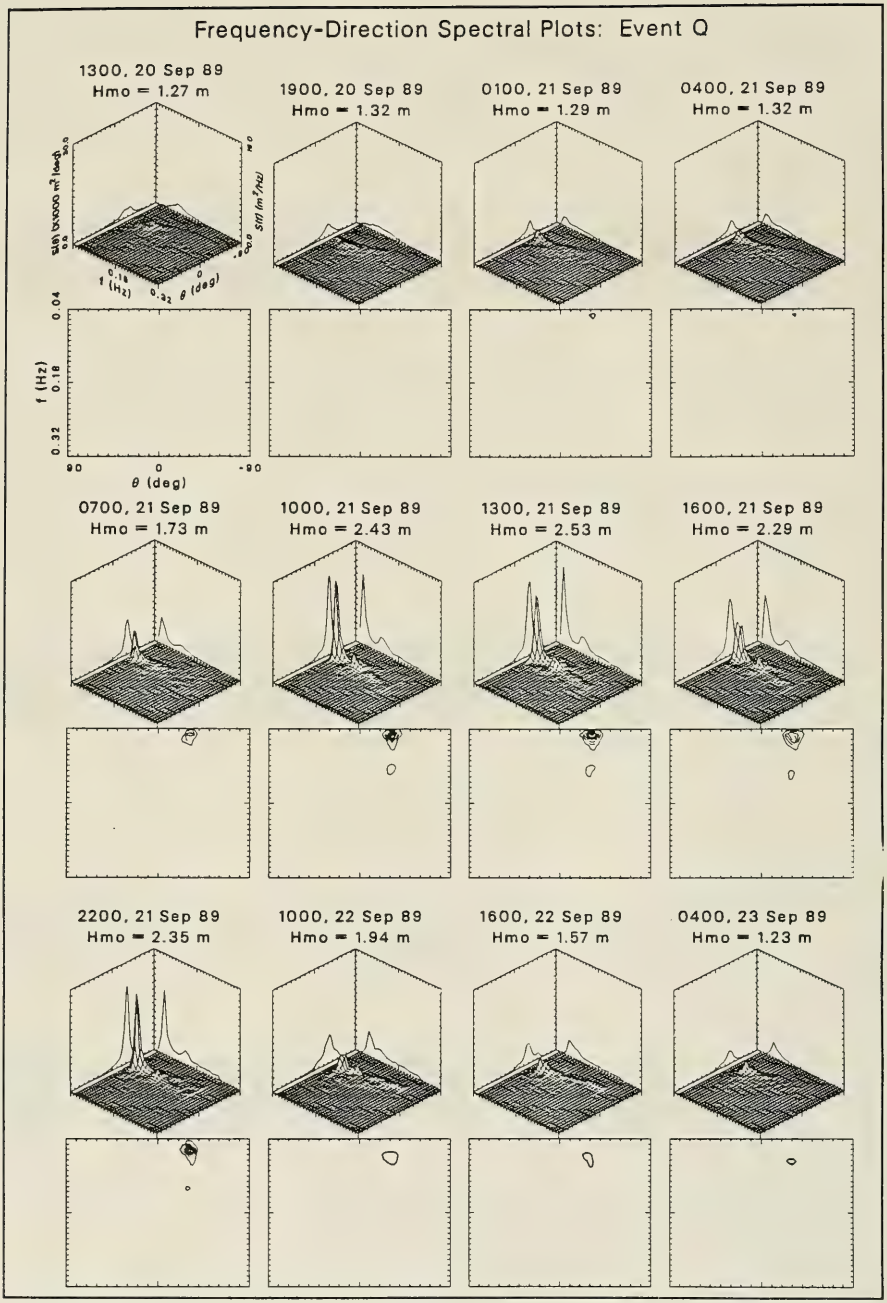
Frequency-Direction Spectral Plots: Event Q
1300, 20 Sep 89
Hmo = 1.27 m
1900, 20 Sep 89
Hmo = 1.32 m
0100, 21 Sep 89
Hmo = 1.29 m
0400, 21 Sep 89
Hmo = 1.32 m
f (Hz)
θ (deg)
0700, 21 Sep 89
Hmo = 1.73 m
1000, 21 Sep 89
Hmo = 2.43 m
1300, 21 Sep 89
Hmo = 2.53 m
1600, 21 Sep 89
Hmo = 2.29 m
2200, 21 Sep 89
Hmo = 2.35 m
1000, 22 Sep 89
Hmo = 1.94 m
1600, 22 Sep 89
Hmo = 1.57 m
0400, 23 Sep 89
Hmo = 1.23 m

Frequency-Direction Spectral Plots: Event Q

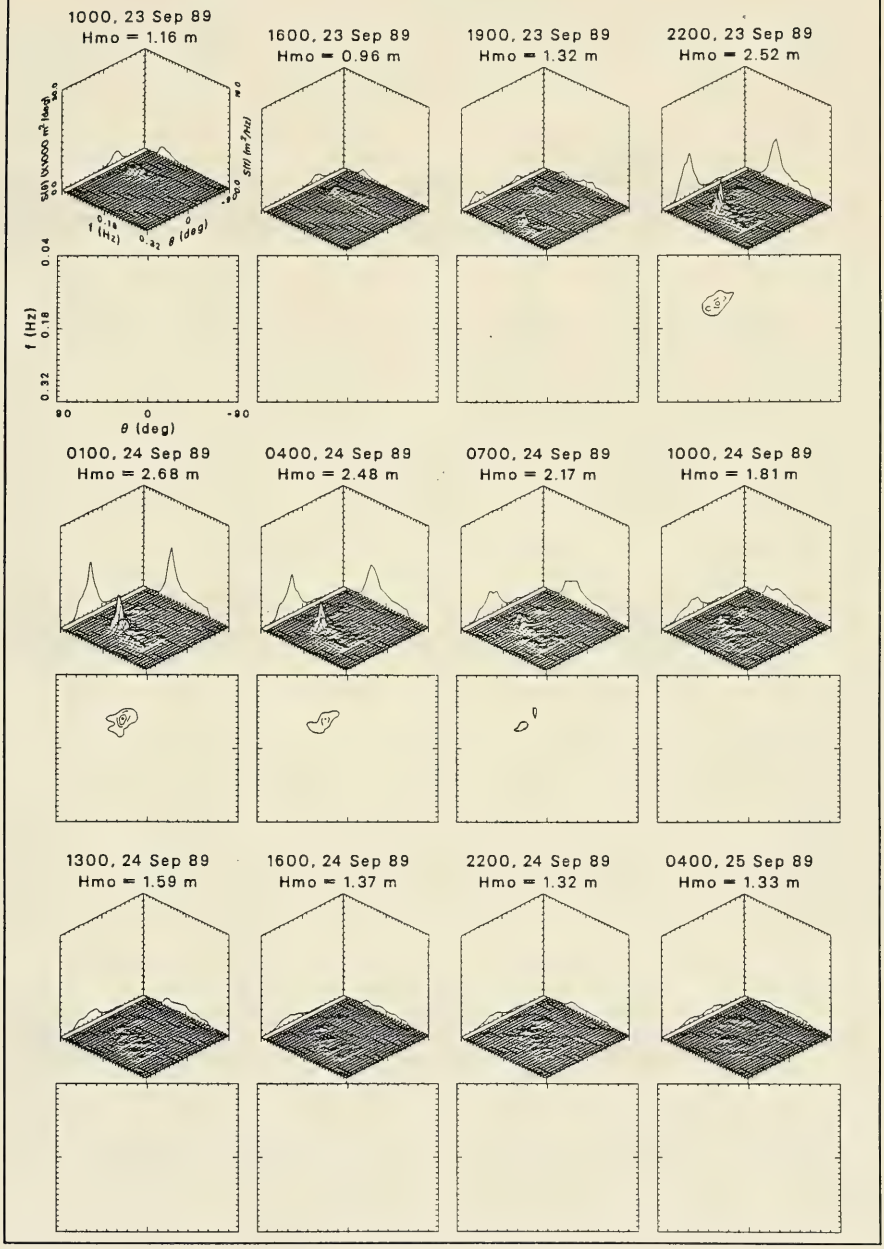

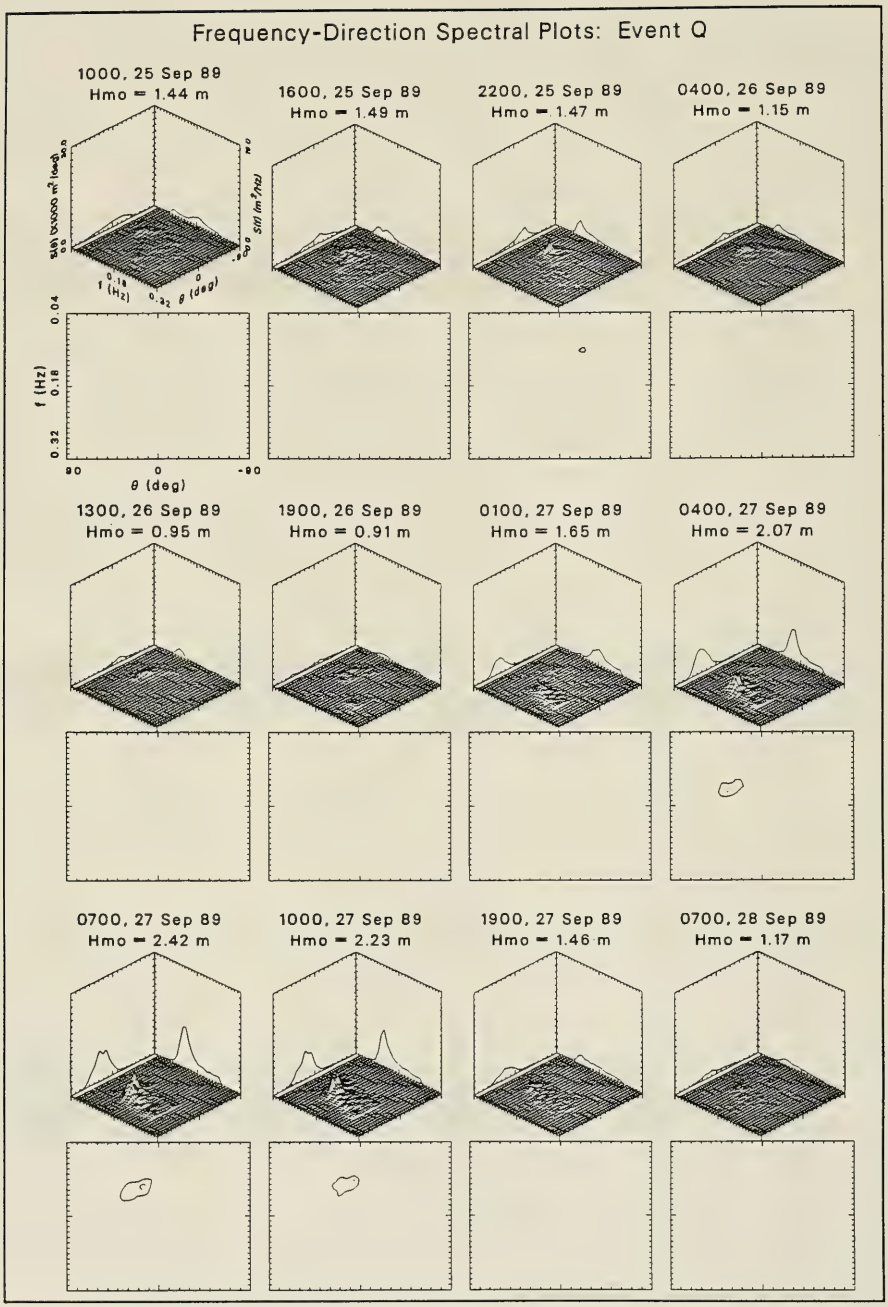
Frequency-Direction Spectral Plots: Event Q
1000, 25 Sep 89
Hmo = 1.44 m
1600, 25 Sep 89
Hmo = 1.49 m
2200, 25 Sep 89
Hmo = 1.47 m
0400, 26 Sep 89
Hmo = 1.15 m
1300, 26 Sep 89
Hmo = 0.95 m
1900, 26 Sep 89
Hmo = 0.91 m
0100, 27 Sep 89
Hmo = 1.65 m
0400, 27 Sep 89
Hmo = 2.07 m
0700, 27 Sep 89
Hmo = 2.42 m
1000, 27 Sep 89
Hmo = 2.23 m
1900, 27 Sep 89
Hmo = 1.46 m
0700, 28 Sep 89
Hmo = 1.17 m
f (Hz)
0.04
0.18
0.32
90
0
-90
θ (deg)

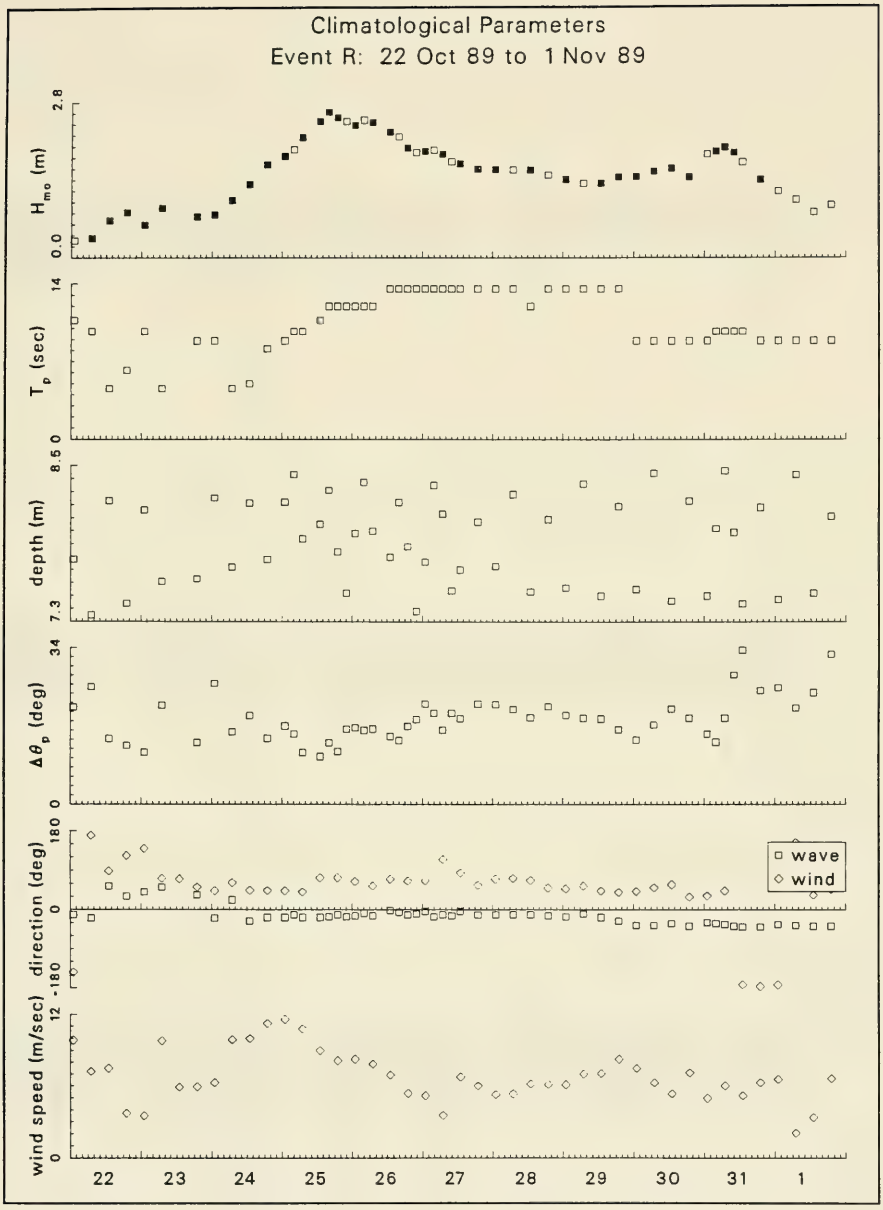
Climatological Parameters
Event R: 22 Oct 89 to 1 Nov 89
H_{mo} (m)
2.8
0.0
T_p (sec)
14
0
depth (m)
8.5
7.3
$\Delta\theta_p$ (deg)
34
0
direction (deg)
180
0
-180
wave
wind
wind speed (m/sec)
12
0
22
23
24
25
26
27
28
29
30
31
1

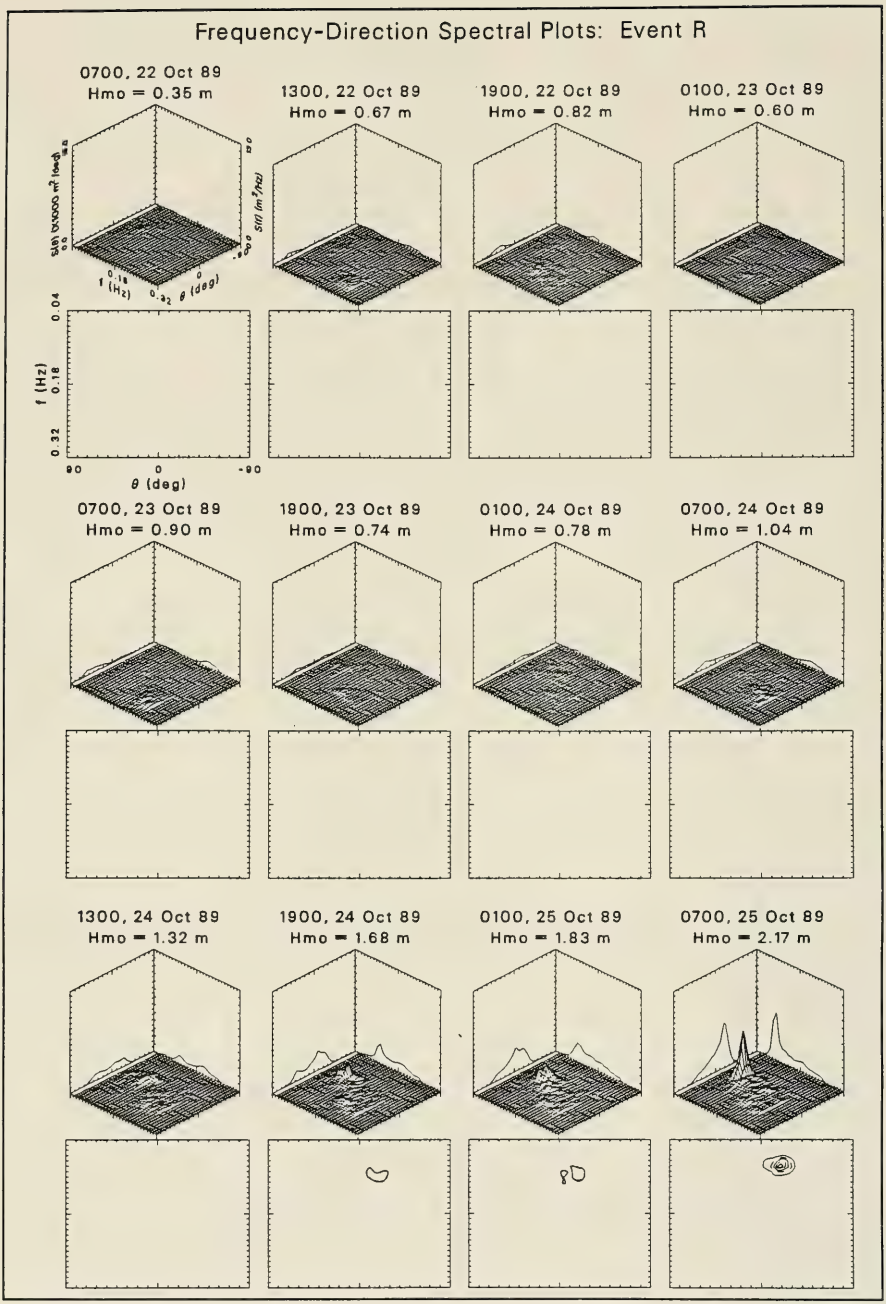
Frequency-Direction Spectral Plots: Event R
0700, 22 Oct 89
Hmo = 0.35 m
1300, 22 Oct 89
Hmo = 0.67 m
1900, 22 Oct 89
Hmo = 0.82 m
0100, 23 Oct 89
Hmo = 0.60 m
0700, 23 Oct 89
Hmo = 0.90 m
1900, 23 Oct 89
Hmo = 0.74 m
0100, 24 Oct 89
Hmo = 0.78 m
0700, 24 Oct 89
Hmo = 1.04 m
1300, 24 Oct 89
Hmo = 1.32 m
1900, 24 Oct 89
Hmo = 1.68 m
0100, 25 Oct 89
Hmo = 1.83 m
0700, 25 Oct 89
Hmo = 2.17 m
f (Hz)
0.04
0.18
0.32
90
0
-90
θ (deg)

Frequency-Direction Spectral Plots: Event R

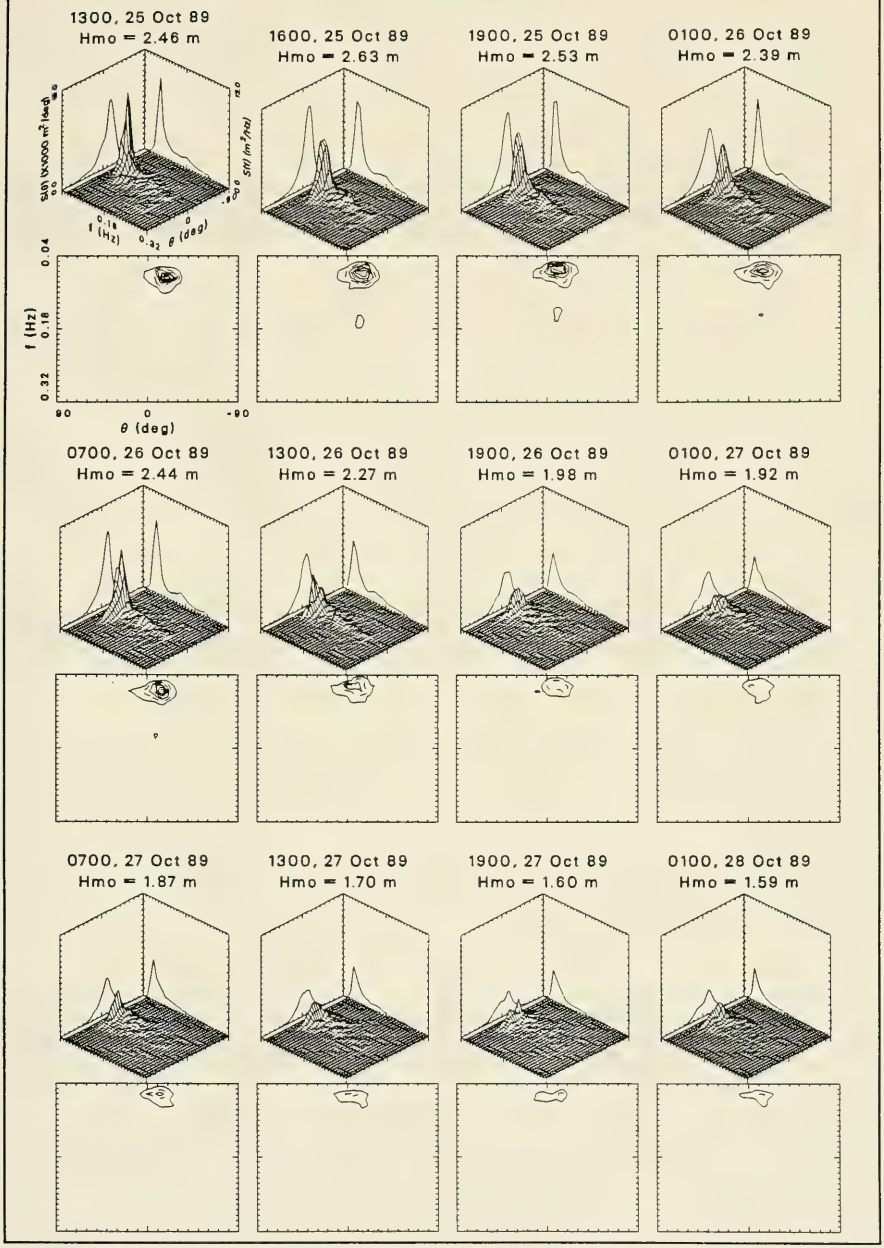

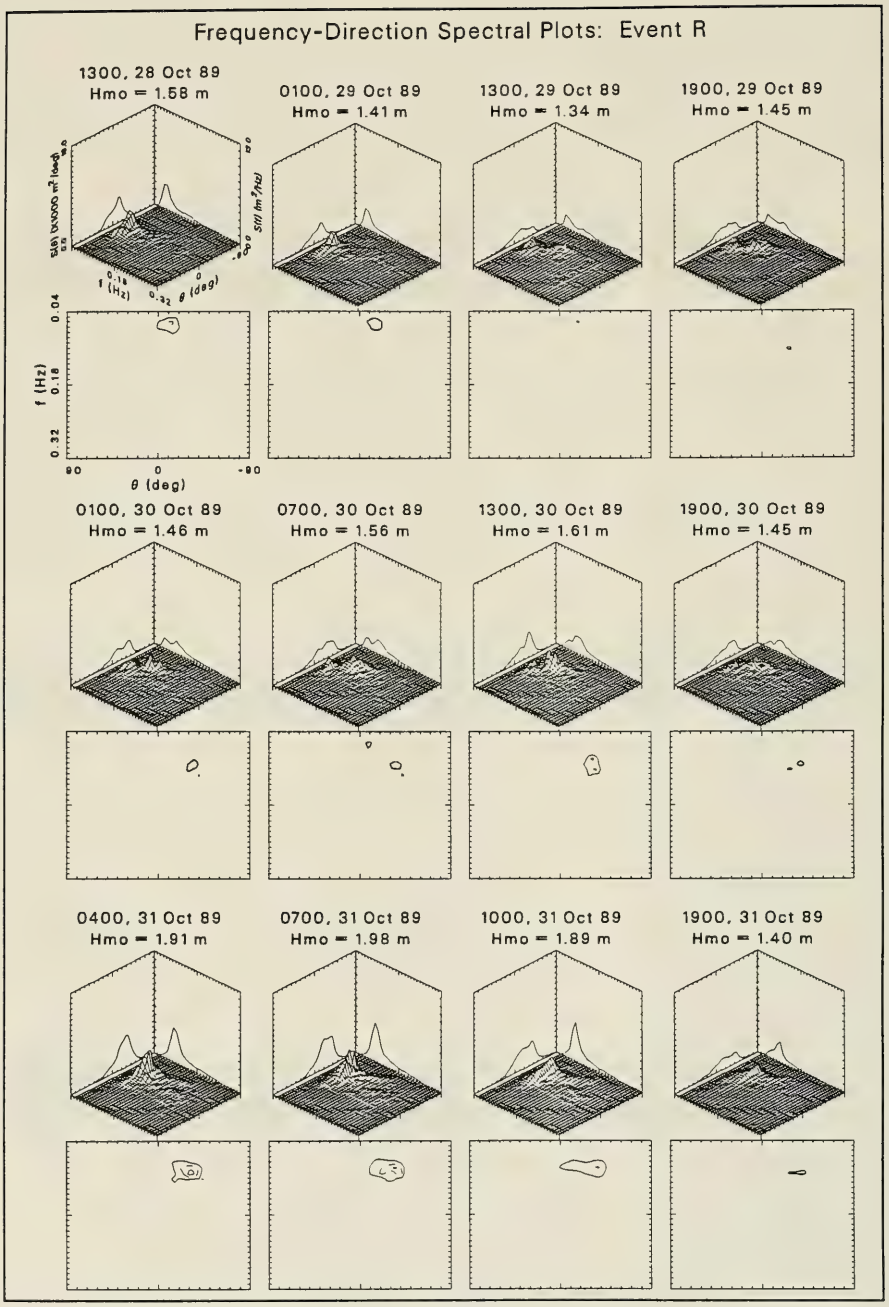
Frequency-Direction Spectral Plots: Event R
1300, 28 Oct 89
Hmo = 1.58 m
0100, 29 Oct 89
Hmo = 1.41 m
1300, 29 Oct 89
Hmo = 1.34 m
1900, 29 Oct 89
Hmo = 1.45 m
f (Hz)
0.04
0.18
0.32
90
0
-90
θ (deg)
0100, 30 Oct 89
Hmo = 1.46 m
0700, 30 Oct 89
Hmo = 1.56 m
1300, 30 Oct 89
Hmo = 1.61 m
1900, 30 Oct 89
Hmo = 1.45 m
0400, 31 Oct 89
Hmo = 1.91 m
0700, 31 Oct 89
Hmo = 1.98 m
1000, 31 Oct 89
Hmo = 1.89 m
1900, 31 Oct 89
Hmo = 1.40 m

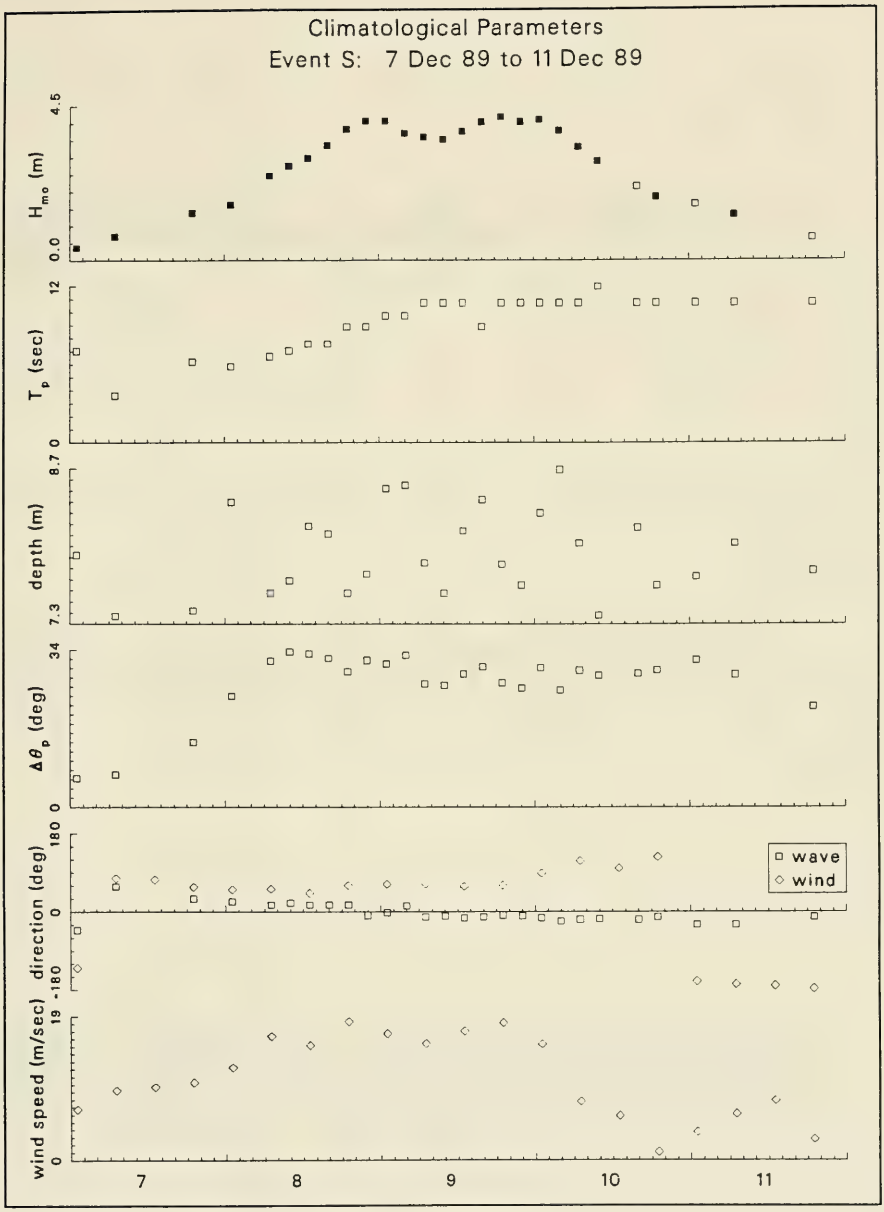
Climatological Parameters
Event S: 7 Dec 89 to 11 Dec 89
H_{mo} (m)
4.5
0.0
T_p (sec)
12
0
depth (m)
8.7
7.3
$\Delta\theta_p$ (deg)
34
0
direction (deg)
180
0
-180
wave
wind
wind speed (m/sec)
19
0
7
8
9
10
11

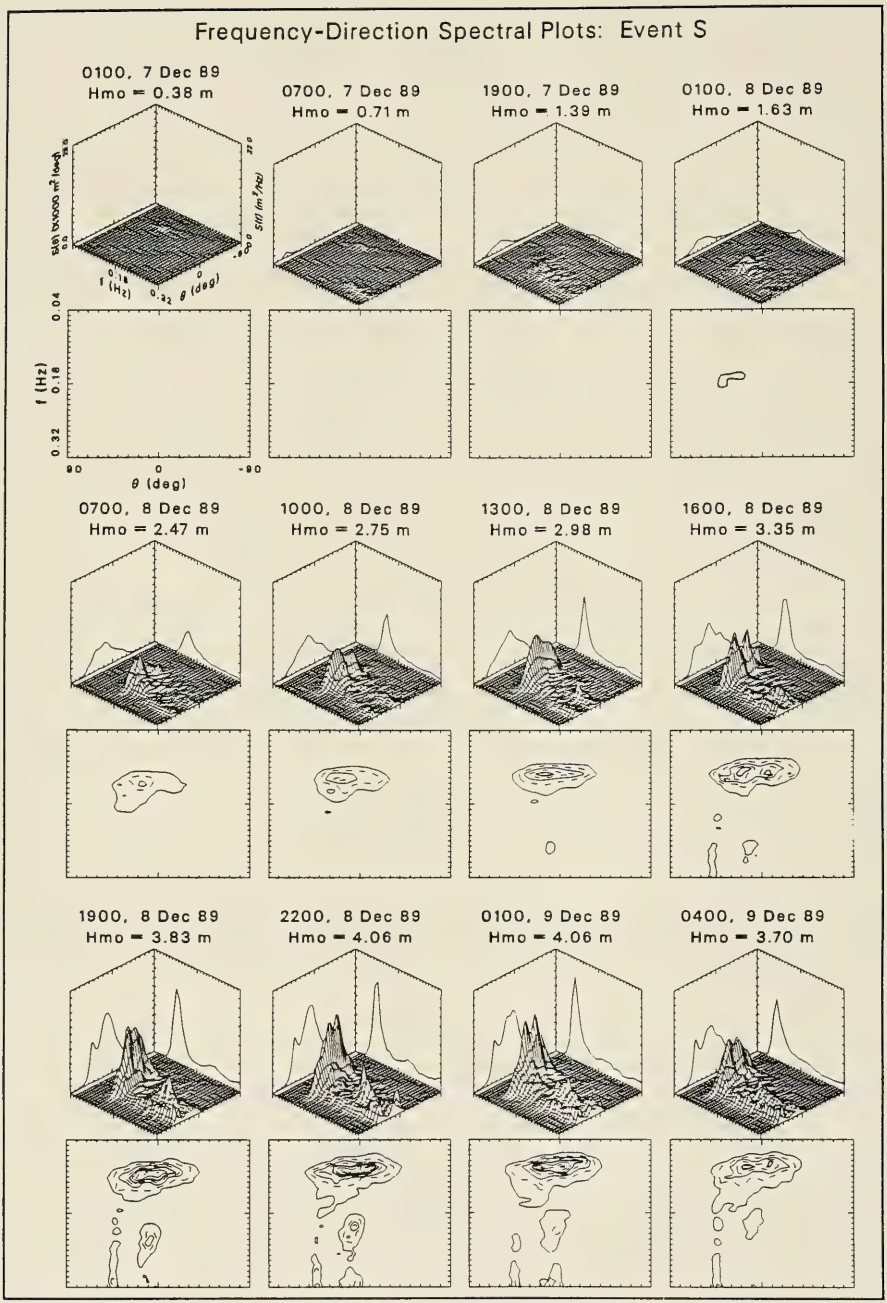
Frequency-Direction Spectral Plots: Event S
0100, 7 Dec 89
Hmo = 0.38 m
0700, 7 Dec 89
Hmo = 0.71 m
1900, 7 Dec 89
Hmo = 1.39 m
0100, 8 Dec 89
Hmo = 1.63 m
f (Hz)
0.04
0.16
0.32
90
0
-90
θ (deg)
0700, 8 Dec 89
Hmo = 2.47 m
1000, 8 Dec 89
Hmo = 2.75 m
1300, 8 Dec 89
Hmo = 2.98 m
1600, 8 Dec 89
Hmo = 3.35 m
1900, 8 Dec 89
Hmo = 3.83 m
2200, 8 Dec 89
Hmo = 4.06 m
0100, 9 Dec 89
Hmo = 4.06 m
0400, 9 Dec 89
Hmo = 3.70 m

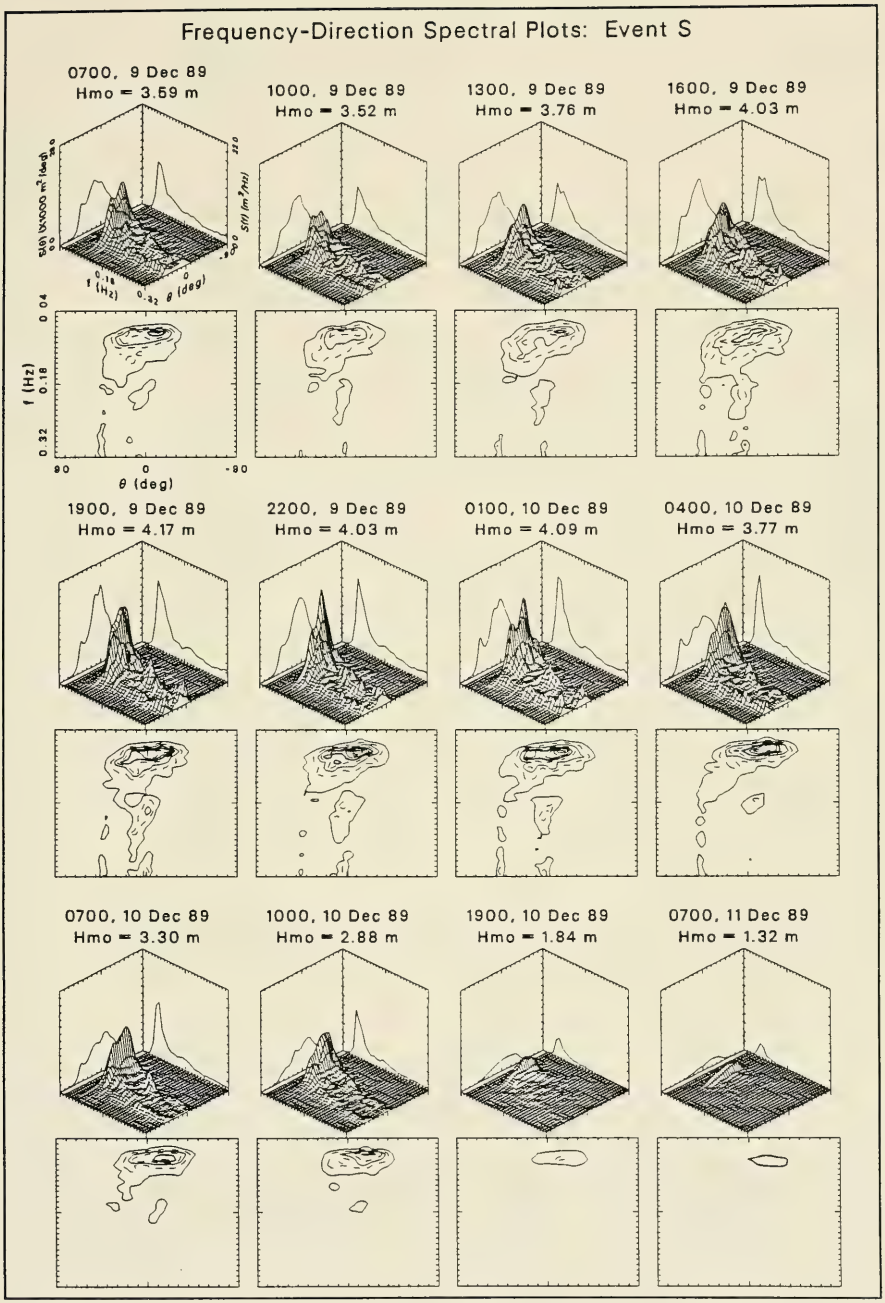
Frequency-Direction Spectral Plots: Event S
0700, 9 Dec 89
Hmo = 3.59 m
1000, 9 Dec 89
Hmo = 3.52 m
1300, 9 Dec 89
Hmo = 3.76 m
1600, 9 Dec 89
Hmo = 4.03 m
1900, 9 Dec 89
Hmo = 4.17 m
2200, 9 Dec 89
Hmo = 4.03 m
0100, 10 Dec 89
Hmo = 4.09 m
0400, 10 Dec 89
Hmo = 3.77 m
0700, 10 Dec 89
Hmo = 3.30 m
1000, 10 Dec 89
Hmo = 2.88 m
1900, 10 Dec 89
Hmo = 1.84 m
0700, 11 Dec 89
Hmo = 1.32 m
f (Hz)
0.04
0.18
0.32
90
0
-90
θ (deg)

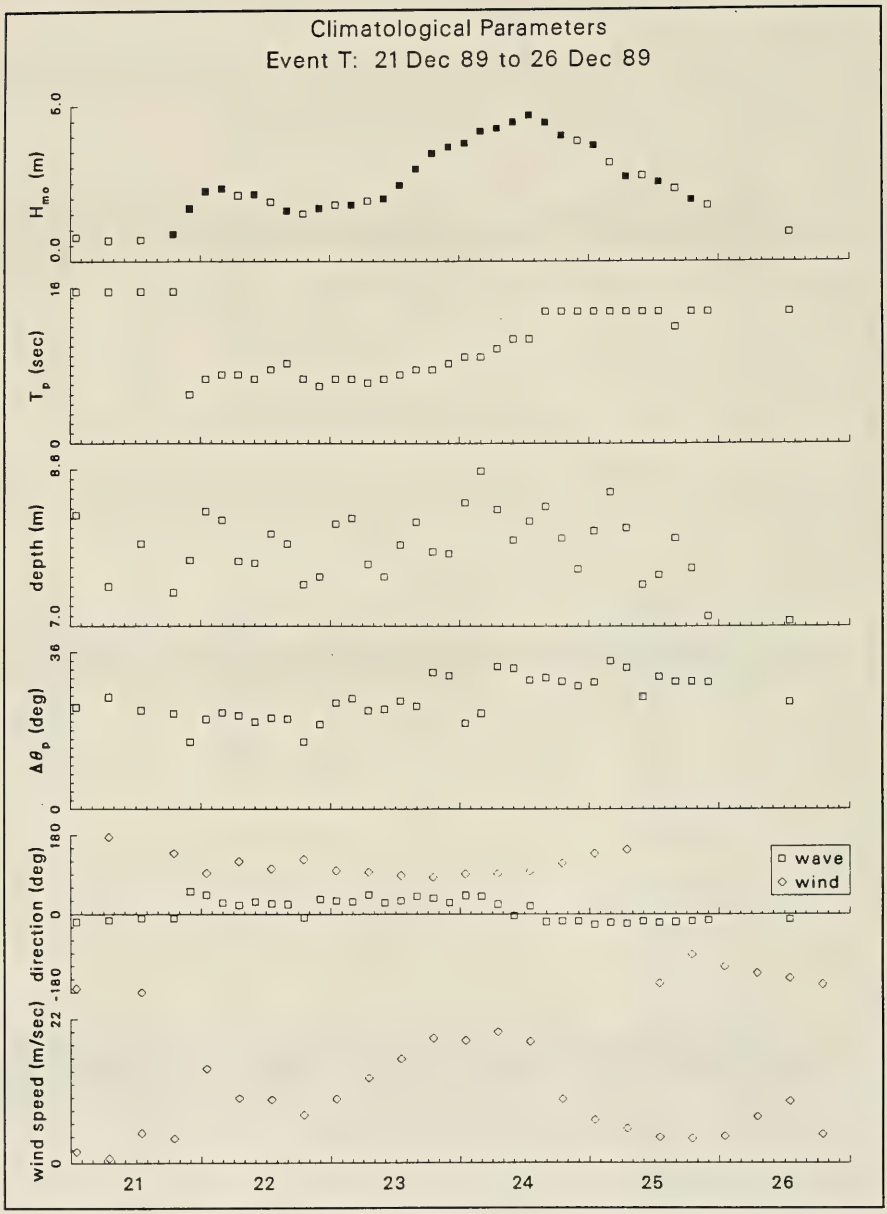
Climatological Parameters
Event T: 21 Dec 89 to 26 Dec 89
H_{mo} (m)
5.0
0.0
T_p (sec)
18
0
depth (m)
8.8
7.0
$\Delta\theta_p$ (deg)
36
0
direction (deg)
180
0
-180
wave
wind
wind speed (m/sec)
22
0
21
22
23
24
25
26

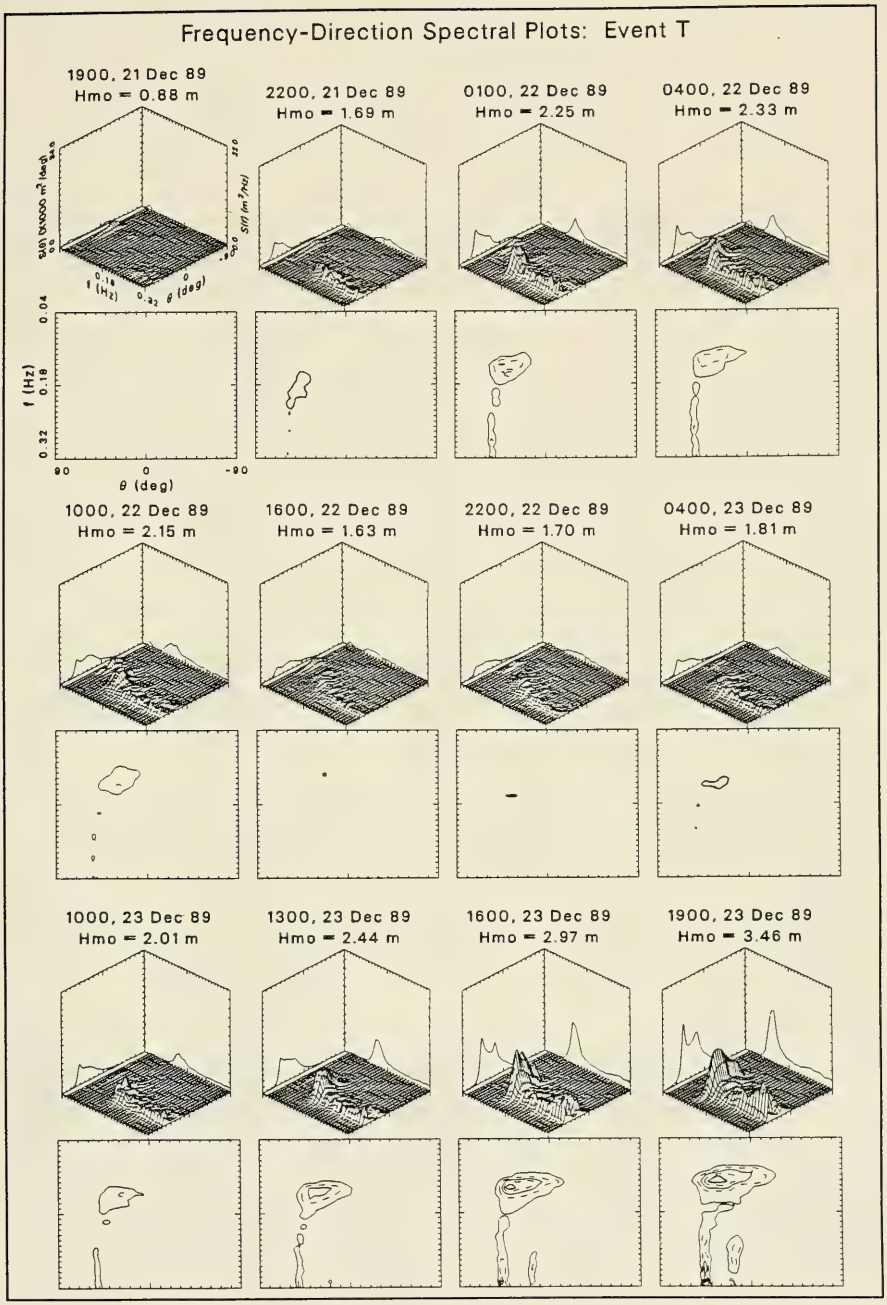
Frequency-Direction Spectral Plots: Event T
1900, 21 Dec 89
Hmo = 0.88 m
2200, 21 Dec 89
Hmo = 1.69 m
0100, 22 Dec 89
Hmo = 2.25 m
0400, 22 Dec 89
Hmo = 2.33 m
f (Hz)
0.04
0.18
0.32
90
0
-90
θ (deg)
1000, 22 Dec 89
Hmo = 2.15 m
1600, 22 Dec 89
Hmo = 1.63 m
2200, 22 Dec 89
Hmo = 1.70 m
0400, 23 Dec 89
Hmo = 1.81 m
1000, 23 Dec 89
Hmo = 2.01 m
1300, 23 Dec 89
Hmo = 2.44 m
1600, 23 Dec 89
Hmo = 2.97 m
1900, 23 Dec 89
Hmo = 3.46 m

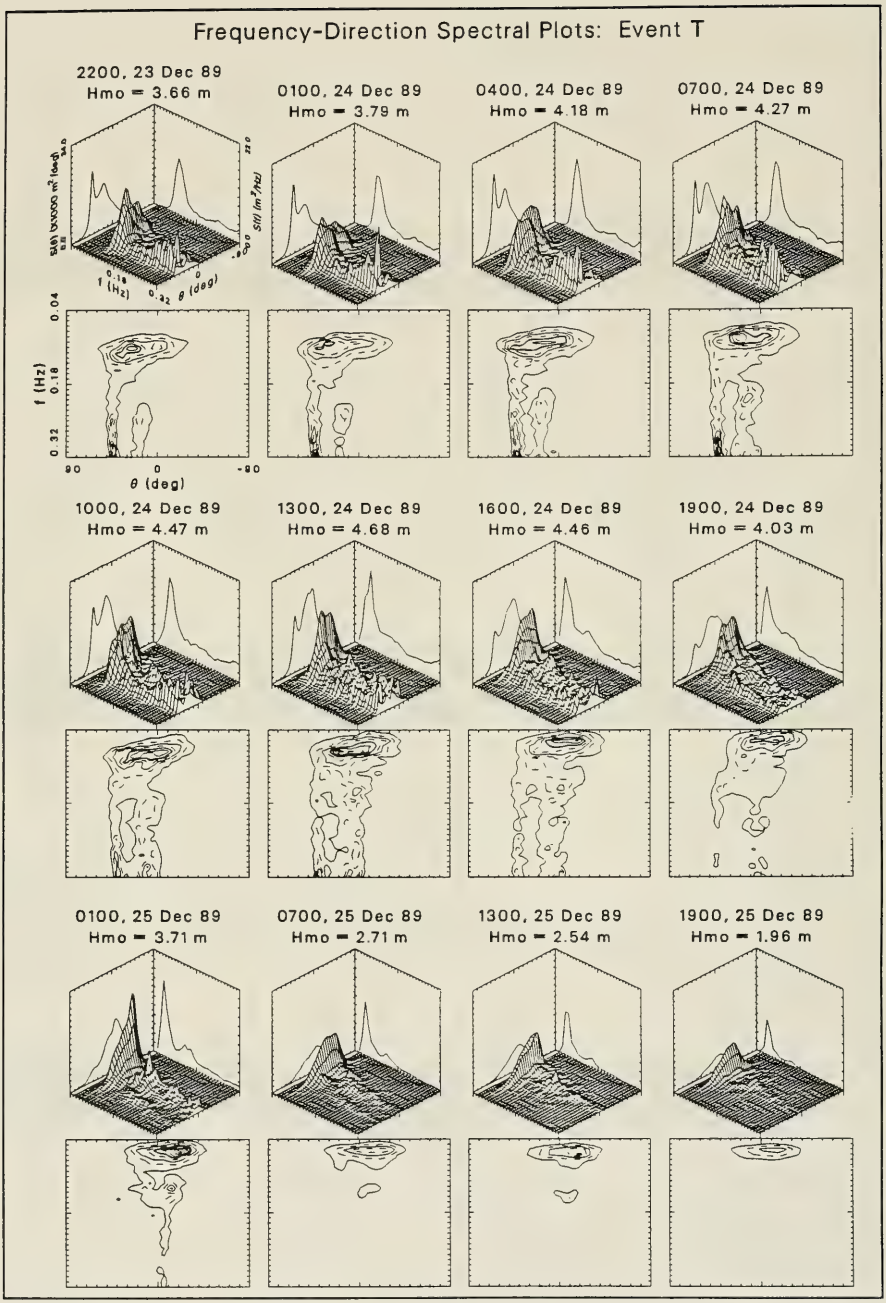
Frequency-Direction Spectral Plots: Event T
2200, 23 Dec 89
Hmo = 3.66 m
0100, 24 Dec 89
Hmo = 3.79 m
0400, 24 Dec 89
Hmo = 4.18 m
0700, 24 Dec 89
Hmo = 4.27 m
f (Hz)
0.04
0.18
0.32
90
0
-90
θ (deg)
1000, 24 Dec 89
Hmo = 4.47 m
1300, 24 Dec 89
Hmo = 4.68 m
1600, 24 Dec 89
Hmo = 4.46 m
1900, 24 Dec 89
Hmo = 4.03 m
0100, 25 Dec 89
Hmo = 3.71 m
0700, 25 Dec 89
Hmo = 2.71 m
1300, 25 Dec 89
Hmo = 2.54 m
1900, 25 Dec 89
Hmo = 1.96 m

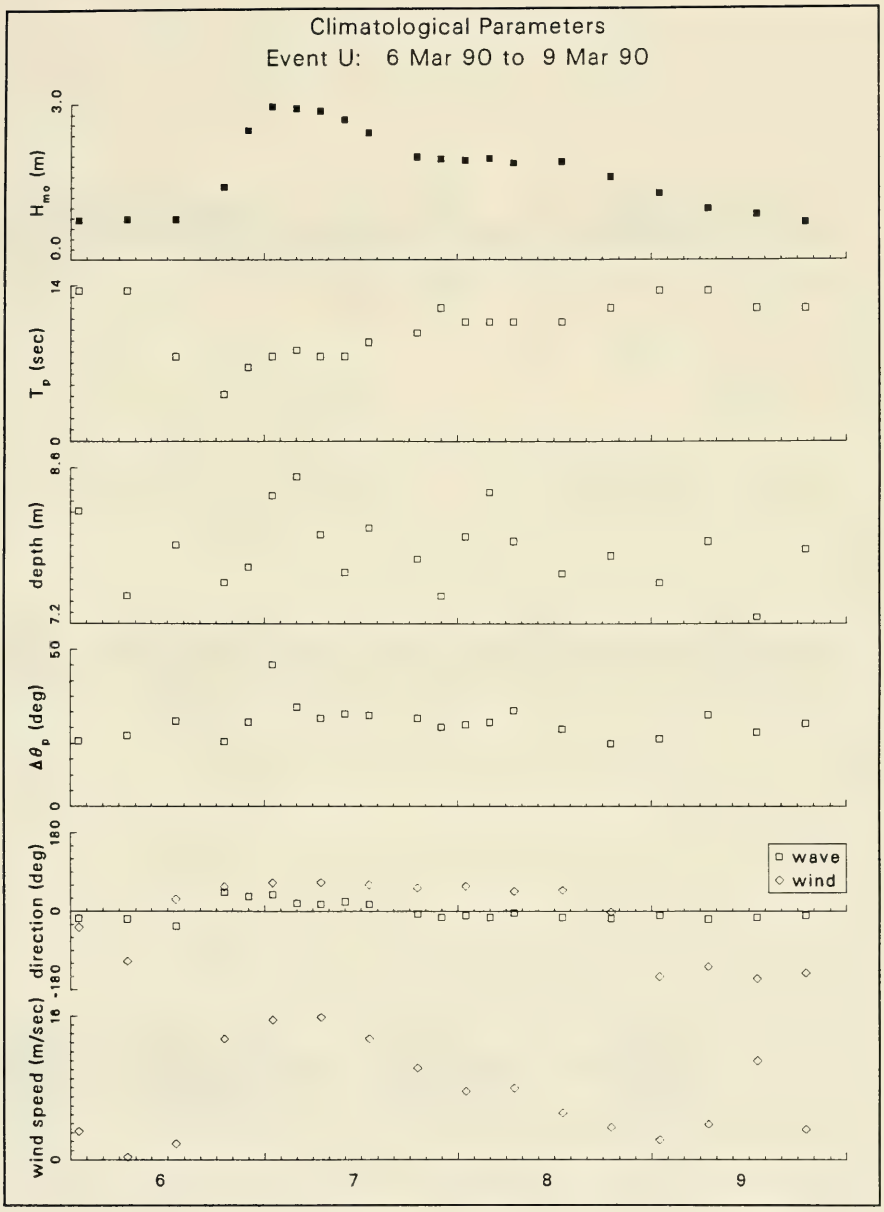
Climatological Parameters
Event U: 6 Mar 90 to 9 Mar 90
H_{mo} (m)
3.0
0.0
T_p (sec)
14
0
depth (m)
8.6
7.2
$\Delta\theta_p$ (deg)
50
0
direction (deg)
180
0
-180
wave
wind
wind speed (m/sec)
16
0
6
7
8
9

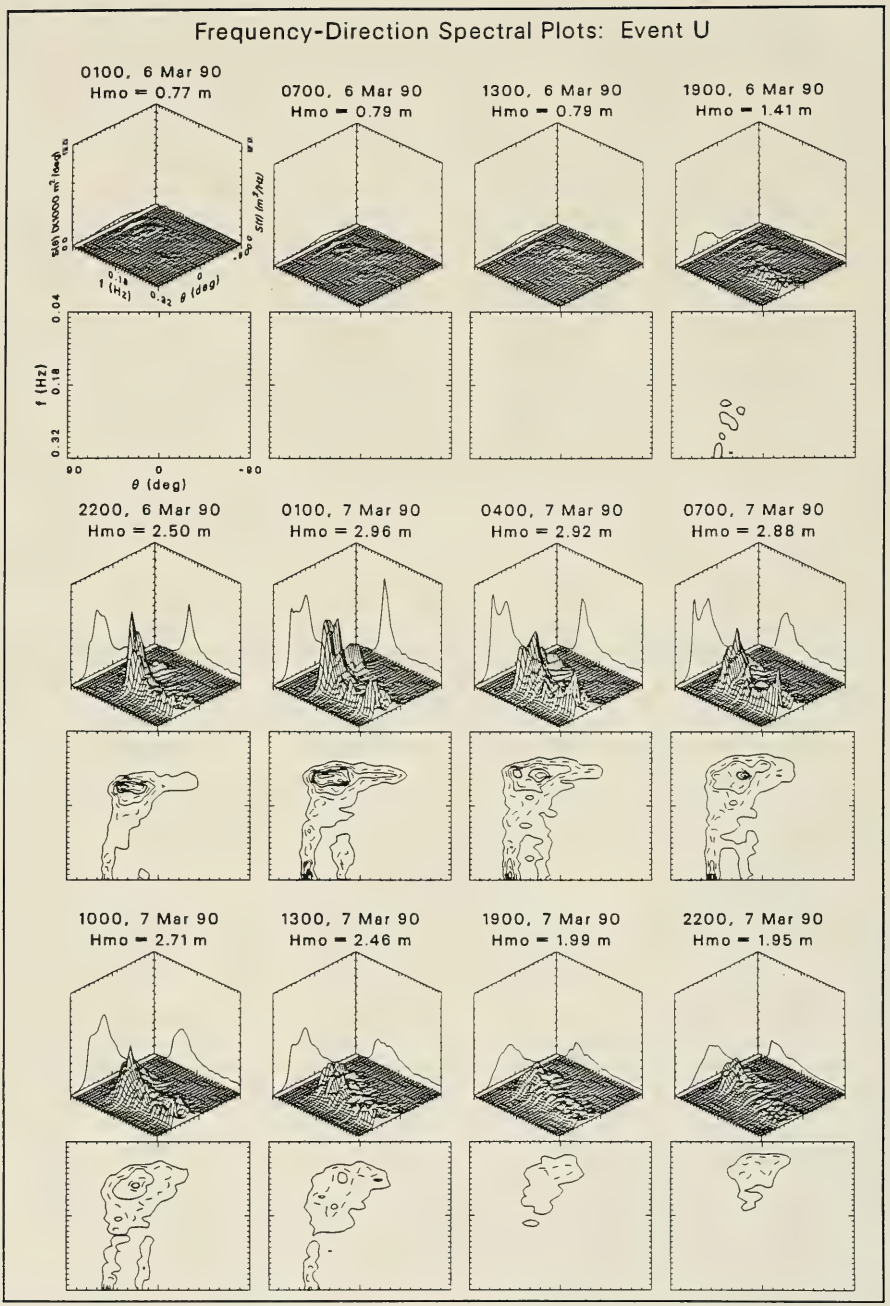
Frequency-Direction Spectral Plots: Event U
0100, 6 Mar 90
Hmo = 0.77 m
0700, 6 Mar 90
Hmo = 0.79 m
1300, 6 Mar 90
Hmo = 0.79 m
1900, 6 Mar 90
Hmo = 1.41 m
f (Hz)
0.04
0.18
0.32
90
0
-90
θ (deg)
2200, 6 Mar 90
Hmo = 2.50 m
0100, 7 Mar 90
Hmo = 2.96 m
0400, 7 Mar 90
Hmo = 2.92 m
0700, 7 Mar 90
Hmo = 2.88 m
1000, 7 Mar 90
Hmo = 2.71 m
1300, 7 Mar 90
Hmo = 2.46 m
1900, 7 Mar 90
Hmo = 1.99 m
2200, 7 Mar 90
Hmo = 1.95 m

Frequency-Direction Spectral Plots: Event U

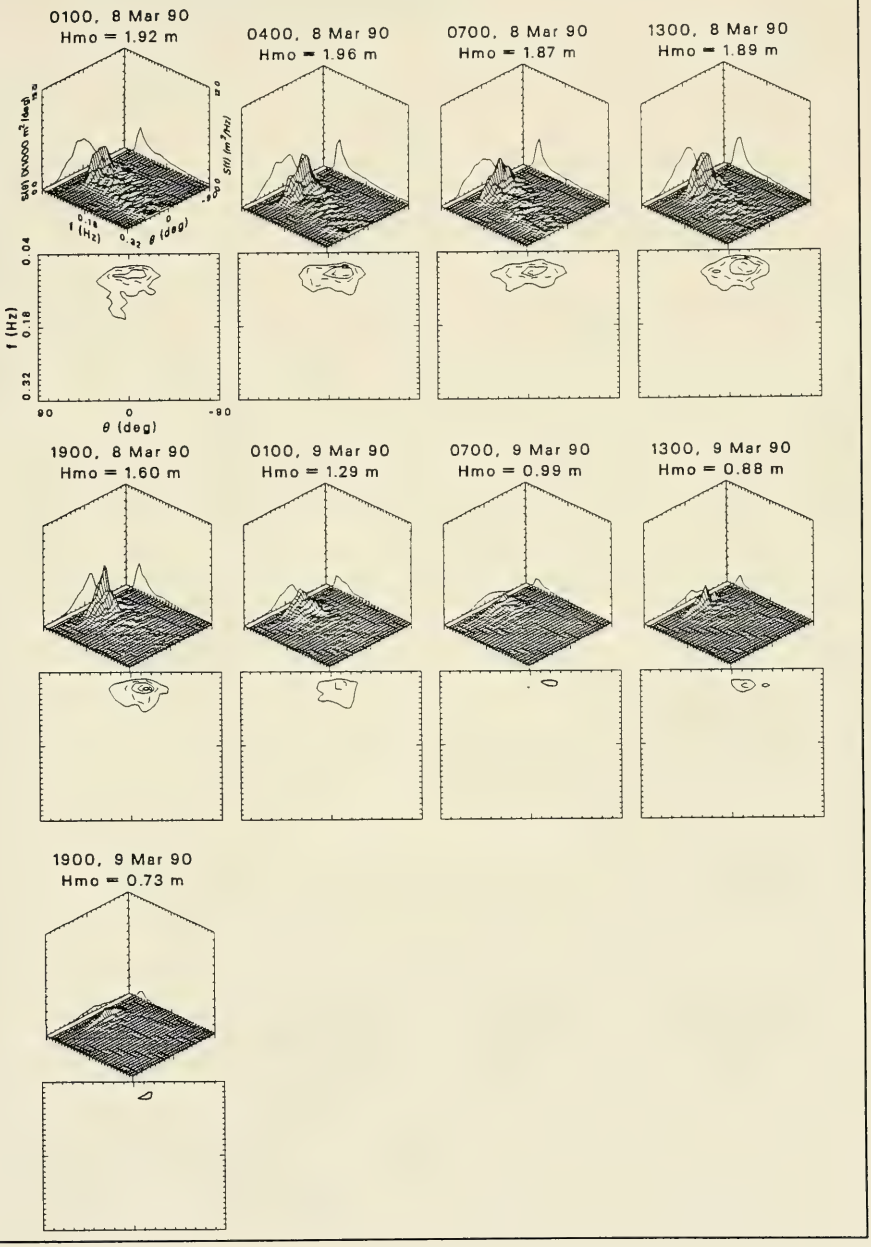

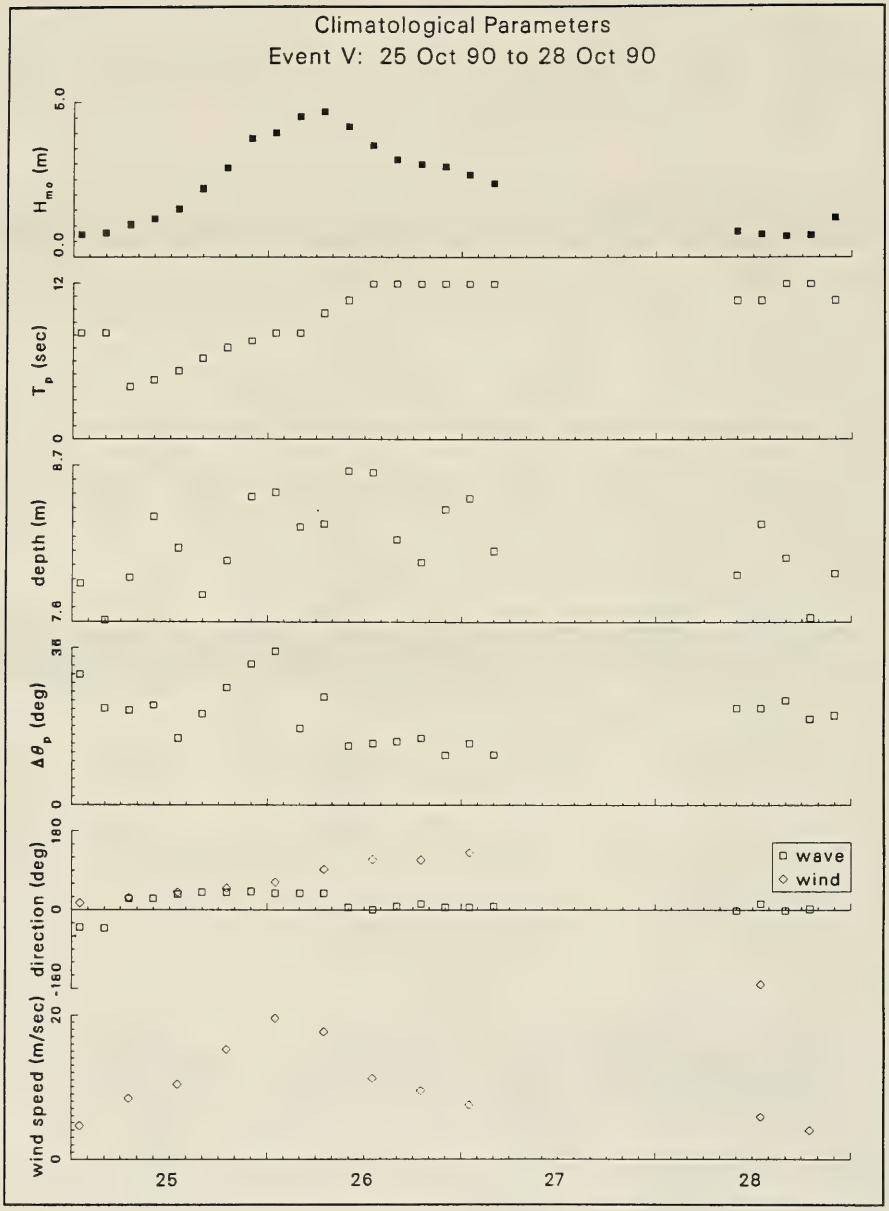
Climatological Parameters
Event V: 25 Oct 90 to 28 Oct 90
H_{mo} (m)
6.0
0.0
T_p (sec)
12
0
depth (m)
8.7
7.8
$\Delta\theta_p$ (deg)
360
0
wave direction (deg)
180
0
-180
wave
wind
wind speed (m/sec)
20
0
25
26
27
28

Frequency-Direction Spectral Plots: Event V

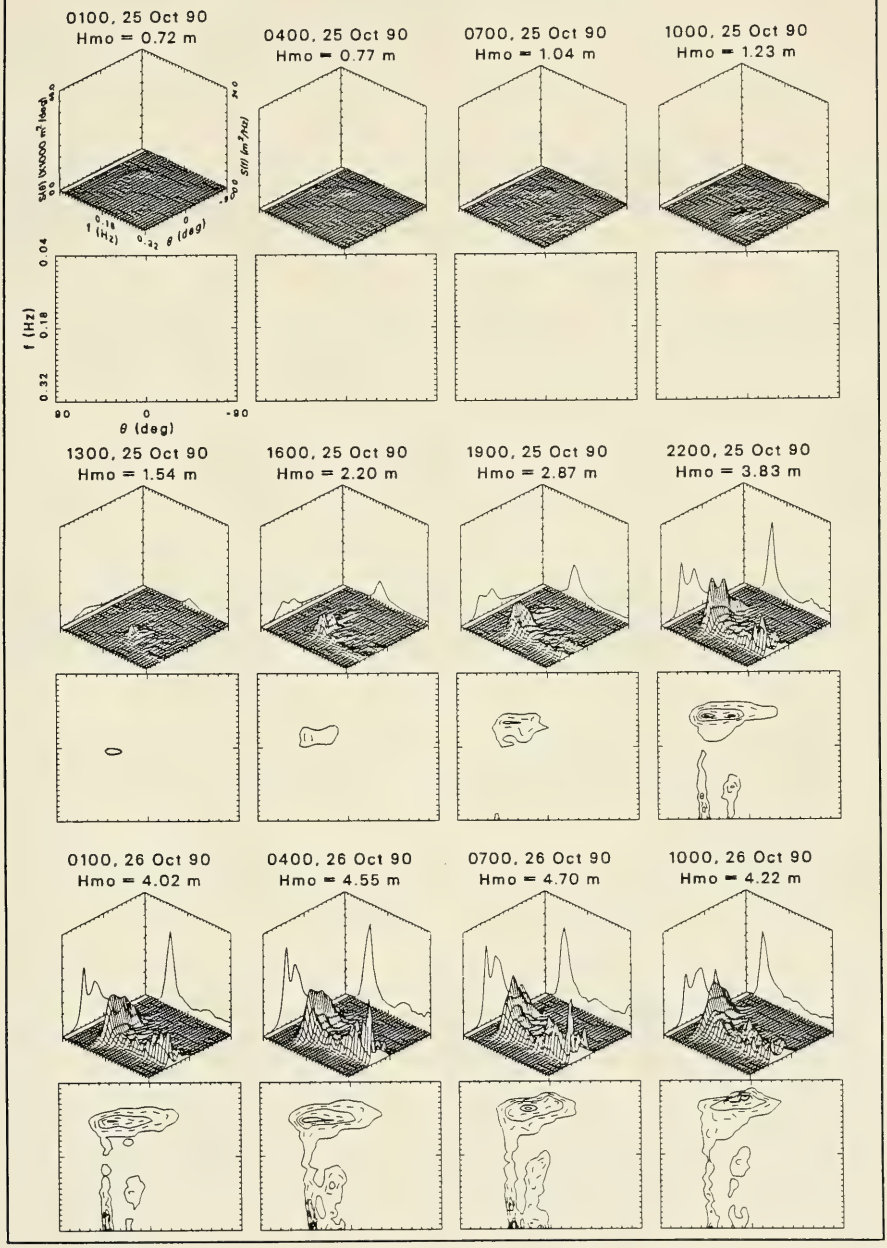

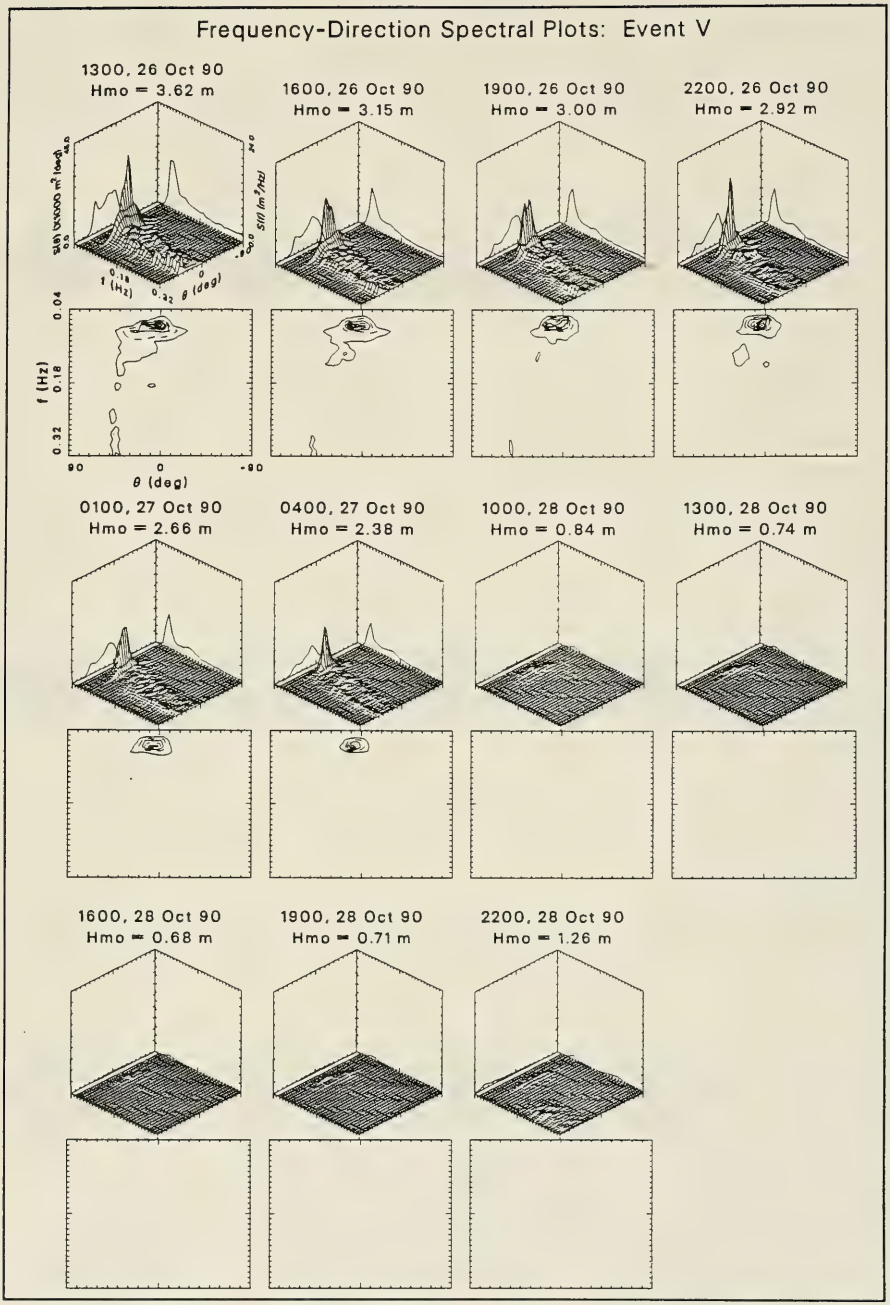
Frequency-Direction Spectral Plots: Event V
1300, 26 Oct 90
Hmo = 3.62 m
1600, 26 Oct 90
Hmo = 3.15 m
1900, 26 Oct 90
Hmo = 3.00 m
2200, 26 Oct 90
Hmo = 2.92 m
f (Hz)
0.04
0.18
0.32
90
0
-90
θ (deg)
0100, 27 Oct 90
Hmo = 2.66 m
0400, 27 Oct 90
Hmo = 2.38 m
1000, 28 Oct 90
Hmo = 0.84 m
1300, 28 Oct 90
Hmo = 0.74 m
1600, 28 Oct 90
Hmo = 0.68 m
1900, 28 Oct 90
Hmo = 0.71 m
2200, 28 Oct 90
Hmo = 1.26 m

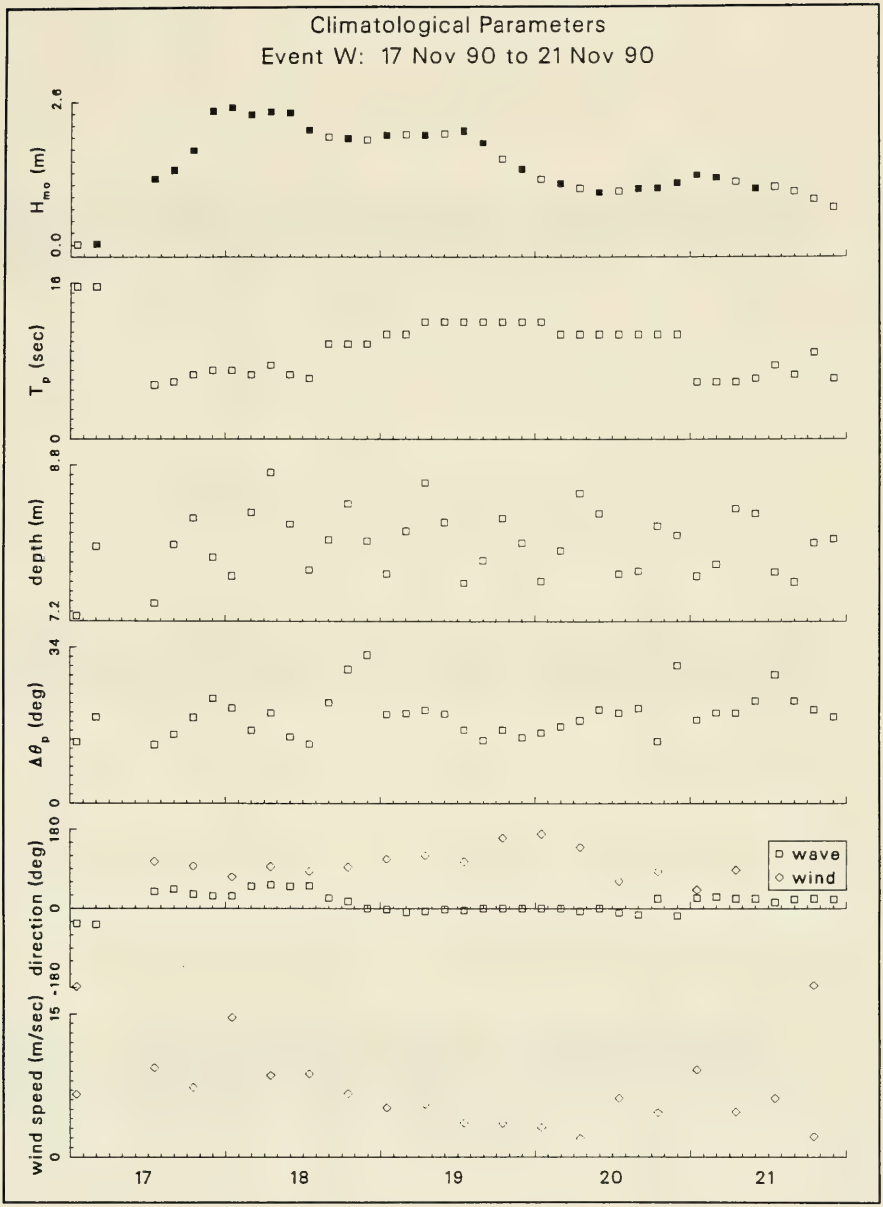
Climatological Parameters
Event W: 17 Nov 90 to 21 Nov 90
H_{mo} (m)
2.6
0.0
T_p (sec)
16
0
depth (m)
8.8
7.2
$\Delta\theta_p$ (deg)
34
0
direction (deg)
180
0
-180
wave
wind
wind speed (m/sec)
15
0
17
18
19
20
21

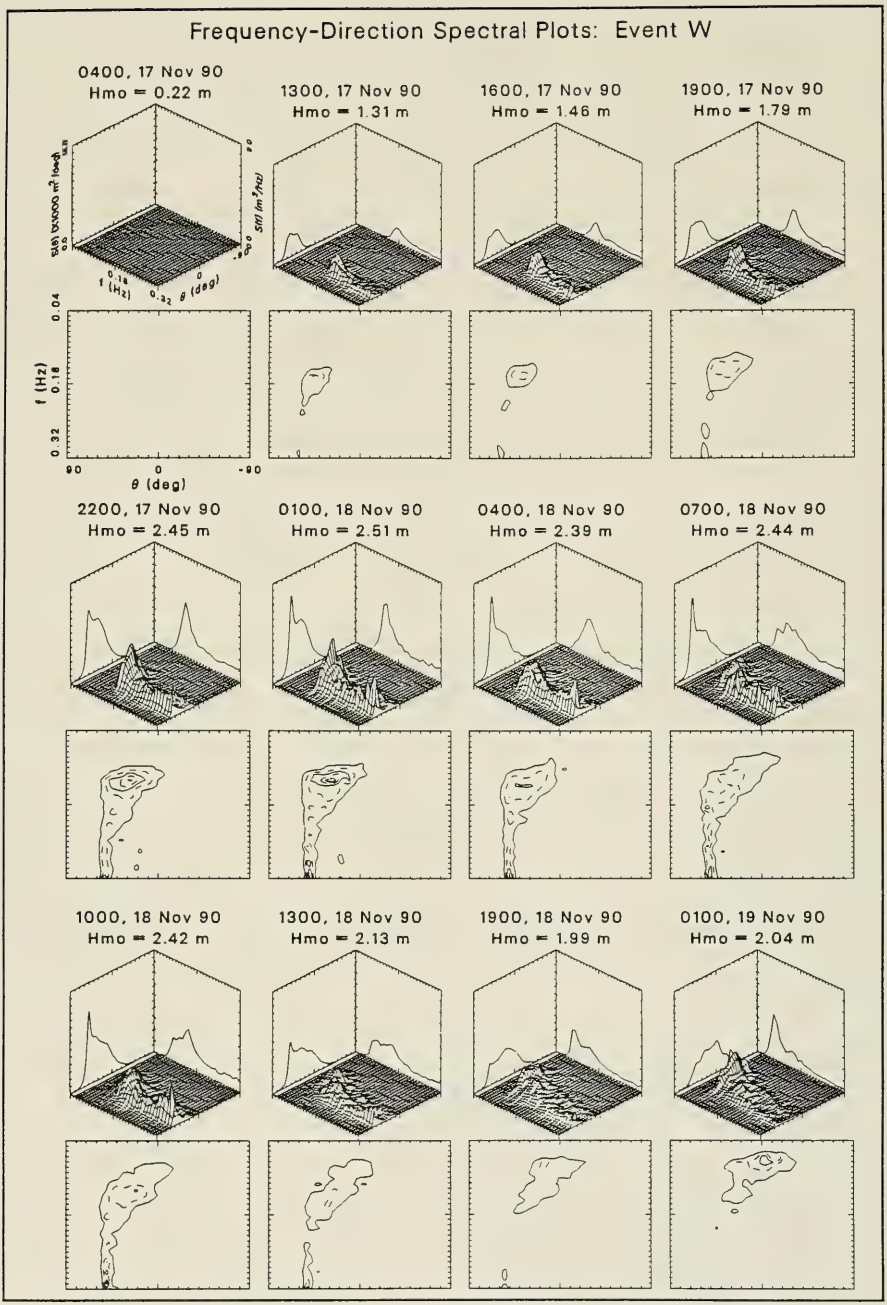
Frequency-Direction Spectral Plots: Event W
0400, 17 Nov 90
Hmo = 0.22 m
1300, 17 Nov 90
Hmo = 1.31 m
1600, 17 Nov 90
Hmo = 1.46 m
1900, 17 Nov 90
Hmo = 1.79 m
f (Hz)
0.04
0.18
0.32
90
0
-90
θ (deg)
2200, 17 Nov 90
Hmo = 2.45 m
0100, 18 Nov 90
Hmo = 2.51 m
0400, 18 Nov 90
Hmo = 2.39 m
0700, 18 Nov 90
Hmo = 2.44 m
1000, 18 Nov 90
Hmo = 2.42 m
1300, 18 Nov 90
Hmo = 2.13 m
1900, 18 Nov 90
Hmo = 1.99 m
0100, 19 Nov 90
Hmo = 2.04 m

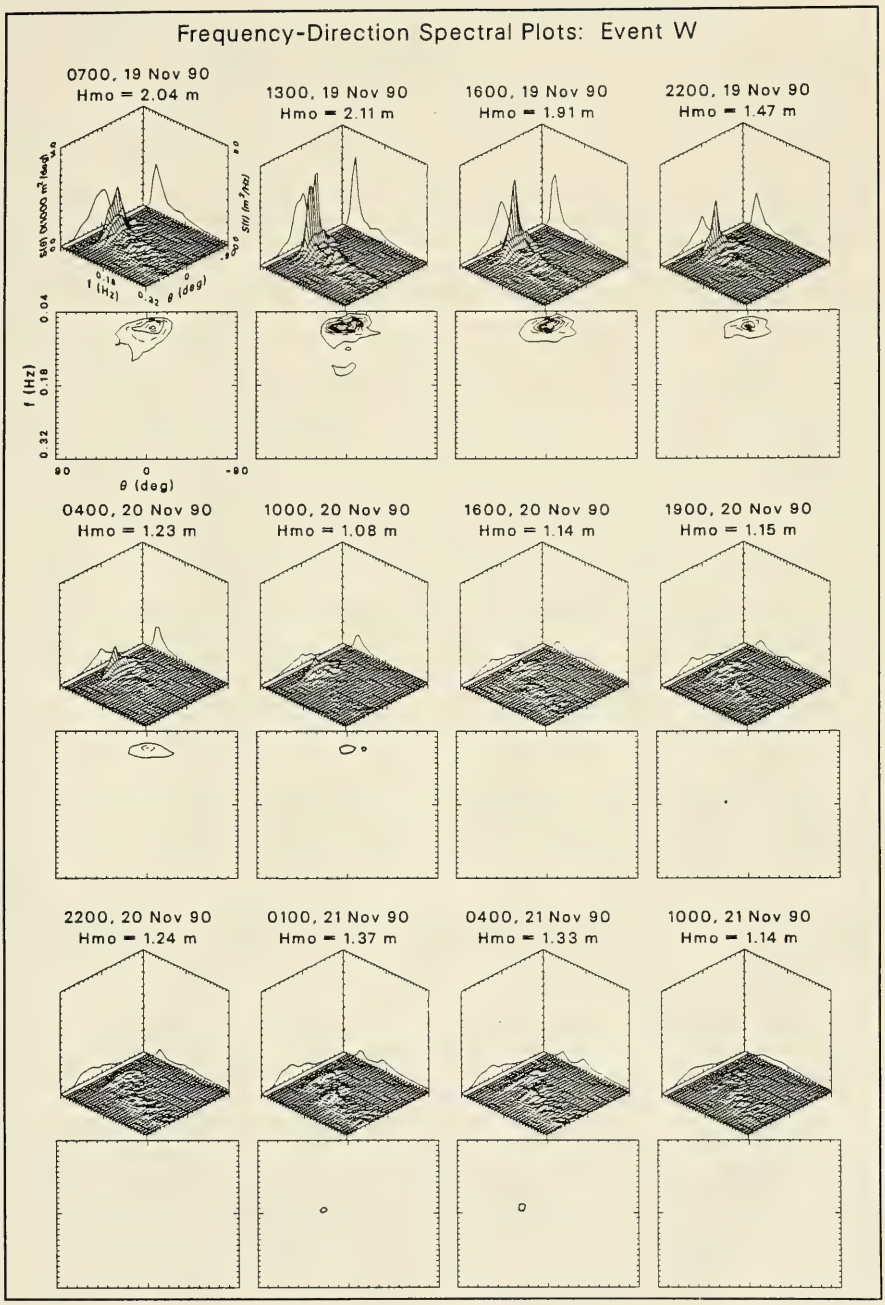
Frequency-Direction Spectral Plots: Event W
0700, 19 Nov 90
Hmo = 2.04 m
1300, 19 Nov 90
Hmo = 2.11 m
1600, 19 Nov 90
Hmo = 1.91 m
2200, 19 Nov 90
Hmo = 1.47 m
f (Hz)
0.04
0.18
0.32
90
0
-90
θ (deg)
0400, 20 Nov 90
Hmo = 1.23 m
1000, 20 Nov 90
Hmo = 1.08 m
1600, 20 Nov 90
Hmo = 1.14 m
1900, 20 Nov 90
Hmo = 1.15 m
2200, 20 Nov 90
Hmo = 1.24 m
0100, 21 Nov 90
Hmo = 1.37 m
0400, 21 Nov 90
Hmo = 1.33 m
1000, 21 Nov 90
Hmo = 1.14 m

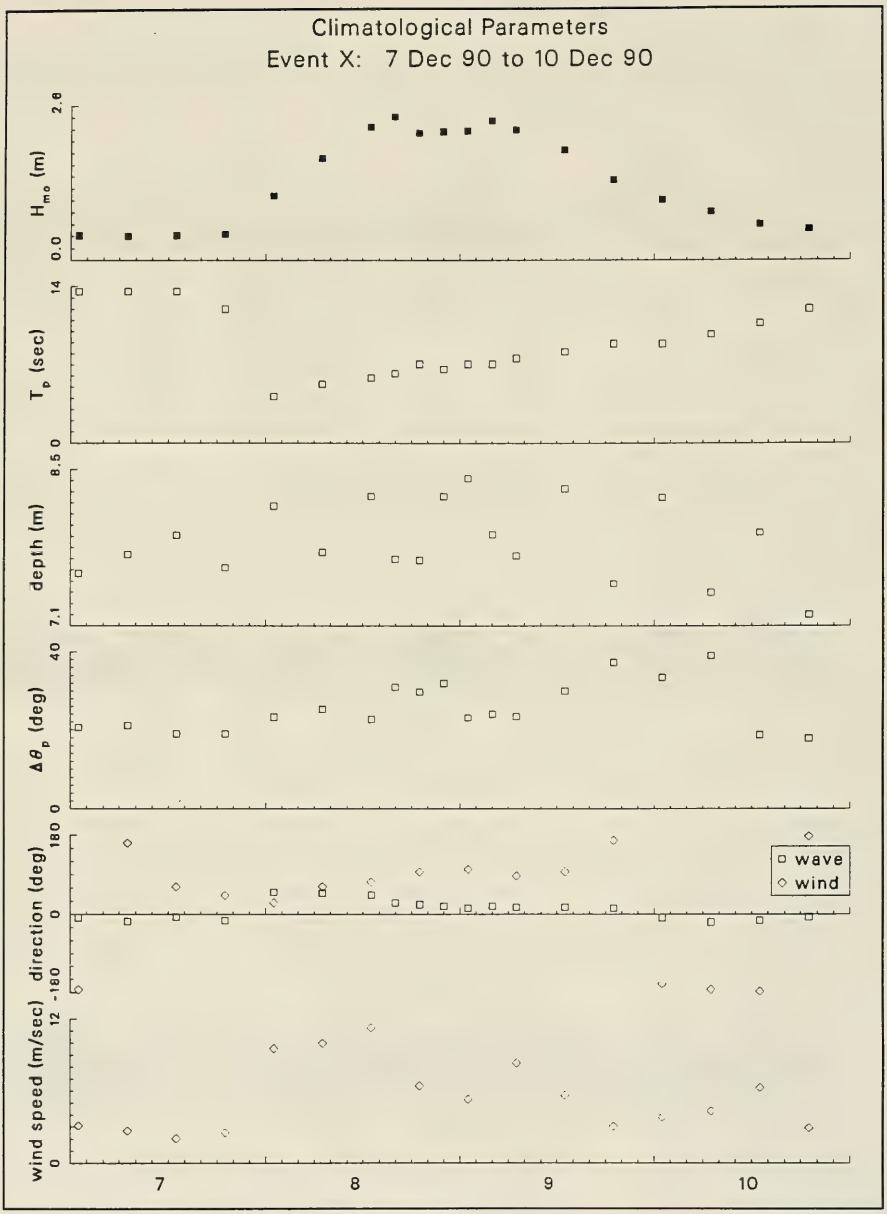
Climatological Parameters
Event X: 7 Dec 90 to 10 Dec 90
H_{mo} (m)
2.8
0.0
T_p (sec)
14
0
depth (m)
8.5
7.1
$\Delta\theta_p$ (deg)
40
0
direction (deg)
180
0
-180
wave
wind
wind speed (m/sec)
12
0
7
8
9
10

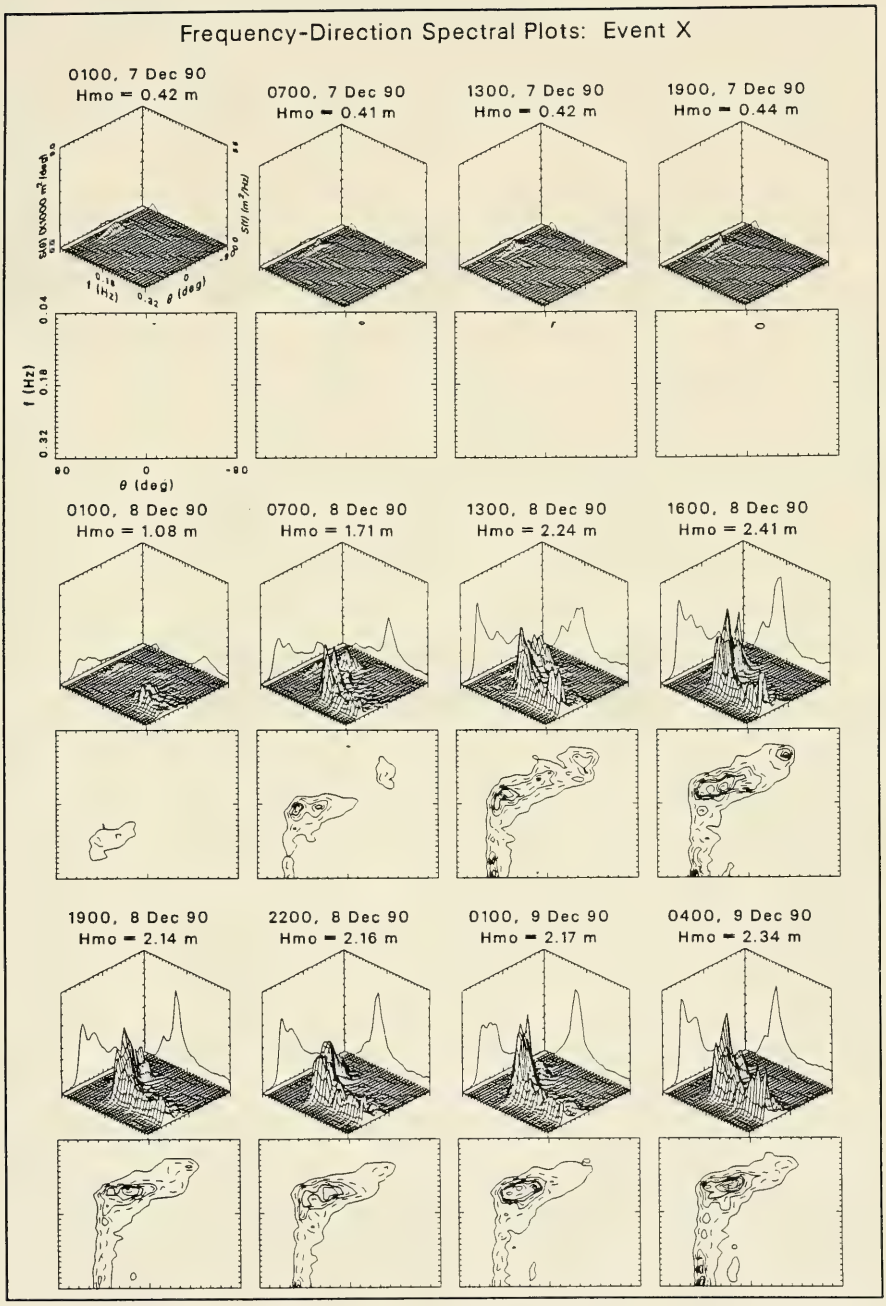
Frequency-Direction Spectral Plots: Event X
0100, 7 Dec 90
Hmo = 0.42 m
0700, 7 Dec 90
Hmo = 0.41 m
1300, 7 Dec 90
Hmo = 0.42 m
1900, 7 Dec 90
Hmo = 0.44 m
f (Hz)
0.04
0.18
0.32
90
0
-90
θ (deg)
0100, 8 Dec 90
Hmo = 1.08 m
0700, 8 Dec 90
Hmo = 1.71 m
1300, 8 Dec 90
Hmo = 2.24 m
1600, 8 Dec 90
Hmo = 2.41 m
1900, 8 Dec 90
Hmo = 2.14 m
2200, 8 Dec 90
Hmo = 2.16 m
0100, 9 Dec 90
Hmo = 2.17 m
0400, 9 Dec 90
Hmo = 2.34 m

Frequency-Direction Spectral Plots: Event X

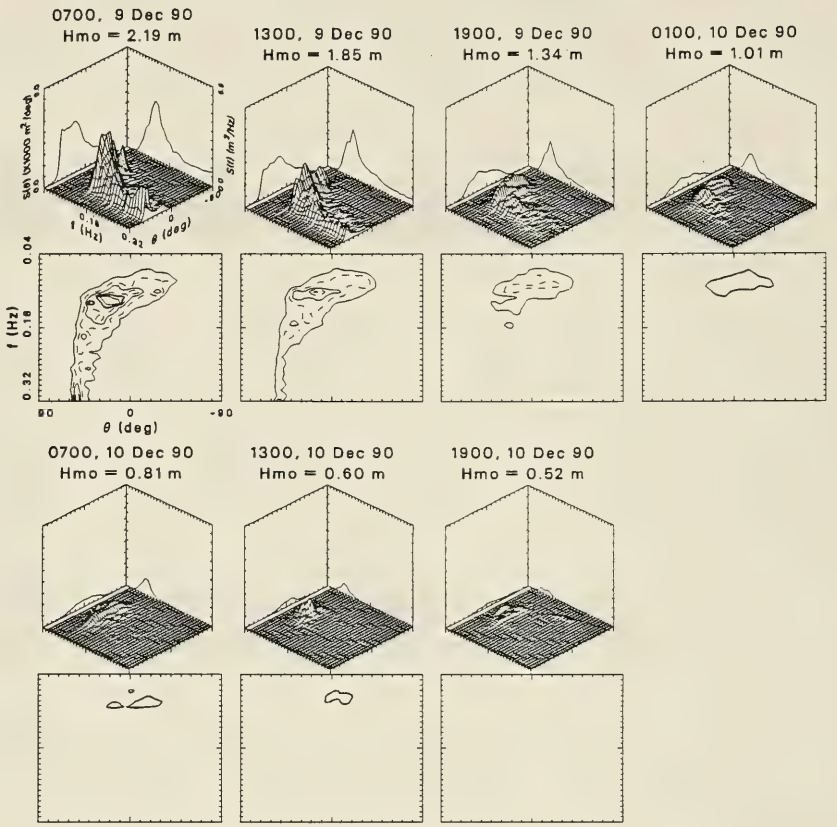

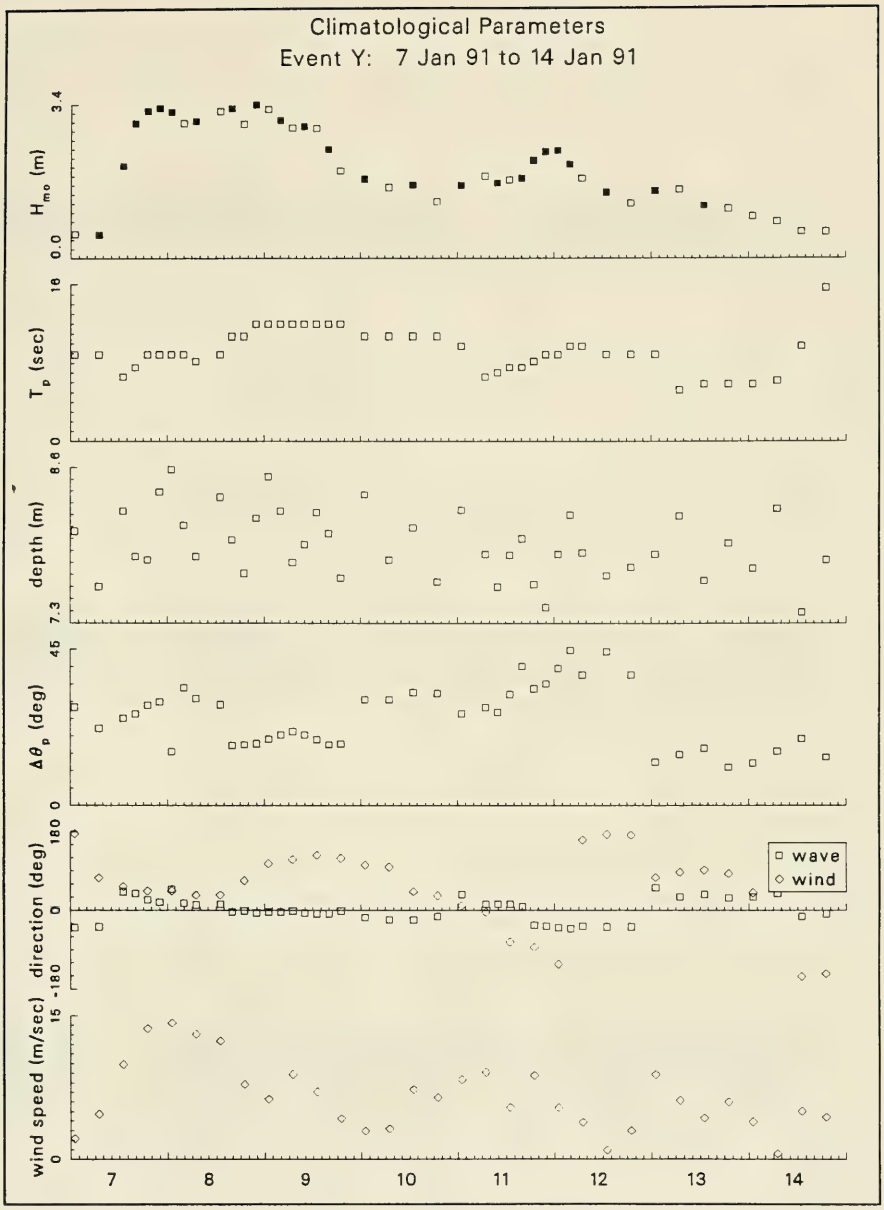
Climatological Parameters
Event Y: 7 Jan 91 to 14 Jan 91
H_{mo} (m)
3.4
0.0
T_p (sec)
18
8.6 0
depth (m)
7.3
$\Delta\theta_p$ (deg)
45
0
direction (deg)
180
0
-180
wave
wind
wind speed (m/sec)
15
0
7
8
9
10
11
12
13
14

Frequency-Direction Spectral Plots: Event Y

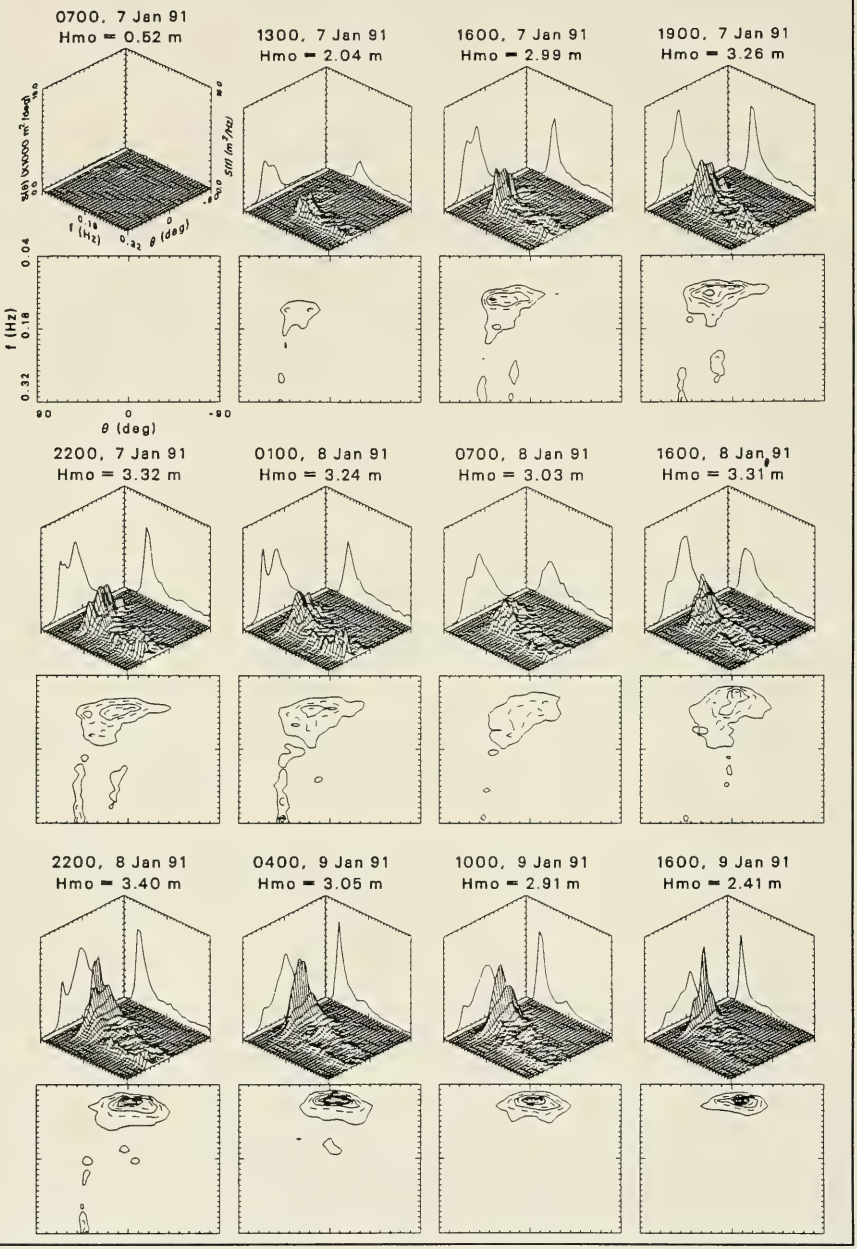

Frequency-Direction Spectral Plots: Event Y

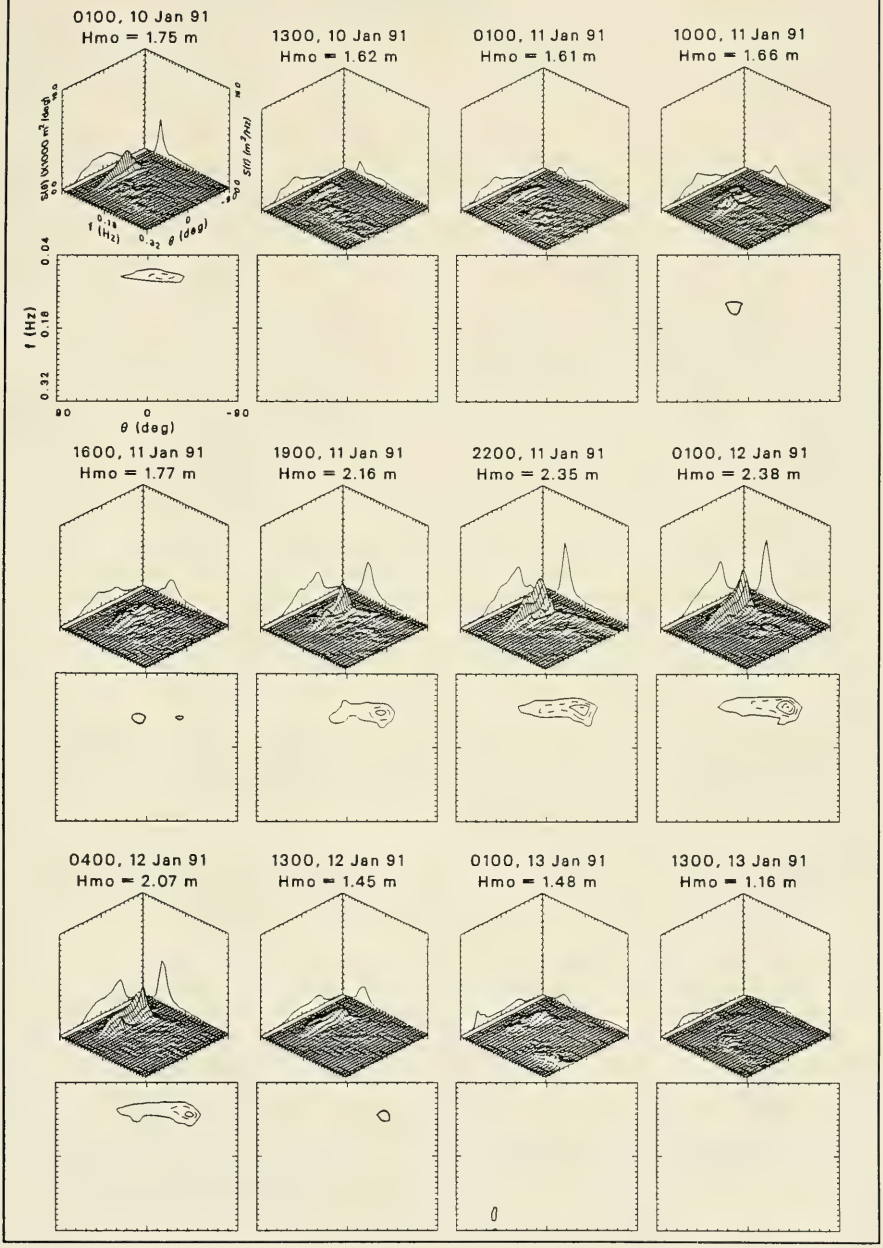

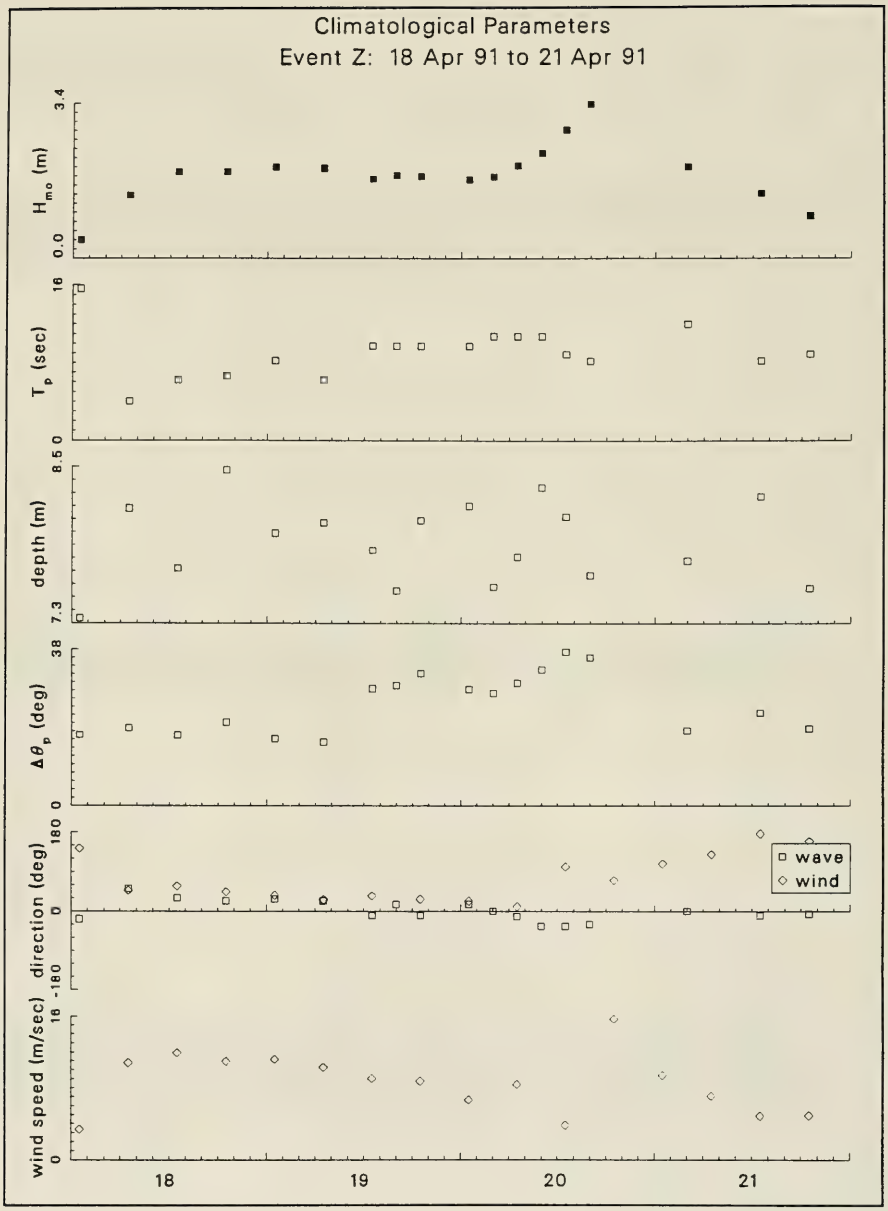
Climatological Parameters
Event Z: 18 Apr 91 to 21 Apr 91
H_{mo} (m)
3.4
0.0
T_p (sec)
16
0
depth (m)
8.5
7.3
$\Delta\theta_p$ (deg)
38
0
direction (deg)
180
0
-180
wave
wind
wind speed (m/sec)
16
0
18
19
20
21

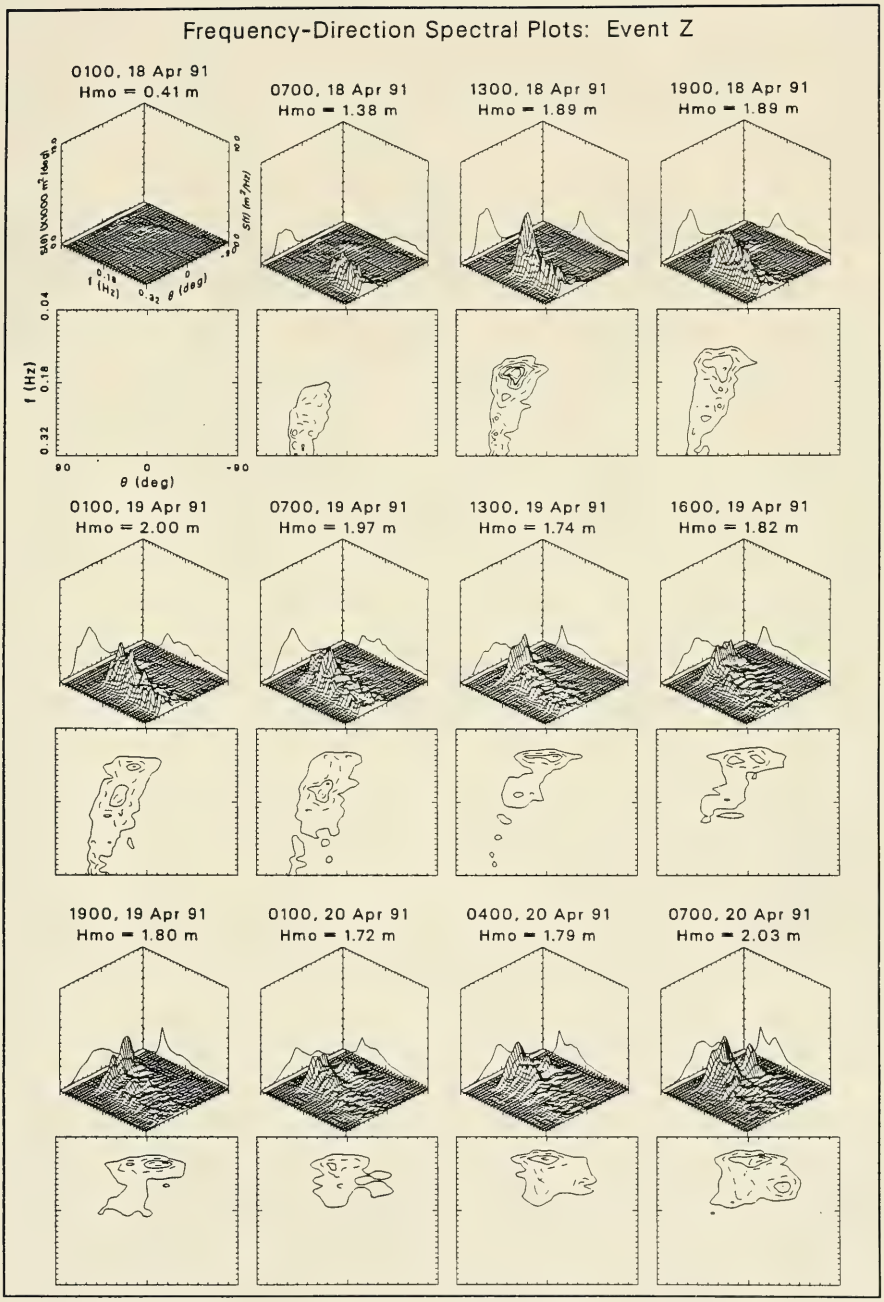
Frequency-Direction Spectral Plots: Event Z
0100, 18 Apr 91
Hmo = 0.41 m
0700, 18 Apr 91
Hmo = 1.38 m
1300, 18 Apr 91
Hmo = 1.89 m
1900, 18 Apr 91
Hmo = 1.89 m
f (Hz)
0.04
0.18
0.32
90
0
-90
θ (deg)
0100, 19 Apr 91
Hmo = 2.00 m
0700, 19 Apr 91
Hmo = 1.97 m
1300, 19 Apr 91
Hmo = 1.74 m
1600, 19 Apr 91
Hmo = 1.82 m
1900, 19 Apr 91
Hmo = 1.80 m
0100, 20 Apr 91
Hmo = 1.72 m
0400, 20 Apr 91
Hmo = 1.79 m
0700, 20 Apr 91
Hmo = 2.03 m

Frequency-Direction Spectral Plots: Event Z

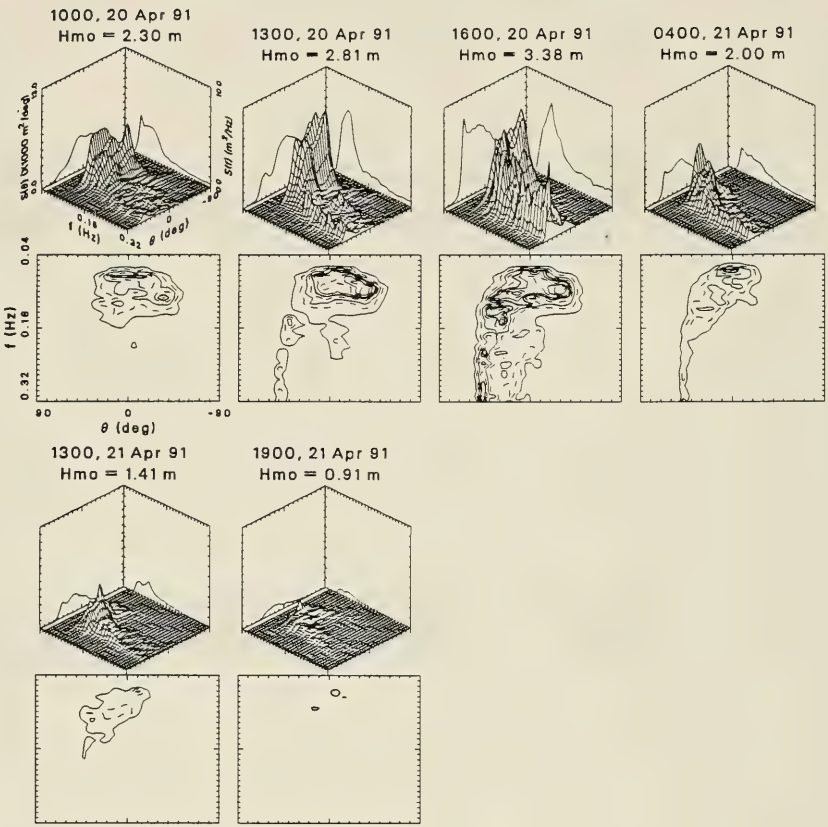

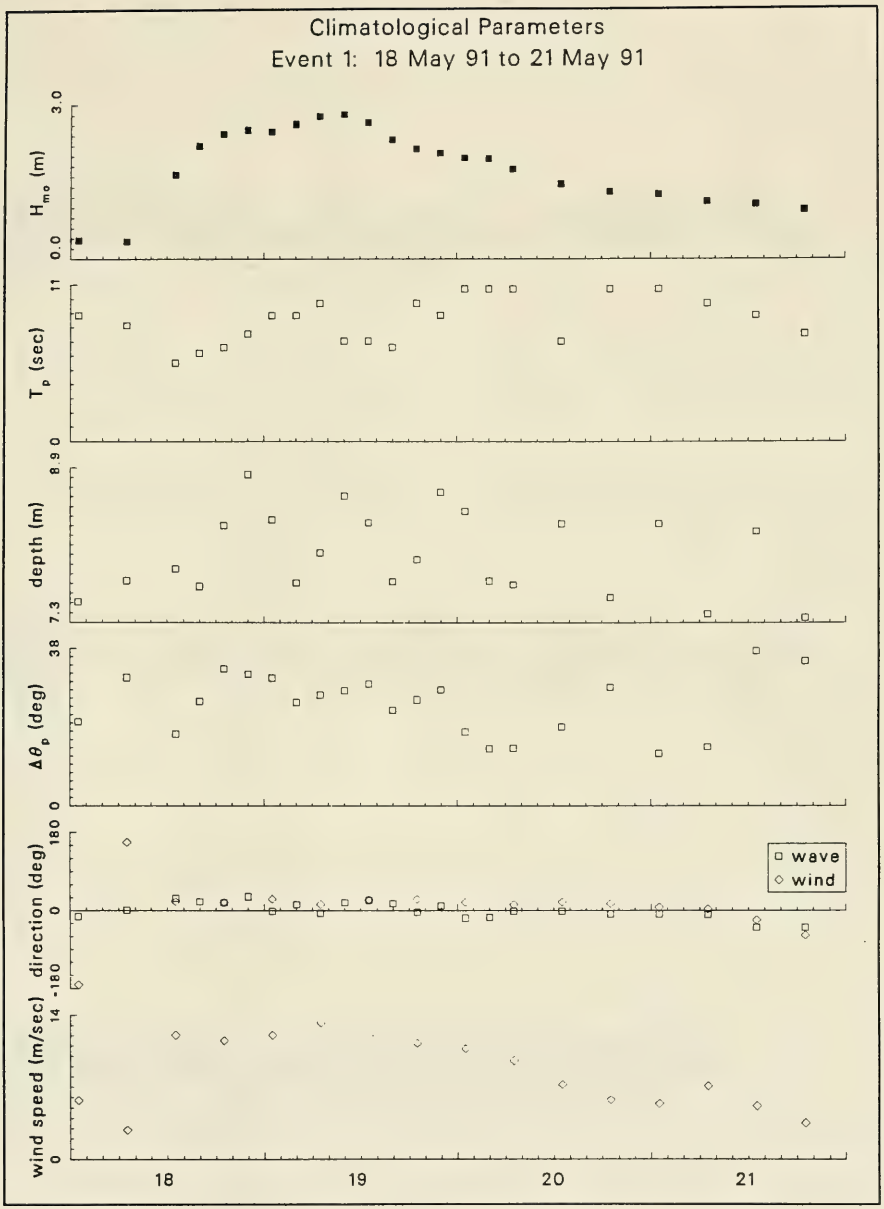
Climatological Parameters
Event 1: 18 May 91 to 21 May 91
H_{mo} (m)
3.0
0.0
T_p (sec)
11
0
depth (m)
8.9
7.3
$\Delta\theta_p$ (deg)
38
0
direction (deg)
180
0
-180
wave
wind
wind speed (m/sec)
14
0
18
19
20
21

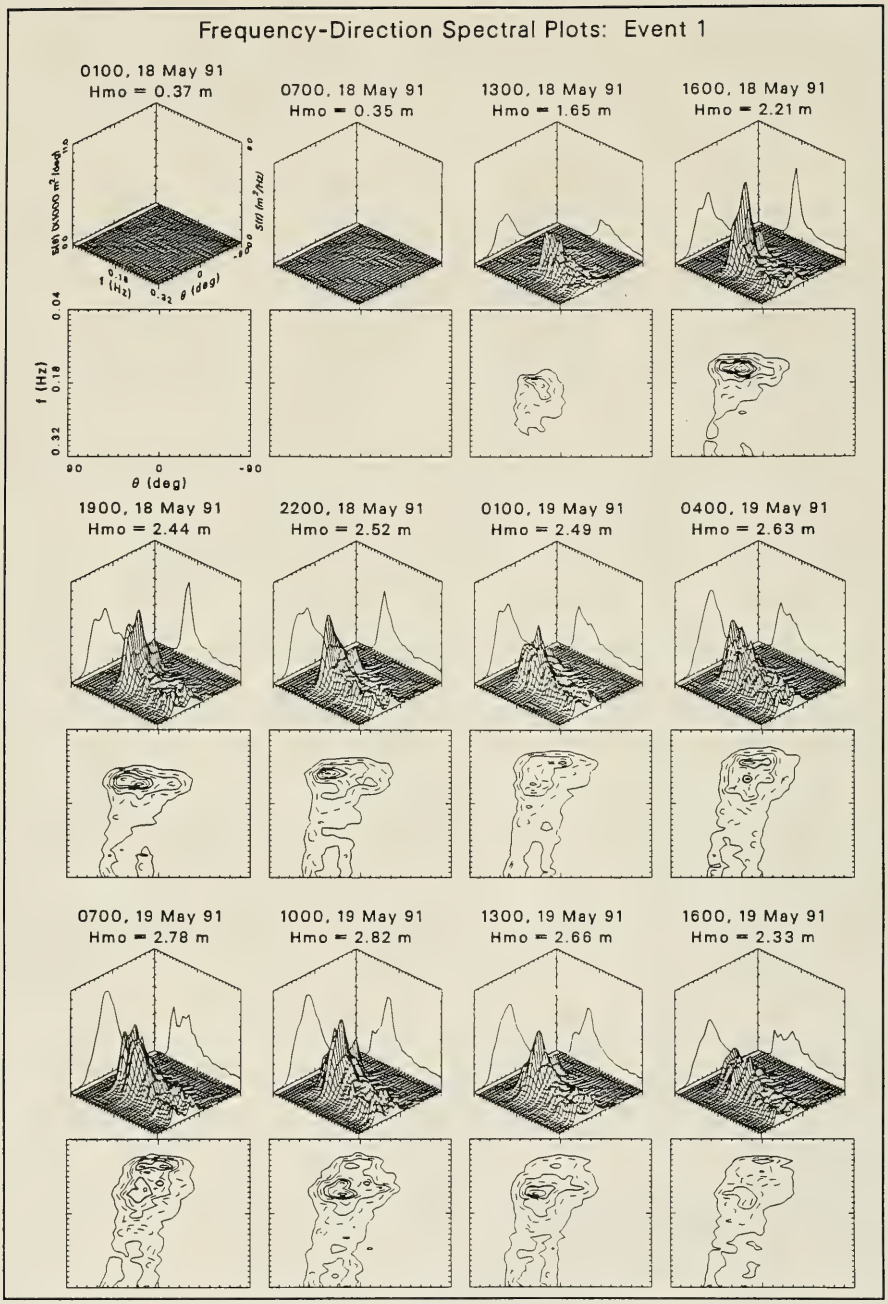
Frequency-Direction Spectral Plots: Event 1
0100, 18 May 91
Hmo = 0.37 m
0700, 18 May 91
Hmo = 0.35 m
1300, 18 May 91
Hmo = 1.65 m
1600, 18 May 91
Hmo = 2.21 m
f (Hz)
0.04
0.18
0.32
90
0
-90
θ (deg)
1900, 18 May 91
Hmo = 2.44 m
2200, 18 May 91
Hmo = 2.52 m
0100, 19 May 91
Hmo = 2.49 m
0400, 19 May 91
Hmo = 2.63 m
0700, 19 May 91
Hmo = 2.78 m
1000, 19 May 91
Hmo = 2.82 m
1300, 19 May 91
Hmo = 2.66 m
1600, 19 May 91
Hmo = 2.33 m

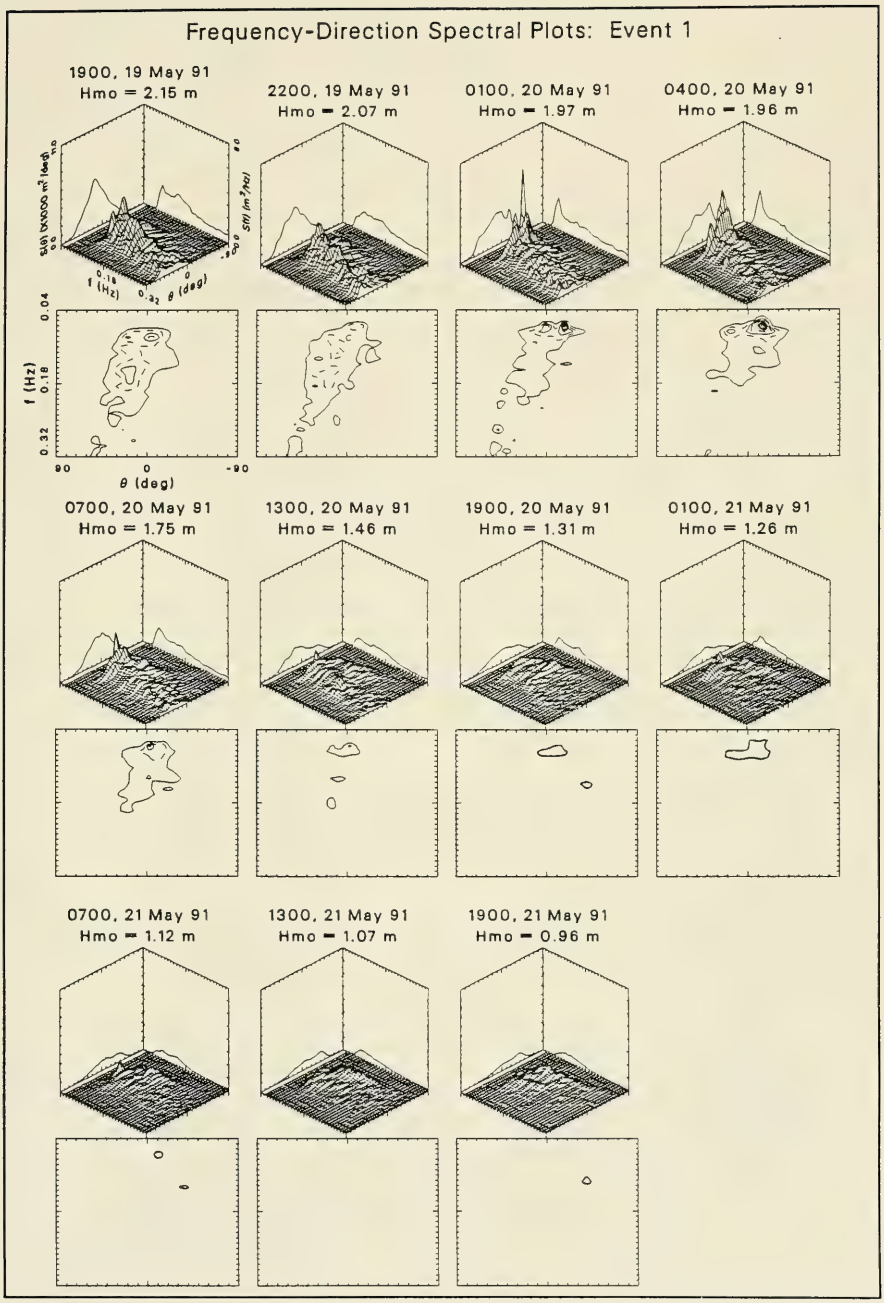
Frequency-Direction Spectral Plots: Event 1
1900, 19 May 91
Hmo = 2.15 m
2200, 19 May 91
Hmo = 2.07 m
0100, 20 May 91
Hmo = 1.97 m
0400, 20 May 91
Hmo = 1.96 m
0700, 20 May 91
Hmo = 1.75 m
1300, 20 May 91
Hmo = 1.46 m
1900, 20 May 91
Hmo = 1.31 m
0100, 21 May 91
Hmo = 1.26 m
0700, 21 May 91
Hmo = 1.12 m
1300, 21 May 91
Hmo = 1.07 m
1900, 21 May 91
Hmo = 0.96 m
f (Hz)
0.04
0.18
0.32
90
0
-90
θ (deg)

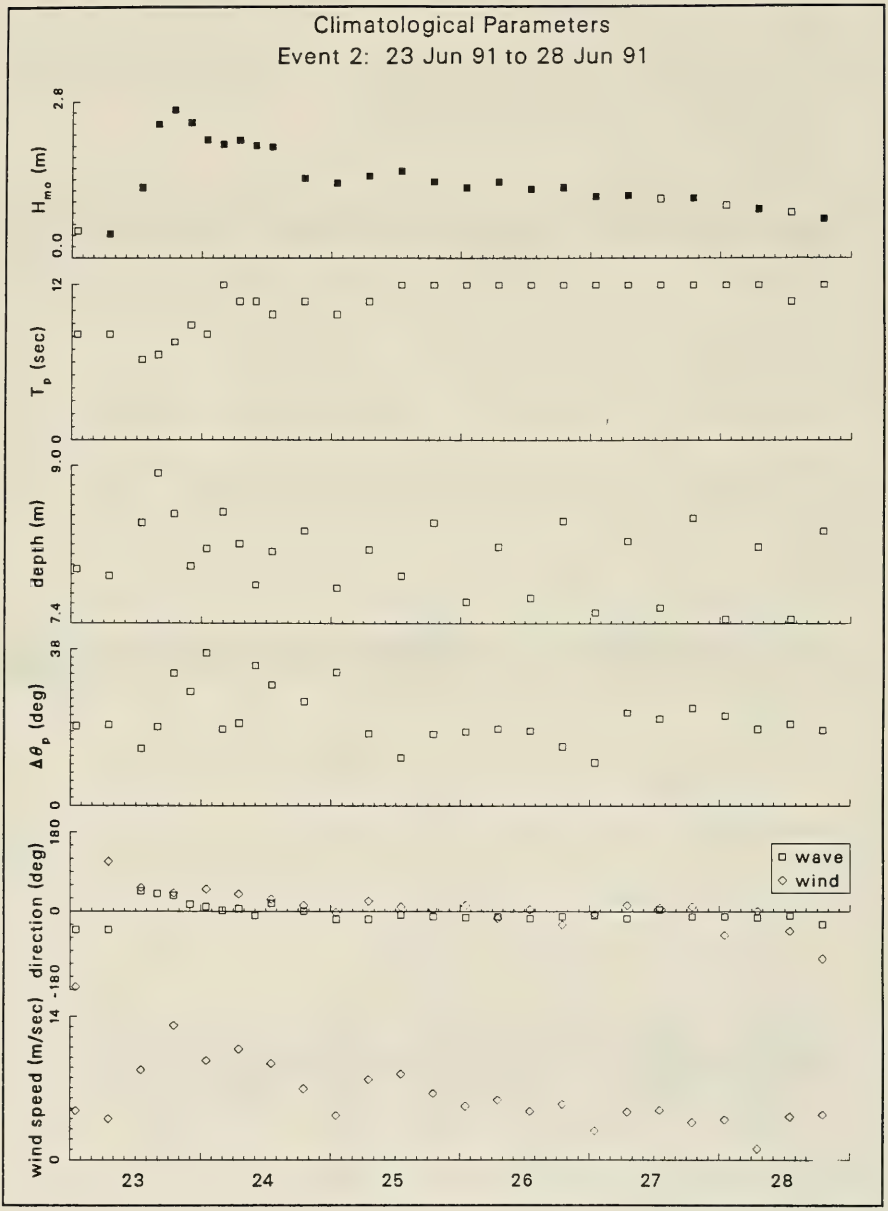
Climatological Parameters
Event 2: 23 Jun 91 to 28 Jun 91
H_{mo} (m)
2.8
0.0
T_p (sec)
12
0
depth (m)
9.0
7.4
$\Delta\theta_p$ (deg)
38
0
direction (deg)
180
0
-180
wave
wind
wind speed (m/sec)
14
0
23
24
25
26
27
28

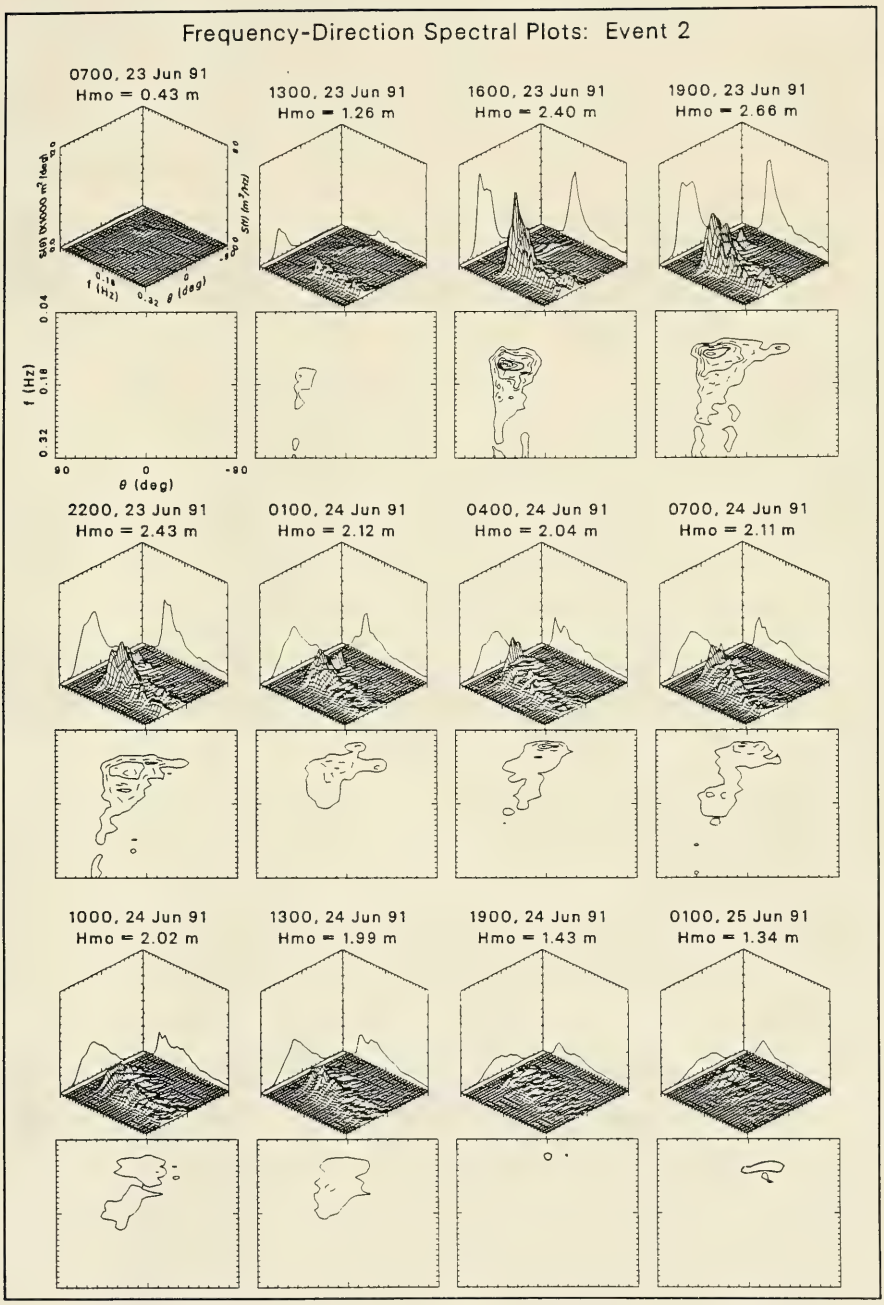
Frequency-Direction Spectral Plots: Event 2
0700, 23 Jun 91
Hmo = 0.43 m
1300, 23 Jun 91
Hmo = 1.26 m
1600, 23 Jun 91
Hmo = 2.40 m
1900, 23 Jun 91
Hmo = 2.66 m
f (Hz)
0.04
0.18
0.32
90
0
-90
θ (deg)
2200, 23 Jun 91
Hmo = 2.43 m
0100, 24 Jun 91
Hmo = 2.12 m
0400, 24 Jun 91
Hmo = 2.04 m
0700, 24 Jun 91
Hmo = 2.11 m
1000, 24 Jun 91
Hmo = 2.02 m
1300, 24 Jun 91
Hmo = 1.99 m
1900, 24 Jun 91
Hmo = 1.43 m
0100, 25 Jun 91
Hmo = 1.34 m

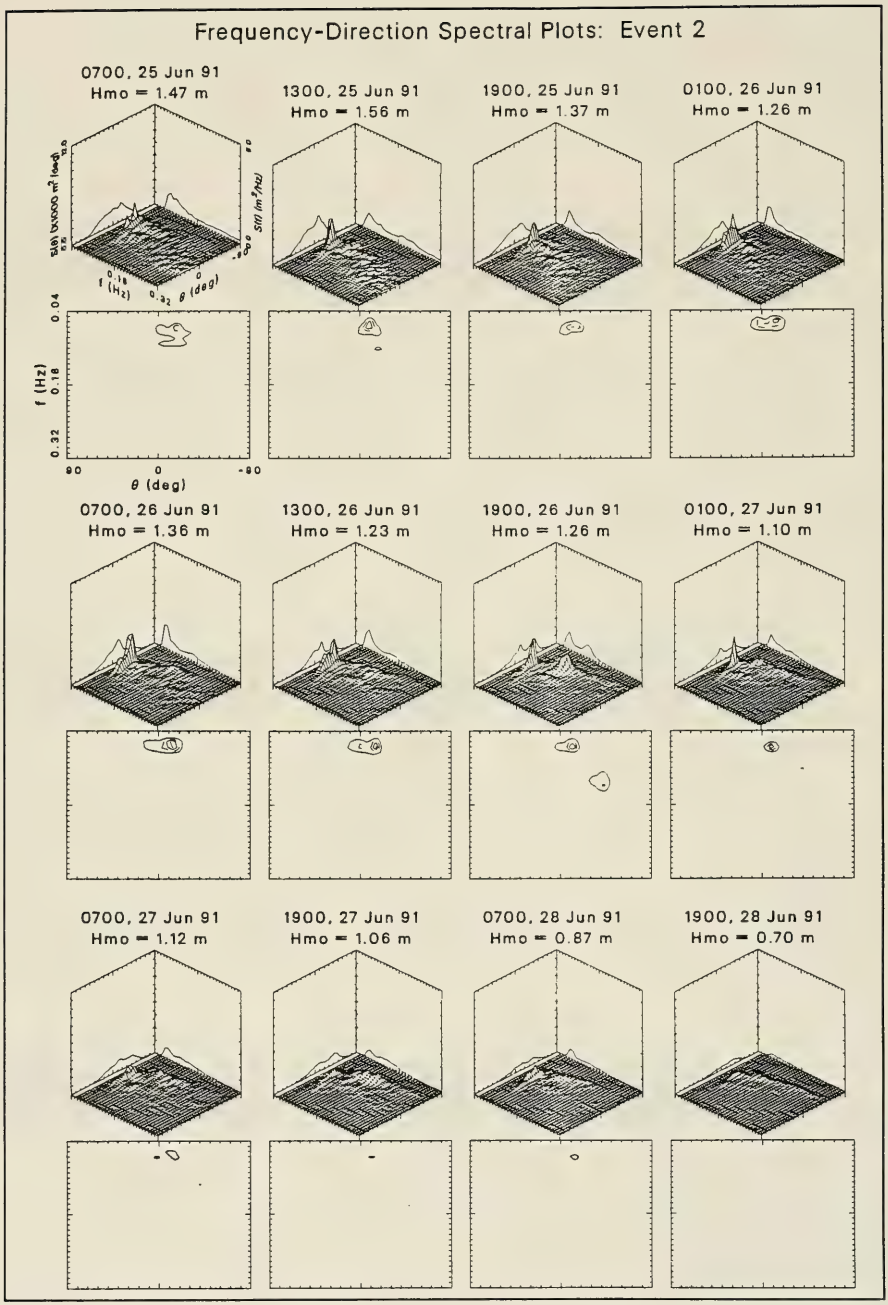
Frequency-Direction Spectral Plots: Event 2
0700, 25 Jun 91
Hmo = 1.47 m
1300, 25 Jun 91
Hmo = 1.56 m
1900, 25 Jun 91
Hmo = 1.37 m
0100, 26 Jun 91
Hmo = 1.26 m
f (Hz)
0.04
0.18
0.32
90
0
-90
θ (deg)
0700, 26 Jun 91
Hmo = 1.36 m
1300, 26 Jun 91
Hmo = 1.23 m
1900, 26 Jun 91
Hmo = 1.26 m
0100, 27 Jun 91
Hmo = 1.10 m
0700, 27 Jun 91
Hmo = 1.12 m
1900, 27 Jun 91
Hmo = 1.06 m
0700, 28 Jun 91
Hmo = 0.87 m
1900, 28 Jun 91
Hmo = 0.70 m

Appendix B
Notation

d	Water depth
f	Cyclic frequency
f_n	Cyclic frequency of n^{th} component wave
f_p	Spectral peak frequency
f_N	High-frequency boundary for a discrete spectrum
f_1	Low-frequency boundary for a discrete spectrum
H_{mo}	Spectrum-based characteristic wave height
$I(f,\theta)$	Direction integral of directional distribution function
IMLE	Iterative Maximum Likelihood Estimation
m	Index integer
M	Upper limit of indices denoted m
MLE	Maximum Likelihood Estimation
n	Index integer
N	Upper limit of indices denoted n
S	Spectral density
$S(f)$	Frequency spectral density
$S(f_n)$	Frequency spectral density at n^{th} discrete frequency

$S(f,\theta)$	Frequency-direction spectral density
$S(f_n,\theta_m)$	Frequency-direction spectral density at n^{th} discrete frequency and m^{th} discrete direction
$S(\theta)$	Direction spectral density
T_p	Characteristic wave period derived from spectral peak
β	Convergence exponent in IMLE method
γ	Convergence coefficient in IMLE method
$\delta\theta_p$	Directional spread of wave energy at spectral peak frequency
Δf	Finite frequency increment
θ	Wave direction
θ_m	Element m of a discrete set of wave directions
θ_M	Upper bound of discrete direction coordinate
θ_p	Peak wave direction
θ_1	Lower bound of discrete direction coordinate
θ_{25}	Angle subtending 25 percent of wave energy
θ_{75}	Angle subtending 75 percent of wave energy

REPORT DOCUMENTATION PAGE

Form Approved
OMB No. 0704-0188

1. AGENCY USE ONLY *(Leave blank)*	2. REPORT DATE	3. REPORT TYPE AND DATES COVERED
	February 1994	Final Report

4. TITLE AND SUBTITLE
Storm Evolution of Directional Seas in Shallow Water

5. FUNDING NUMBERS

6. AUTHOR(S)
Charles E. Long

7. PERFORMING ORGANIZATION NAME(S) AND ADDRESS(ES)

U.S. Army Engineer Waterways Experiment Station
Coastal Engineering Research Center
3909 Halls Ferry Road
Vicksburg, MS 39180-6199

8. PERFORMING ORGANIZATION REPORT NUMBER

Technical Report
CERC-94-2

9. SPONSORING/MONITORING AGENCY NAME(S) AND ADDRESS(ES)

U.S. Army Corps of Engineers
Washington, DC 20314-1000

10. SPONSORING/MONITORING AGENCY REPORT NUMBER

11. SUPPLEMENTARY NOTES

Available from National Technical Information Service, 5285 Port Royal Road, Springfield, VA 22161

12a. DISTRIBUTION/AVAILABILITY STATEMENT

Approved for public release; distribution is unlimited

12b. DISTRIBUTION CODE

13. ABSTRACT *(Maximum 200 words)*

Measured storm wave frequency-direction spectra are presented to illustrate the evolution of wind wave energy distributions near times of high energy. Twenty-nine storm events, extracted from a 5-year database, are identified and described. Instrumentation consists of a nine-element linear array of bottom-mounted pressure gauges distributed along the 8-m isobath about 900 m offshore of Duck, NC, site of the Field Research Facility (FRF) of the U.S. Army Engineer Waterways Experiment Station, Coastal Engineering Research Center. Iterative Maximum Likelihood Estimation is used to determine directional distributions of wave energy. Events, identified by elevation and duration of wave energy, are due to both localized storms and long-period swell radiating from major weather events in the distant, deep Atlantic Ocean. Frequency-direction spectra associated with storms known as "northeasters" have a curiously recurrent pattern of broad directional distributions at low frequencies near the spectral peaks and distinct bimodal distributions over a broad range of high frequencies. Reasons for this behavior are not obvious but require clarification because such wave patterns do not conform to conventional models used in engineering design. The differences may lead to substantial variations in design results.

14. SUBJECT TERMS
Frequency-direction spectra
Storms
Wave climate
Wind Waves

15. NUMBER OF PAGES
131

16. PRICE CODE

17. SECURITY CLASSIFICATION OF REPORT	18. SECURITY CLASSIFICATION OF THIS PAGE	19. SECURITY CLASSIFICATION OF ABSTRACT	20. LIMITATION OF ABSTRACT
UNCLASSIFIED	UNCLASSIFIED